A mouse intensive care unit to study TNF-induced sepsis and acid-induced lung injury

Von der Fakultät für Mathematik, Informatik und Naturwissenschaften
der RWTH Aachen University zur Erlangung des akademischen Grades
einer Doktorin der Naturwissenschaften genehmigte Dissertation

vorgelegt von

Diplom-Biologin Lucy Kathleen Reiss

aus London

Berichter: Univ.-Prof. Dr. Stefan Uhlig
Univ.-Prof. Dr. Werner Baumgartner

Tag der mündlichen Prüfung: 25. Juni 2012

Summary

Acute lung injury (ALI) is a life threatening heterogeneous lung disease caused by a variety of intra- and extra-pulmonary inflammatory insults, including ventilator-induced lung injury, sepsis and gastric aspiration. So far no curative therapy is available for patients suffering from ALI and its more severe form acute respiratory distress syndrome (ARDS), which have a mortality of approximately 40%. Animal models are indispensable to elucidate the pathomechanisms of ALI and to develop successful therapeutic strategies. Although mice are the most frequently used species in laboratory practice, their small size poses a challenge regarding the measurement of respiratory and cardiovascular parameters. As a result, mouse models giving comprehensive information on the mechanisms of ALI under consideration of the physiological consequences are largely lacking. The present thesis aimed to examine the pathomechanisms of ALI in different injury models under consideration of clinically relevant physiological parameters.

Therefore, a mouse intensive care unit (ICU) was developed that facilitates non-injurious mechanical ventilation under permanent physiological monitoring resulting in stable pulmonary and cardiovascular functions. For this purpose the role of recruitment manoeuvres (RM) at low and moderately high levels of tidal volume (V_T) (8 versus 16 mL/kg) and positive end-expiratory pressure (PEEP) (2 versus 6 cmH_2O) was examined. The current study demonstrated that protective non-injurious ventilation of mice requires the application of recurrent short RM to avoid atelectasis and further confirmed a protective effect of low V_T and an increased PEEP level. Stable cardiovascular functions were achieved by intra-arterial volume substitution, regulation of body temperature and adequate anaesthesia. This setup provided all necessary parameters to determine experimental ALI, including oxygenation, pulmonary inflammation, oedema formation and histopathology, and is therefore useful for studies on ALI.

A further objective was to examine the effect of a lethal systemic dose tumour necrosis factor (TNF) on the lungs of wild-type and acid sphingomyelinase-deficient ($ASM^{-/-}$) mice. The pro-inflammatory cytokine TNF and the ceramide-generating enzyme ASM both play an important role in the pathogenesis sepsis, which is the main cause for extra-pulmonary ALI. The mouse ICU with its life supporting features facilitated to conduct this study. Despite of the supportive strategies, TNF caused septic shock, which was lethal in a significant number of wt mice. Of note, $ASM^{-/-}$ mice were protected from the cardiovascular depression and mortality, validating a pivotal role of ASM in sepsis. Somewhat surprisingly, TNF-induced sepsis did not cause lung injury.

Finally, a model was required that causes a reproducible lung injury and allows the investigation of the effectiveness of therapeutic drugs in ALI, in particular the usefulness of steroids, which is currently under debate. For this purpose the model of acid-induced lung injury was chosen, because it resembles important clinical features of intra-pulmonary ALI. Instillation of acid with pH 1.5 caused inflammation and profound structural changes in the lung, leading to a loss of lung functions and severe hypoxemia. Treatment with the glucocorticoid dexamethasone proved to be anti-inflammatory, but did not prevent physiological dysfunction. In contrast, acid with pH 1.8 induced moderate lung injury with mild hypoxemia and predominantly inflammatory processes that were susceptible to dexamethasone. For the first time it was shown in an animal model of intra-pulmonary lung injury that steroid treatment significantly improved not only neutrophil recruitment and oedema formation, but also lung functions and oxygenation. A further therapeutic approach with the anti-inflammatory drug quinine failed to improve lung injury.

In conclusion, the mouse ICU established here allows non-injurious ventilation under monitoring of clinically relevant parameters, provides life supporting measures, as shown in the TNF model, and is useful to conduct injury models. A final cluster analysis revealed three patterns of ALI: a ‘classical’ inflammation-dependent pathway and two injury mechanisms that are not related to inflammation, namely low-volume injury and chemical damage. These results suggest that the clinical effectiveness of anti-inflammatory drugs, such as steroids, may depend on the aetiology of ALI.

Zusammenfassung

Akutes Lungenversagen (Acute Lung Injury/ALI) ist eine heterogene Lungenerkrankung, die durch eine Vielzahl von intra- und extra-pulmonalen Stimuli ausgelöst werden kann. Dazu gehören unter anderem der beatmungsinduzierte Lungenschaden, Sepsis und die Aspiration des Mageninhaltes. Bislang gibt es keine kurative Therapie für ALI und seine schwerere Form Acute Respiratory Distress Syndrome (ARDS). Die Mortalität der Patienten mit ALI/ARDS liegt deshalb bei ca. 40%. Tiermodelle sind unentbehrlich, um die Pathomechanismen zu erforschen, die zu ALI führen, und um wirksame Therapien zu entwickeln. Mäuse sind die am häufigsten eingesetzte Spezies in experimentellen Tiermodellen. Die Messung von respiratorischen und kardiovaskulären Parametern stellt jedoch bedingt durch ihre kleine Größe eine Herausforderung dar. Bisher gibt es kaum Mausmodelle für ALI, die einen umfassenden Einblick in die Mechanismen der Entstehung des Lungenschadens bieten und gleichzeitig die physiologischen Konsequenzen beleuchten. In der aktuellen Studie sollten die Pathomechanismen von ALI in verschiedenen Schadensmodellen unter Einbeziehung physiologischer Parameter untersucht werden.

Das erste Ziel dieser Studie bestand darin, eine Maus-Intensivstation zu etablieren, die es ermöglicht, Mäuse unter permanenter Überwachung respiratorischer und kardiovaskulärer Parameter zu beatmen. Es sollten Bedingungen definiert werden, unter denen diese Parameter über mehrere Stunden konstant bleiben. Von besonderem Interesse war dabei die Auswirkung von Rekrutierungsmanövern (RM) bei niedrigem und moderat erhöhtem Tidalvolumen (V_T) (8 versus 16 mL/kg) sowie verschiedenen positiv endexpiratorischen Drücken (PEEP) (2 versus 6 cmH_2O). Die aktuelle Studie zeigt, dass eine protektive Beatmung von Mäusen die Applikation von regelmäßigen RM zur Vermeidung von Atelektasen erfordert. Des Weiteren sind ein niedriges V_T und moderater PEEP nötig, um die Lunge nicht durch die Beatmung zu schädigen. Stabile Kreislaufbedingungen wurden durch intra-arterielle Volumengabe, Regulation der Körpertemperatur und eine angemessene Anästhesie erreicht. Das hier etablierte Beatmungsmodell liefert alle Parameter die nötig sind, um experimentelles ALI zu diagnostizieren, einschließlich von Oxygenierung, pulmonaler Entzündung, Ödembildung und Histopathologie, und bietet dadurch eine optimale Grundlage für Schadensmodelle.

Ein weiteres Ziel war es, erstmalig den Effekt einer letalen systemisch applizierten Dosis „tumour necrosis factor" (TNF) auf die Lunge zu untersuchen. Es wurden Wildtyp und Saure Sphingomyelinase-defiziente ($ASM^{-/-}$) Mäuse in diese Studie eingeschlossen. Das pro-inflammatorische Zytokin TNF und das Ceramid-generierende Enzym ASM spielen beide eine wichtige Rolle in der Pathogenese der Sepsis, welche die Hauptursache für extra-

pulmonales ALI ist. Die Maus-Intensivstation erwies sich als sehr geeignet, diese Untersuchung durchzuführen. Trotz der lebenserhaltenden Maßnahmen war die TNF-induzierte Sepsis in einer signifikanten Anzahl von Wildtyp Mäusen letal. Interessanterweise waren die $ASM^{-/-}$ Mäuse vor kardiovaskulärer Dekompensation und Mortalität geschützt, wodurch gezeigt werden konnte, dass die ASM beim letalen Verlauf der Sepsis eine entscheidende Rolle spielt. Überraschenderweise wurde jedoch durch die TNF-induzierte Sepsis kein Lungenschaden verursacht.

Abschließend wurde ein intra-pulmonales Schadensmodell benötigt, in dem ein reproduzierbarer Lungenschaden die Grundlage für die Erforschung therapeutisch wirksamer Medikamenten liefern sollte. Im Vordergrund stand dabei die Untersuchung der Wirksamkeit von Steroiden bei ALI, die bislang kontrovers diskutiert wird. Zu diesem Zweck wurde das Modell des Säure-induzierten Lungenschadens gewählt, da es wichtige klinische Merkmale von ALI widerspiegelt. Die Instillation von Säure mit pH 1.5 verursachte sowohl Entzündung als auch strukturelle Veränderungen in der Lunge, begleitet von einer Beeinträchtigung der Lungenmechanik und schwerer Hypoxämie. Eine Behandlung mit dem Glucocorticoid Dexamethason wirkte anti-entzündlich, verhinderte aber nicht die physologische Dysfunktion. Im Gegensatz dazu induzierte die Instillation von Säure mit pH 1.8 einen moderaten Lungenschaden, der vornehmlich durch inflammatorische Vorgänge und moderate Hypoxämie charakterisiert war und durch Dexamethason vollständig verhindert werden konnte. Im Rahmen des hier etablierten Tiermodelles wurde zum ersten Mal die Wirksamkeit von Steroiden bei intra-pulmonalem ALI nicht nur auf inflammatorischer, sondern auch auf physiologischer Ebene nachgewiesen. Ein anderer therapeutischer Ansatz, mit dem ebenfalls anti-inflammatorisch wirksamen Chinin, konnte den Lungenschaden in diesem Modell nicht beeinflussen.

Zusammenfassend lässt sich aussagen, dass die hier etablierte Maus-Intensivstation eine protektive Beatmung unter der permanenten Überwachung klinisch relevanter Parameter ermöglicht. Dieser Versuchsaufbau eignet sich auf Grund der lebenserhaltenden Maßnahmen sowohl für Sepsismodelle als auch für die Erforschung von ALI. Eine abschließende Clusteranalyse ließ drei unterschiedliche Schadensmuster von ALI erkennen: einen „klassischen“ inflammatorischen Weg sowie zwei entzündungsunabhängige Mechanismen, von denen einer mit Atelektasen und der andere mit chemischer Verletzung assoziiert war. Diese Ergebnisse deuten darauf hin, dass die klinische Wirksamkeit von anti-inflammatorischen Medikamenten, wie beispielsweise den Steroiden, von der Ätiologie des ALI abhängig ist.

List of abbreviations

AECC	American-European Consensus Conference
ALI	Acute lung injury
ARDS	Acute respiratory distress syndrome
ASM	Acid sphingomyelinase
AT I	Angiotensin I
BAL	Bronchoalveolar lavage
BSA	Bovine serum albumin
C	Compliance
ELISA	Enzyme-linked immunosorbent assay
FiO_2	Fraction of inspired oxygen
f	Frequency
G	Tissue damping
H	Tissue elastance
HCl	Hydrochloric acid
HE	Hematoxylin Eosin
HMGB1	High-mobility group protein B1
HSA	Human serum albumin
IL-6	Interleukin-6
ICAM-1	Intercellular adhesion molecule 1
IP-10	Interferon gamma-induced protein 10
ip	intraperitoneal
it	intratracheal
iv	intravenous
KC	Keratinocyte-derived chemokine
LPS	Lipopolysaccharide
LPC	Lysophosphatidylcholine
MA	Moderate acid
MIP-2	Macrophage inflammatory protein-2
MV	Mechanical ventilation
NaCl	Sodium chloride
NFκB	Nuclear factor kappa-light-chain-enhancer of activated B cells
NO	Nitric oxide
NPD	Niemann-Pick disease
PBS	Phosphate buffered saline
PCT	Procalcitonin
PEEP	Positive end-expiratory pressure

PLA2	Phospholipase A2
R	Resistance
R_{aw}	Airway resistance
RM	Recruitment manoeuvre
ROS	ROS: reactive oxygen species
SA	Severe acid
TNF	Tumour necrosis factor
VILI	Ventilator-induced lung injury
V_T	Tidal volume
wt	wild-type
zVAD-fmk	Carbobenzoxy-valyl-alanyl-aspartyl-[O-methyl]-fluoromethylketone

Table of contents

1 Introduction

1.1 Anatomy of the human lung

The respiratory system can be divided into an extra-thoracic tract with nose and larynx and an intra-thoracic tract to which the trachea, the bronchi and the lungs belong [1]. The lung (*pulmo*) is a paired organ, comprising a right lung with three lobes and a left lung with two lobes (Fig. 1.1). When reaching the hilus of the lung, the trachea bifurcates into a right and a left main bronchus of which one enters each lung. The intrapulmonary bronchi further branch into three right and two left lobular bronchi with ten segmental bronchi in each lung. The bronchi finally split into terminal and respiratory bronchioles which terminate, on average in the 23rd generation, in the alveoli. The air conducting part of the respiratory system is the anatomical dead space of the lung (~150 mL). The respiratory bronchioles divide into two alveolar ducts that end in alveolar sacs, were the gas exchange takes place. Each terminal bronchiole carries about 200 alveoli, which comprise one morphological unit called *acinus.* 5-10 *acinini* form one lobulus, a unit with about 1 mL gas volume. The total lung capacity of the human lung is about 5 L, whereof about 0.5 L is the average tidal volume [2]. The lobuli form bronchopulmonal segments, of which the right lung has ten and the left mostly only nine. Each segment is supplied with a segmental bronchus and a furcation of the *arteria pulmonalis*. The alveoli are covered by a dense capillary network (*vasa publica*), containing about 200 mL of blood that is involved in gas exchange on a surface area of about 140 m^2. Gas exchange takes place by diffusion over the alveolar-capillary barrier, a thin layer of only 2 µm, which consists of alveolar epithelial pneumocytes type I, an interstitial space and vascular endothelial cells [3]. Besides of the pneumocytes type I, also the surfactant producing epithelial pneumocytes type II, non-ciliated bronchiolar clara cells and alveolar macrophages are cell types that are unique to the lung. Beyond these, 40 other types of epithelial, connective tissue and blood cells are located in the lung [4]. The nourishment of the lung is provided by a second vascular network, the *vasa privata*. The lung is innervated by the *plexus pulmonalis* containing parasympathetic fibers of the *nervus vagus,* responsible for bronchoconstriction, and fibres of the *truncus sympathicus,* causing bronchodilatation [5]. The innervation is restricted to the peribronchial and perivascular musculature. The primary function of the lung is the gas exchange, during which O_2 diffuses from the alveoli into the blood and CO_2 from the blood into the air spaces. In addition, the lung has several other important functions e.g. filtration of the blood, synthesis of mucus and surfactant, uptake, storage and detoxification of foreign substances, cytochrome p-450 metabolism [6] and processing of hormones and vasoactive substances [7,8].

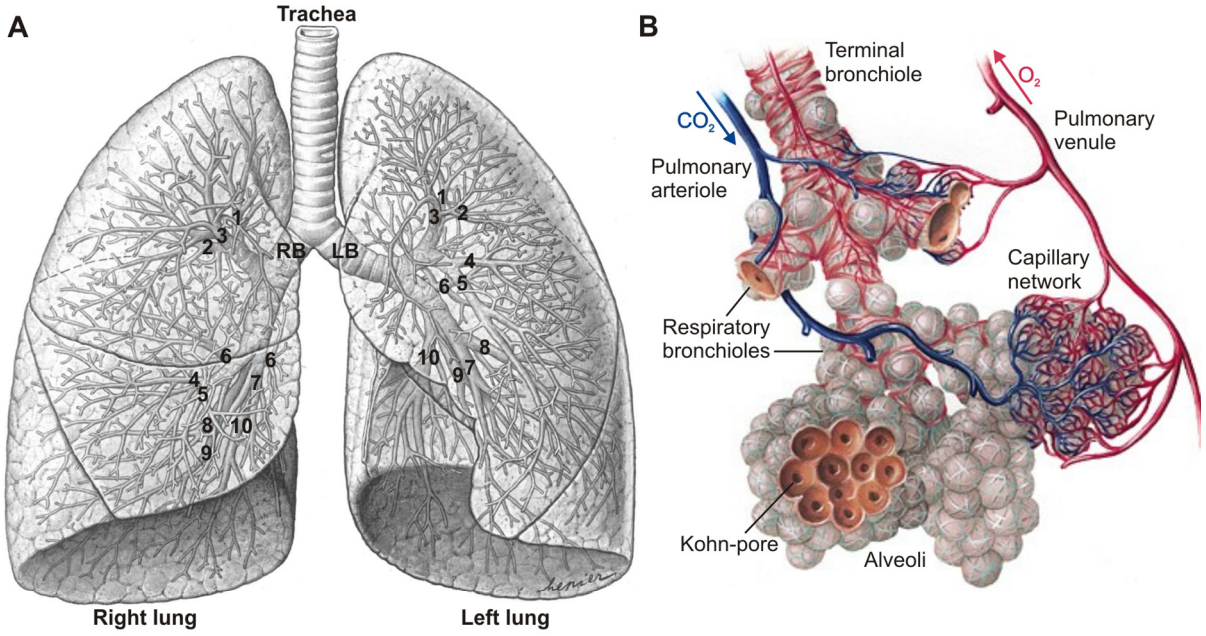

Fig. 1.1: The human lung. A. Right and left lung with right main bronchus (RB) and left main bronchus (LB), which derive from the trachea, entering the lungs at the hilus. The bronchial tree with lobular and segmental bronchi is projected from ventral on to the lungs. Segmental bronchi are indicated by numbers from 1 to 10. **B.** Terminal respiratory unit consisting of a terminal bronchiole with several respiratory bronchioles. The air conducting part ends in the alveoli, where gas exchange takes place. CO_2-rich blood, coming from the heart, enters the lung via the pulmonary arterioles, gas exchange takes place in the capillary network and O_2-rich blood leaves the lung via the pulmonary venules. The sum of alveoli derived from one terminal bronchiole is termed acinus. Figures are modified according to Sobotta [9].

1.2 Physiology of the lung

The lung is an elastic structure without own musculature. Each lobe is surrounded by a visceral pleura, which has direct contact to the parietal pleura that lines the rib cage. The lung follows all movements of the rib cage. Ventilation takes place by movement of the diaphragm and the intercostal muscles. Two forces oppose each other during breathing: the centripetal retraction of the lung, which is mainly due to the elastic properties of the lung, and the centrifugal retraction of the thorax, which depends on the muscle tone of the respiratory muscles. The elastic properties of the lung are facilitated by collagen and elastic fibres in the walls of the alveoli, bronchioles and capillaries on the one hand and by the phospholipid-rich surfactant, which lines the alveoli and prevents alveolar collapse by reducing the alveolar surface tension [10,11], on the other hand. During ventilation, air always moves from the high to the low pressure area. The driving force is the transpulmonary pressure, which is determined by the intra-alveolar pressure minus the subatmospheric pleural pressure, which is caused by the recoil of the lung. During inhalation, the thorax is expanded by muscle contraction, leading to a passive expansion of the lung, a decrease in the alveolar pressure and inflow of air until the alveolar pressure equals the atmospheric pressure. In the exhalation phase, the chest cavity becomes smaller by muscle relaxation, the alveolar

pressure increases above the atmospheric pressure and air streams out. The ability of the lungs to expand is expressed by the pulmonary compliance (C), which is defined as volume change (ΔV) per unit of pressure change (ΔP) across an elastic structure:

$$C = \frac{\Delta V}{\Delta P}$$

The volume-pressure curve is non-linear. C is highest at the residual volume, i.e. the volume that remains in the lungs after maximal exhalation, and decreases with increasing lung volume. Also, C depends on the size of the lungs. Larger lungs have a higher C than small lungs. The measurement of C indicates how easily the lung is inflated and is the inverse value of the elastance that indicates the stiffness of the lung [12].

Besides of the elastic forces of the lung, which have to be overcome only during inspiration, the resistance of the lung plays a role during inspiration and expiration. The pulmonary resistance (R) is composed of the airway resistance and to a lesser degree also forces of friction in the lung tissue. Pulmonary resistance is defined as pressure change (ΔP) between alveolar pressure and atmospheric pressure divided by flow (V_{flow}):

$$R = \frac{\Delta P}{V_{flow}}$$

About 90% of the airway resistance is due to central and only about 10% to peripheral airways. Airway resistance depends on various parameters including the airway calibre, the air flow or breathing rate and the type of flow, determined by the size and form of the airway. As a result, small airways have a higher resistance than large airways at a constant flow [12].

1.3 Assessment of lung mechanics

One way of describing lung mechanics is inverse modelling i.e. construction of mathematical models that predict structural changes, based on experimental measurement of mechanical function [13]. In the following only those two models will be discussed that were actually applied in this thesis, namely the ’single-compartment model’ and the ’constant phase model’. The models are illustrated in Fig. 1.2.

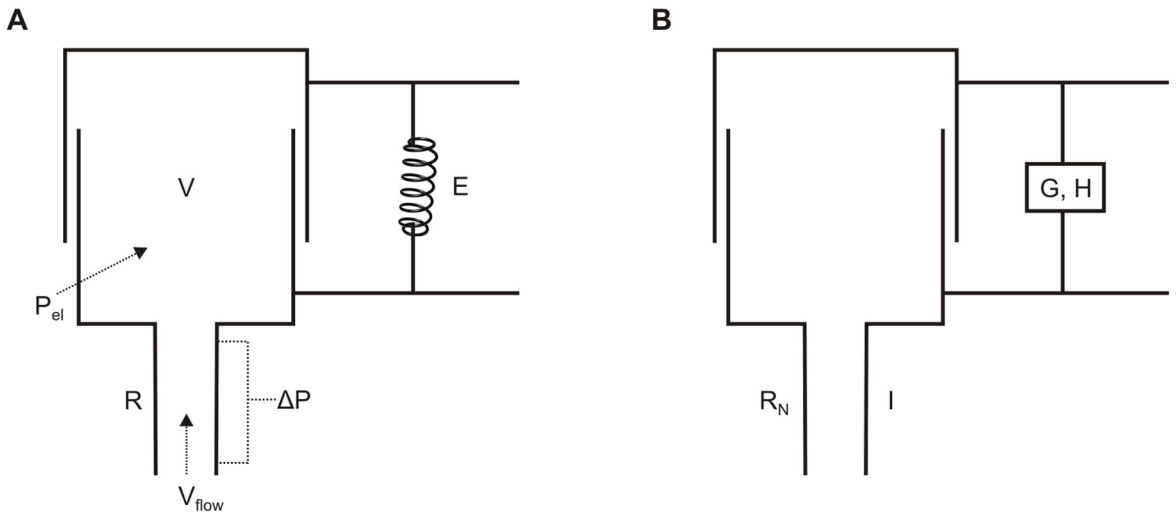

Fig. 1.2: Models of the lung. A. Single-compartment model. The lung is described as one compartment formed by two telescope canisters, which are connected by an elastic spring representing the tissue properties. The airways are described by an open tube. V: volume of the compartment, E: elastance of the spring (E=1/C), R: flow resistance, P_{el}: elastic recoil pressure, ΔP: pressure difference between the ends of the tube. **B.** Constant-phase model. The model is based on the single compartment model, but here the tissue properties are frequency-independent. G and H: tissue impedance, R_N: Newtonian flow resistance, I: gas inertance. The figure is modified according to J.H.T. Bates [14].

1. The linear first-order single compartment model is a simple model that describes the lung as an elastic structure with one compartment, comparable to a balloon, which is filled via a stiff tube, which represents the properties of the conducting airways [15]. A slightly modified version of the single compartment model is depicted in Fig. 1.2A. Despite of its simplicity, the model reflects anatomical and functional aspects of the lung. It can be described by the following equation:

$$P = V_{flow}R + \frac{V}{C} + P_0$$

The total pressure across the model from the entrance of the tube to the outside of the elastic structure is the sum of the elastic recoil pressure ($P_{el} = V/C$) and the pressure difference between the ends of the tubing ($\Delta P = V_{flow}R$) plus the positive-endexpiratory pressure (P_0) that keeps the lung open [14]. Fitting the airway opening pressure and flow measured in a subject to this model allows calculation of the dynamic resistance and compliance.

Another approach, in which the lung is assumed as a linear dynamic system, is the calculation of the pulmonary input impedance (Z) [16]. The impedance reflects how difficult it is to get a certain quantity through a system. In the lung, the impedance relates flow and pressure. The term input derives from the fact that both parameters are measured at the same site, the entrance of the lung. To determine Z, a flow (V_{flow}) is applied to the lung and the pressure P is measured. V_{flow} and P are transformed by a Fourier transformation so that

they can be expressed as a function of frequency instead of time, before the impedance is calculated [14]:

$$Z = \frac{P(f)}{V_{flow}(f)}$$

One mode of applying a suitable flow to the lungs is to induce a sine-wave at a specific frequency. A more common method, known as the forced oscillation technique (FOT), involves application of multiple sinusoidal frequencies at the same time, which are higher than the frequency of breathing (< 0.5 Hz) [13,17]. FOT is also relevant in clinical praxis, as it can be superimposed on the breathing pattern and allows non-invasive assessment of lung functions [18,19].

2. A more advanced model of the lung is the constant phase model, in which the tissue component is independent of frequency and therefore constant, which is not the case in the single compartment model (Fig. 1.2B) [20]. Assessing the impedance by FOT, followed by constant phase analysis is a method that reveals accurate impedance data even in mice in which the small size and low air flow hinder other methods of lung function measurement [15,21]. A frequency spectra < 20 Hz was found to result in precise fits for the impedance also in several other species [22,23]. The input impedance of the constant phase model is described with the following equation [20]:

$$Z = R_N + i\omega I + \frac{G - iH}{\omega^{\alpha}} \qquad \text{and} \qquad \alpha = \frac{2}{\pi}\tan^{-1}\frac{H}{G}$$

(Z: pulmonary input impedance; R_N: Newtonian resistance; $i = \sqrt{-1}$: imaginary unit; $\omega = 2\pi f$: angular frequency, I: inertance, G: tissue damping, H: tissue elastance)

The impedance has a so called real part (R_N), which strongly resembles the resistance in the central airways (R_{aw}) [21], and an imaginary part, which describes the tissue component, comprising a dissipative part (G: tissue damping) and an elastic part (H: tissue elastance) (Fig. 1.2B) [24]. The imaginary part, also termed reactance, results from breathing and depends on the the elasticity of the lung. The ratio G/H is termed hysteresivity (η) and describes the relation between the dissipated and the stored energy. [25]. Although hysteresivity was shown to be relatively constant in one individual, it is discussed that an increase in hysteresivity accounts for structural heterogeneity in the lungs, as it increases with bronchoconstriction [26,27]. The advantage of fitting the constant phase model to the input impedance of the lung is that it allows to distinguish between central and peripheral respiratory mechanics [28].

1.4 Acute lung injury and acute respiratory distress syndrome

Acute respiratory distress syndrome (ARDS) is a life threatening heterogeneous lung disease that was first described in 1967, when the use of mechanical ventilation was rare [29]. In 1994 the American-European Consensus Conference (AECC) on ARDS defined four criteria, on which the diagnosis is based to date (Table 1.1). In this definition ARDS is distinguished from the less severe acute lung injury (ALI). The criteria include acute onset, bilateral chest infiltrates, pulmonary arterial occlusion pressure ≤ 18 mmHg or lack of evidence for cardiogenic oedema and a Horovitz index (pO_2/FiO_2) ≤ 200 mmHg for ARDS and ≤ 300 mmHg for ALI, respectively [30]. According to a cohort study including over 1000 patients in the USA, ALI has an incidence of 79 per 100,000 with a mortality around 40%. Of the patients with ALI who were ventilated for more than 24 hours, 21% developed ARDS [31], demonstrating that ALI has a progressive character. ARDS patients are at high risk of developing multiple organ failure, which is the predominant cause of death in ARDS [32,33].

Table 1.1: Clinical and experimental criteria for ARDS and ALI

Criterion	Clinical	Experimental
Timing	Acute onset	Acute onset
Oedema / inflammation	Radiograph: bilateral chest infiltrates	Histological evidence Inflammatory response
Type of oedema	Non-cardiogenic	Alterations of the alveolar capillary barrier
Oxygenation	PaO_2/FiO_2 ≤ 200 mmHg (ARDS) PaO_2/FiO_2 ≤ 300 mmHg (ALI)	Physiological dysfunction

Clinical criteria according to the American-European consensus conference on ARDS in 1994 [30]. Experimental criteria were suggested by the American Thoracic Society workshop report in 2011 [34].

In addition to defining ARDS, the AECC distinguished pulmonary ARDS, caused by insults directly affecting the lung parenchyma e.g. pneumonia, gastric aspiration or inhalation, from extra-pulmonary ARDS, resulting from an acute systemic inflammatory response such as sepsis or trauma [30]. Clinically, direct ARDS is characterised by a stronger increase in lung elastance and appears more resistant to therapeutic interventions, e.g. positive end-expiratory pressure (PEEP), prone positioning or recruitment manoeuvres than indirect ARDS [35].

Therapeutic approaches in ARDS are restricted mainly to supportive care, involving mechanical ventilation (MV). Although MV is mandatory in ARDS patients, it bears the risk of

inducing and worsening lung injury, especially in the typically inhomogeneously damaged ARDS lungs, a well characterised process termed ventilator-induced lung injury (VILI) [36-38]. The only clinical intervention that resulted in significant improvement of mortality, shown in a phase III trial, was reduction of tidal volume (V_T) from 12 mL/kg to 6 mL/kg [39]. The effectiveness of pharmacological treatments, e.g. inhaled NO or corticosteroids, lacks sufficient clinical evidence [40]. Though steroids are potent anti-inflammatory drugs in general, steroid-therapy of ARDS patients resulted in diverse clinical outcome [41,42]. However, a beneficial effect of steroids in ARDS is indicated by some clinical studies, especially when given in the later fibrotic phase [43,44]. The development of novel effective therapies is an important objective in current research, with a special focus on the molecular mechanisms that underlie the pulmonary inflammation involved in ALI/ARDS [45].

1.5 Animal models of acute lung injury

The basis for the development of novel therapies is a better understanding of the complex pathomechanisms that lead to ALI/ARDS. For this purpose, animal models are indispensable. One difficulty with animal models of ALI is that they do not show exactly the same features as the human respiratory failure, although they are based on typical risk factors of ALI [46]. Considering the different aetiologies of ALI, one approach to find new therapeutic targets is searching for molecular mechanisms that are common in different animal models. Given the importance of inflammation in the progression of lung injury, it is obvious that pro-inflammatory pathways are in the main focus of investigation [47].

A further problem is the definition of ALI in animal models. Well defined criteria are important to validate that the model actually works and for evaluation whether tested therapies are successful. Of the four criteria applied in humans (Table 1.1), the bilateral infiltration and the non-cardiogenic origin of oedema are difficult to assess in the frequently used small laboratory animals, i.e. mice and rats. Moreover, not all research laboratories may have access to a blood gas analyser for measurement of oxygenation. The question, how to standardise ALI in animal models, led to a first definition of ALI in animals by the American Thoracic Society [34]. This definition includes the following five experimental criteria for ALI: acute onset, histological alterations, inflammatory response, permeability of the alveolar capillary barrier and evidence of physiological dysfunction, e.g. hypoxemia as depicted in Table 1.1. Of these criteria, acute onset and at least three of the other criteria should be fulfilled to determine that ALI has occurred.

Finally, the choice of a suitable model and species is crucial, and depends on the mechanism under investigation. Species differences, such as the presence or absence of pulmonary intravascular macrophages, NO production or genetic variations regarding Toll-like or chemokine receptors have to be taken into account [46]. Models of ALI should ideally be based on the aetiologies that lead to human lung injury and can therefore be classified in models of intra- and extra-pulmonary ALI.

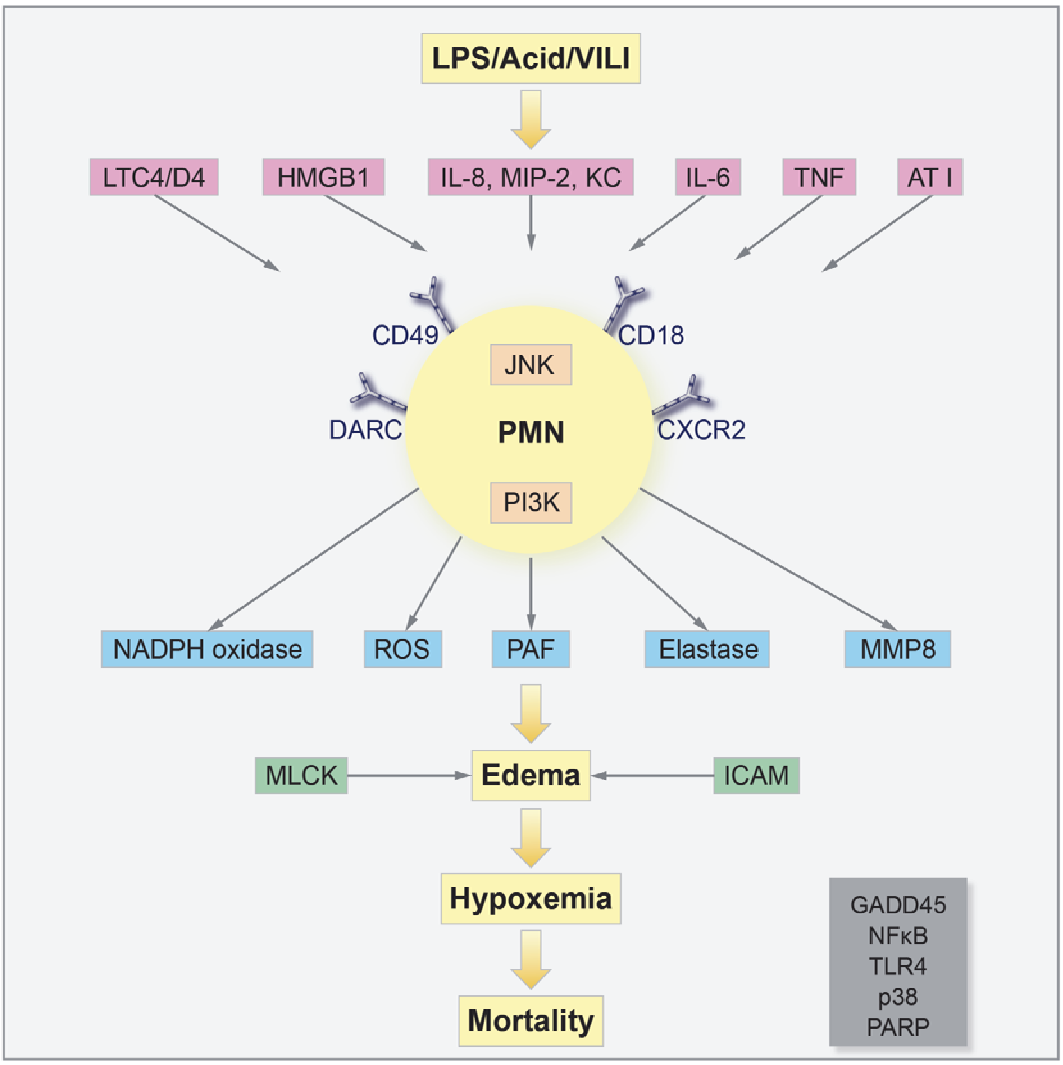

Fig. 1.3: Mechanisms of pulmonary inflammation caused by endotoxin- (LPS), acid- and ventilator-induced lung injury (VILI). Mediators are released in the lung in response to an insult recruit and activate neutrophils, which are provided with specific receptors and kinases that modulate the immune response. Activated neutrophils liberate several effectors, which target the alveolar-capillary barrier and cause oedema formation. Progressive oedema leads to hypoxemia and may have lethal consequences. Mediators are depicted in pink: LTC4/D4: leukotriens C4 and D4; HMBG1: high-mobility group protein B1; IL-8: interleukin-8, MIP-2: macrophage inflammatory protein-2, KC: keratinocyte-derived chemokine; IL-6: interleukin-6; TNF: tumour necrosis factor; AT I: angiotensin II receptor type I. Polymorphonuclear leukocyte (PMN) receptors are dark blue: DARC: Duffy antigen receptor for chemokines; CD49: cluster of differentiation 49; CD18: cluster of differentiation 18; CXCRC2: CXC chemokine receptor 2. Kinases are shown in orange: JNK: c-Jun terminal kinase; PI3K: phosphatidylinositol-3 kinase. Products of PMNs / neutrophils are depicted in light blue: NADPH oxidase; ROS: reactive oxygen species; PAF: platelet activating factor; the protease elastase; MMP8: matrix metalloproteinase-8. Endothelial proteins are green: MLCK: myosin light chain kinase; ICAM: intercellular adhesion molecule. Molecules that are not directly related to neutrophils are listed in the grey box: GADD45: growth arrest and DNA damage; NFκB: nuclear factor kappa-light-chain-enhancer of activated B cells; TLR4: Toll-like receptor 4; the kinase p38; PARP: poly [ADP-ribose] polymerase.

1.6 Experimental intra-pulmonary acute lung injury

Three widely used models of intra-pulmonary ALI are: instillation of bacterial endotoxin (biological insult), instillation of acid (chemical insult) and injurious ventilation (mechanical insult). In Fig. 1.3 common mechanisms of pulmonary inflammation in response to these three stimuli are depicted, illustrating the outcome of a large number of experimental studies reviewed recently [47]. The pathway drawn reflects the hierarchical connection between four main features of ALI: neutrophils, oedema formation, hypoxemia and mortality. In response to the insult, soluble mediators, such as cytokines and chemokines, are liberated. Neutrophils interact with these mediators via surface-bound receptors, sequester in the lung and release effector molecules, e.g. platelet activating factor (PAF), reactive oxygen species (ROS) and elastase. These products damage the alveolar capillary barrier, thereby inducing oedema formation and exacerbating lung injury. As a result, oxygenation is increasingly impaired finally leading to death. Of these common mechanisms, some may represent promising pharmacological targets. In all three models, neutrophils played a central role. Therapies directed against neutrophils directly [48-50], CXCR2 chemokine receptors or their neutrophil-attracting ligands (IL-8, MIP-2, KC) [51-53] indicated beneficial effects on lung injury. Further targets with good prospects were lipid mediators such as leukotrienes (LTC4/D4) and PAF. Inactivation of the leukotriene-producing enzyme 5-lipoxygenase as well as of PAF-receptors were beneficial regarding all aspects of lung injury [54-56]. In comparison, inhibition of angiotensin II receptor (AT I) activation, tumour necrosis factor (TNF), and high-mobility group protein B1 (HMGB1) were found to be only moderately protective [57-59]. Of note, in most studies summarised in Fig. 1.3, mechanisms leading to neutrophil sequestration or oedema formation were in the main focus, rather than oxygenation, physiological dysfunction or mortality, which were mostly ignored [47].

1.7 Acid-induced lung injury

In the following, the model of acid-induced lung injury will be characterised more detailed, because it was employed in the present thesis. The basis for this model is that gastric aspiration, which occurs for instance as complication during anaesthesia, leads to acute pneumonitis [60]. The pulmonary consequences of gastric aspiration are related to the composition of the gastric content on the one hand, which cotains particles and bacteria, and to the acidic pH on the other hand [61]. In one experimental study, the aspiration of 2 mL/kg gastric contents at a pH 5.9 induced the same level of injury as pure acid at pH 1.8 [62], demonstrating that the pH alone is not the only harmful factor.

The severity of acid-induced lung injury depends on the pH and the volume of the instilled acid as well as on time. In most experimental studies, a volume of 1-4 mL/kg acid with a pH between 1 and 2 is instilled into the lung. Regarding the pH, the margin between a lethal pH (< 1.2) and a non-injurious pH (> 2.5) is rather small. In this range, an almost linear dose-response curve between acid pH and lung permeability can be drawn. Changes in acid volume have a certain influence as well, regarding the fact that very small volumes ≤ 0.5 mL/kg of acid pH 1.5 are only minimally injurious compared to volumes > 1mL/kg [63].

Concerning the time course, the injury follows a biphasic pathogensis, with a first peak after about 1 hour and a second peak after 4 hours. The first peak is characterised by an increase in permeability before neutrophils are recruited to the lung and is probably due to a physiochemical reaction to the acid. The later phase is characterised by neutrophil infiltration and an acute inflammatory response [63], suggesting that the physiochemical injury is followed by inflammatory organ damage. In fact, neutrophils were shown to be necessary for the full development of lung injury, whereby in the pathogenesis of the second phase, the production of serine proteases (e.g. elastase) by neutrophils seems to play a more important role than the neutrophil-derived oxygen radicals [50]. The progression of injury was examined by electron microscopy of murine tracheas, where acid at pH 1.5 led to desquamation of the superficial cell layer with complete loss of ciliated and non-ciliated cells between 6 and 48 hours after instillation. Onset of regeneration was observed after 3 days and was completed after 7 days [64].

In conclusion, the advantages of this model include that it is based on a clinically relevant aetiology and reflects important hallmarks of the pathogenesis of ALI in humans. Regarding the technical issues, the model shows a good reproducibility, but the clinical implications of the narrow margin between injurious and non-injurious doses are unclear [46].

1.8 Experimental extra-pulmonary acute lung injury

Models of extra-pulmonary ALI include a variety of indirect insults that are characterised as clinically relevant inducers of ALI such as sepsis, trauma, shock, burn injury or mass transfusion [65]. Common experimental approaches to trigger the onset of sepsis are the intravenous (i.v.) application of endotoxin or bacteria [46,66]. A model that aims to mimic bone trauma is based on i.v. injection of oleic acid [67]. These approaches target the capillary endothelium rather than the alveolar epithelium, as the stimulus is administered via the venous route. Further indirect insults, which resemble known clinical phenomena, are pulmonary and non-pulmonary ischemia-reperfusion or peritonitis induced by cecal ligation

and puncture. The disadvantage of these models is that they require complex surgery [68,69]. All these models of extra-pulmonary ALI have in common that they usually cause milder lung injury than the direct insults. In addition, most of the indirect models are subjected to a higher biological variability, which can affect reproducibility [46].

1.9 The role of tumour necrosis factor (TNF) in the lung

TNF was characterised originally as an anti-tumour agent [70], but it became soon clear that it plays a pivotal role as pro-inflammatory cytokine in host-defence, acute inflammation and apoptosis [71,72]. TNF can be produced by several populations of leukocytes and triggers the production of many other pro-inflammatory cytokines and chemokines [73]. As described above, sepsis models are commonly used to induce extra-pulmonary ALI (chapter 1.8). Interestingly, high levels of TNF were found in response to i.v. endotoxin application [74,75] and application of TNF induced similar metabolic responses as endotoxin in humans [76]. Experimental studies revealed that i.v. administered TNF causes a lethal depression of the systemic circulation, comparable to the cardiovascular collapse in septic shock [77,78]. This observation lead to the hypothesis that septic shock is caused by an overwhelming host defence reaction that is characterised by production of high amounts of pro-inflammatory cytokines, including TNF. A patient trial in 1987 revealed that a fatal outcome of sepsis was correlated with high TNF levels [79]. As a consequence of these findings, anti-inflammatory strategies were suggested to be salutary in sepsis [80]. The benefit of anti-TNF therapy in septic shock was investigated in baboons and later also in mice, which were protected from the lethal effects of endotoxin after pre-treatment with an anti-TNF antibody [81,82]. Based on the success in animal studies, several randomised controlled trials were designed to investigate the effectiveness of anti-TNF therapies, of which some even reached phase III. In these clinical trials either anti-TNF antibodies or soluble receptors were used to inhibit TNF in sepsis patients. In several anti-TNF antibody trials this therapy had a small beneficial effect on mortality [80,83]. In one phase II trial, using an anti-TNF antigen binding fragment, mortality was reduced and the number of ventilator- and intensive care unit (ICU) -free days was increased [84]. Furthermore, high IL-6 levels, which correlated with a fatal outcome, were reduced by anti-TNF antibodies in several studies [84-86]. Of note, treatment with soluble TNF receptors increased mortality in three trials, especially at high doses [80].

TNF plays an important role in the pathogenesis of many pulmonary diseases. Increased TNF levels were found in bronchopulmonary secretions of patients with ARDS [87]. Persistently high levels of the cytokines TNF, IL-6, IL-1 and IL-8 in the BAL of ARDS patients correlated with a poor outcome [88]. In models of intra-pulmonary lung injury, TNF was

relateded to neutrophil-dependent mechanisms that promote oedema formation [89,90], as indicated in Fig. 1.3. Blocking of TNF by antibodies, receptor-knockout and soluble TNF fusion protein, was beneficial in these models [57,91,92]. Only few studies examined the pulmonary effects of i.v. injected TNF. In sheep, infusion of 0.01 mg/kg human recombinant TNF over 30 min resulted in a pathophysiology comparable to endotoxin-induced lung injury [93]. In a study in rats, infusion of 0.1 mg/kg/day human recombinant TNF for 5 days resulted in 20% mortality and an increase in lung weight by 38%, although no effect on microvascular permeability was found [94]. Of note, TNF doses were fairly low in both studies and little is known about the effects of high plasma levels of TNF on the lung *in vivo*.

TNF interacts with two cell-surface receptors, of which p55 is expressed in most tissues and p75 only on cells of the immune system [95]. The receptor p55 appears to promote oedema formation by reducing the expression of subunits of the epithelial sodium channel ENaC, which is responsible for epithelial sodium transport, the driving force for fluid removal [96]. Further, TNF promotes oedema formation by neutrophil-dependent mechanisms that target the vascular endothelium. The interaction of neutrophils with the endothelium via the integrin complex CD11/CD18 and the endothelial intercellular adhesion molecule 1 (ICAM-1) is a prerequisite for neutrophil-related oedema [97]. In experiments with isolated perfused lungs, TNF caused oedema formation only, when neutrophils were also added to the lungs [90]. This mechanism was shown to be PAF dependent [98] and illustrates why PAF alone induces pulmonary oedema in isolated perfused lungs [99], but TNF alone does not. In addition, some mechanisms affect the endothelium directly, as shown in experiments with endothelial cells *in vitro*. These include the generation of ROS from endothelial mitochondria in response to TNF exposure [100], a mechanism that was shown to involve ceramide [101], the structural reorganisation of the endothelial monolayer and the cytostatic effect of TNF on endothelial cells [102].

In contrast to the p55 receptor, p75 seems to have a protective role in the lung [103]. The dual role of TNF in pulmonary oedema can be attributed not only to the two receptors, but also to the structure of TNF. The cytokine is comprised of a receptor-binding domain that is involved in the development of pulmonary oedema and a lectin-like domain, that is distinct from the receptor-binding site and has positive effects on alveolar liquid clearance [73]. The TIP peptide, a synthetic circular 17 amino acid peptide mimicking the lectin-like domain, increases oedema reabsorption by up-regulation of sodium uptake in type II pneumocytes and furthermore protects the alveolar barrier integrity by unknown mechanisms. Several experimental studies indicate a therapeutic use of the TIP peptide in pulmonary oedema [96].

1.10 The role of sphingolipids in the lung

Apart from their structural function in cell membranes, sphingolipids exert an important function as signalling molecules. Sphingolipids are implicated in the pathogenesis of several respiratory diseases including chronic obstructive pulmonary disease (COPD), cystic fibrosis, asthma and ALI [104] Particularly the alveolar-capillary barrier integrity is regulated by sphingolipids, wherein also TNF plays a role. Apparently, one mechanism leading to ENaC inhibition depends on the activation of ceramide by TNF [105]. By binding to p55, TNF activates the neutral and the acid sphingomyelinase, enzymes that hydrolyse the membrane protein sphingomyelin into ceramide [106,107], which forms lipid microdomains. Ceramide is a signalling molecule that acts on several protein kinases, e.g. the protein kinase C (PKC) [108], which regulates ENaC activity [109]. A further TNF-induced pathway includes activation of the endothelial nitric oxide synthase (eNOS) via the neutral sphingomyelinase and the kinases PI3K and Akt [110,111]. This pathway links ceramide production to vasodilatation via NO liberation [112]. Of note, eNOS also plays a crucial role in regulation of pulmonary vascular permeability, as both too little and too much NO can cause pulmonary oedema [99].

The acid sphingomyelinase (ASM) appears in a lysosomal and a secretory form [113]. The secretory form, which hydrolyses sphingomyelin in the cell membrane, has been associated with the pathogenesis of sepsis and ALI. Patients with sepsis exhibited increased levels of ASM activity, which correlated with mortality [114]. One proposed mechanism involving the lysosomal ASM implies that caveolin-1 is recruited to the ceramide-rich domains (caveolae) formed by ASM, through which endothelial NO is decreased and endothelial Ca^{2+} is increased, promoting pulmonary oedema [99]. The physiologic importance of ASM is further demonstrated by the consequences of ASM-deficiency, which is responsible for a recessively inherited lysosomal lipid storage disorder called Niemann-Pick disease (NPD) type A and B. Type A NPD is a neurovisceral form leading to early death in childhood, whereas type B NPD is a non-neuropathic, visceral form with a longer life expectancy [115]. ASM-deficiency is caused by mutations in the *SMPD1* gene. The pathophysiology of NPD is characterised by the accumulation of sphingomyelin and other lipids, causing cell abnormalities which lead to visceral organ complications, including progressive pulmonary dysfunction with repetitive respiratory infections [116]. Experimentally, ASM-deficient ($ASM^{-/-}$) mice were shown to be a valuable tool for the investigation of the important role of the ASM in sepsis and ALI. In endotoxemia and in models of intra-pulmonary ALI, pharmacological blocking of ASM and ASM-deficiency protected from vascular barrier disruption [117-119] and reduced mortality due to septic shock [114,117]. These findings indicate that ASM may be another interesting therapeutic target for the treatment of ALI [104], particularly in conjunction with sepsis.

Finally, the generation of ceramide by ASM in the caveolae was also shown to be involved in apoptosis [120]. Interestingly, ceramide activates not only the well-known caspase-dependent pathway, but also a caspase-independent mechanism. Whereas caspase-dependent extrinsic apoptosis is induced by ligands that bind to so called death receptors, e.g. TNF and p55, the caspase-independent pathway is proposed to be predominantly stress-induced, e.g. by UV radiation [121-123]. This was also shown *in vivo* in $ASM^{-/-}$ mice, which were protected from radiation-induced ceramide-generation and apoptosis [124]. Nevertheless, formation of ceramide by ASM was also shown in response to TNF, resulting in activation of the transcription factor NFκB, one important regulator of apoptosis [107]. Furthermore, enzymatic degradation of ceramide and inhibition of ASM were shown to increase cell survival in TNF-treated cells [125], indicating a pivotal role of ASM in TNF-induced cell death.

1.11 Mechanical ventilation in mice

MV of mice is increasingly used in biomedical research. While the mechanisms of VILI have been explored intensively [37], experimental conditions required to keep physiological parameters stable in mice during ventilation for several hours are not well defined. Major reasons for this are the focus on the mechanisms of VILI and the lack of comprehensive monitoring of pulmonary and cardiovascular key parameters in most studies.

Monitoring of key physiological parameters is standard during MV of humans and should be aimed also in experimental research. These key parameters need to reflect both the pulmonary (e.g. V_T, airway pressure) and the cardiovascular (e.g. heart rate, blood pressure) consequences of MV as well as oxygenation and acid-base status. Although MV may affect all these parameters, these entities have rarely been assessed together in the same study in mice. Table 1.2 summarises ventilation studies, in which either lung impedance was measured or ventilation was performed for at least four hours. The table reveals that many studies that have focused on lung mechanics examined only a relatively short period of ventilation [126-129] and only one study fulfilled both inclusion criteria [48]. Interestingly, studies in which mice were ventilated for more than three hours often provided cardiovascular parameters, but neglected the examination of lung functions [130-133]. Some studies even completely lacked physiological parameters, although in several cases the authors referred to preliminary experiments that were not included in the published data [134-137]. Thus, without comprehensive information on physiological parameters, it seems difficult to properly assess, standardise and compare the various ventilation strategies.

Table 1.2: Comparison of mouse ventilation models

Reference	Experimental design				Monitored parameters			
	Ventilation	V_T [ml/kg]	PEEP [cmH_2O]	RM	Lung functions	BGA	BP / cardiac activity	SpO_2
[126]	30min	7 / 10	2 / 0	*	+	-	- / P	+
[128]	60min	8	6 / 3	**	+	-	-	-
[129]	140min	30 / 10	2 / 0	2x / min	+	+	- / ECG	-
[127]	150min	8	6 / 2	1x / 5min or 1x / 75min	+	-	- / P	+
[48]	4h	25 / 7	-	-	+	-	- / ECG	-
[134]	4h	20 / 6	2	-	-	-	-	-
[137]	4h	30	-	-	-	-	-	-
[135]	4h	20 / 7	0-2	-	-	-	-	-
[132]	4h	8	4	-	-	+	+ / -	-
[136]	5h	30 / 6	-	-	-	-	- / -	-
[133]	5h	15 / 7.5	2	-	-	+	+ / +	-
[53]	6h	24	-	-	-	-	+ / P	-
[130]	6h	12	6	*	-	+	+ / P	+
[138]	4h / 8h	20 / 10	2	1x / h	-	-	+ / -	-
[131]	8h	12	2	-	-	+	+ / -	-
Present study	6h	16 / 8	2	1x / 5min or 1x / 60min or no RM	+	+	+ / ECG, P	+

The table lists those ventilation studies that analysed lung functions by measurement of lung impedance and studies in which mice were ventilated for at least four hours. V_T: tidal volume, PEEP: positive end-expiratory pressure, RM: recruitment manoeuvre, BGA: blood gas analysis, BP: blood pressure, P: pulse, ECG: electrocardiogram, SpO_2: pulse oximetry. * One RM at the beginning of ventilation. ** Two RM at the beginning of ventilation.

Studies on the mechanisms of VILI have identified several beneficial ventilation strategies, among them low V_T ventilation and application of recruitment manoeuvres (RM) as well as high PEEP. Although RM have a sound physiological basis, it remains unclear how they should be applied [139]. In principal, RM may be used to reopen atelectatic lung areas in injured lungs or to prevent atelectasis in healthy lungs. The latter application requires lower recruitment pressures and hence can be applied more frequently. Without RM, pulmonary compliance is likely to decrease as shown already many years ago in anaesthetised dogs both during spontaneous breathing and during MV [140]. In addition, regular short RM have proved to be useful in models of isolated rat and mouse lungs [141,142]. In mechanically ventilated mice the usefulness of RM with the specific aim to keep pulmonary compliance and other lung functions constant has been explored only sporadically. Previous RM studies in healthy mice have focused on short periods of ventilation and potential lung injury, but did not compare ventilation with and without RM over several hours [127,129]. Further, the effect

of RM on blood pressure in mice is not well defined, although increased intrathoracic pressure might decrease cardiac output [143]. The beneficial effects of PEEP have been demonstrated in several animal studies [144-146]. PEEP helps to prevent repetitive alveolar collapse and preserves surfactant function [37,147]. While it is widely accepted that adequate PEEP together with low V_T is a protective ventilation strategy, the effects of recurrent RM in this setting are unknown.

1.12 Aim of the study

ALI is a life threatening condition, for which to date only symptomatic therapy, such as MV, is available. Animal models are indispensable to elucidate the pathomechanisms of ALI and to develop therapeutic approaches. MV of mice is increasingly used in experimental studies on lung injury, but conditions for ventilation of mice resulting in stable physiological conditions are poorly defined. In most studies, monitoring of clinically relevant physiological parameters is omitted and validation of pulmonary injury is based on inflammatory parameters only. Mouse models of ALI giving comprehensive information on the mechanisms of lung injury under consideration of the physiological consequences are largely lacking.

Thus, the first objective is to establish an 'ICU–like' setup that allows ventilation of mice under permanent monitoring of respiratory and cardiovascular parameters and to define conditions under which these parameters are stable over several hours. Of particular interest is the impact of recurrent RM at different V_T and PEEP levels. While it is widely accepted that adequate PEEP together with low V_T is a protective ventilation strategy, the effects of recurrent RM in this setting are unknown. Furthermore, pulmonary inflammation should be assessed by quantifying microvascular permeability, neutrophil recruitment to the lung, pro-inflammatory mediators and a lung injury score, in order to identify the most protective ventilation strategy. Altogether, the setup should include all relevant criteria for the diagnosis of experimental ALI, so that it can be employed as basis for lung injury models.

This mouse ICU should then be used to examine the unexplored effects of high systemic TNF levels on the lung. TNF plays a major role as mediator of sepsis and ALI and high systemic levels might even cause lung injury. A setup that provides life supportive measures ought to be suitable to avoid lethal the cardiovascular depression, a TNF-related side effect known from experimental and clinical trials, and allow investigation of the impact of TNF on the lung. A further aim is to define the role of ASM and caspases in the TNF-induced pathophysiology.

In addition, intra-pulmonary lung injury is planned to be induced by acid-instillation, a model that resembles crucial features of ALI in humans. Based on the experimental criteria of ALI, the therapeutic effectiveness of the glucocorticoid dexamethasone should be tested. The usefulness of steroids in ALI is still under debate, since the outcome in clinical studies is inconclusive and experimental studies lack information on the physiological consequences. This part of the study aims to provide further insight into the complex role of steroids in ALI by taking the severity of lung injury into account. A final objective is to analyse the injury models for possible pathophysiological patterns in ALI.

2 Material and methods

2.1 Mice

Ventilation and acid-instillation experiments were performed with female C57BL/6 N mice (Charles River, Sulzfeld, Germany) aged 8 to 12 weeks, weighing 20 to 25 grams. The effects of TNF were investigated in female and male C57Bl/6x129/SvEv wild-type (wt) and acid sphingomyelinase-deficient ($ASM^{-/-}$) mice aged 8 to 10 weeks, weighing 25 to 30 grams, kindly provided by Prof. Dieter Adam (Institute of Immunology, Christian Albrechts University, Kiel, Germany). The experimental protocols were in accordance with the German animal protection law and approved by regional governmental authorities (Landesamt für Natur, Umwelt und Verbraucherschutz NRW, permission numbers: AZ 8.87-50.10.35.085 and AZ 8.87-50.10.37.09.287).

2.2 Drugs, chemicals, kits, equipment and software

2.2.1 Drugs and infusions used for mice

Bovine serum albumin	Serva electrophoresis, Heidelberg, Germany
Braunol 7.5%	B. Braun Melsungen AG, Melsungen, Germany
Dexamethasone dihydrogen phosphate	Merck Pharma GmbH, Darmstadt, Germany
Fentanyl	Janssen-CILAG GmbH, Neuss, Germany
Heparin sodium salt	Sigma-Aldrich, Dorset, UK
Human serum albumin	Baxter, Unterschleißheim, Germany
Hypochloric acid solution	Merck Pharma GmbH, Darmstadt, Germany
Ketamine	CEVA, Düsseldorf, Germany
Isoflurane	Abbott GmbH & Co. KG, Wiesbaden, Germany
Isotonic sodium chloride 0.9%	B. Braun Melsungen AG, Melsungen, Germany
Quinine hydrochloride dihydrate	Sigma-Aldrich, Steinheim, Germany
Ringer's solution	B. Braun Melsungen AG, Melsungen, Germany
Sodium hydrogen carbonate 8.4%	Fresenius Kabi GmbH, Bad Homburg, Germany
Sodium pentobarbital	Merial GmbH, Hallbergmoos, Germany
TNF (murine)	Peprotech, Rocky Hill, CT, USA
Xylazine	CEVA, Düsseldorf, Germany
Xylocain 1%	AstraZeneca GmbH, Wedel, Germany
zVAD-fMK	Bachem AG, Bubendorf, Switzerland

2.2.2 Chemicals

Chloroform	AppliChem, Darmstadt, Germany
Diff-Quick staining	Medion Diagnostics, Düdingen, CH
Eosin	Merck, Darmstadt, Germany
Ethanol 70%	Otto Fischar GmbH, Saarbrücken, Germany
H_2O_2 30%	Merck, Darmstadt, Germany
Methanol	AppliChem, Darmstadt, Germany
Mayers Hämalaun	Merck, Darmstadt, Germany
Roti Histofix 4%	Carl Roth GmbH, Karlsruhe, Germany
Sphingomyelin	Sigma-Aldrich, Steinheim, Germany
TMB substrate reagent	R+D Systems, Abingdon, UK
Tween20	Serva electrophoresis, Heidelberg, Germany
Vitro-Clud mounting medium	Langenbrinck, Emmendingen, Germany

2.2.3 Commercial kits

BSA ELISA	Bethyl Laboratories, Montgomery, USA
Cell death detection ELISA	Roche Applied Science, Mannheim, Germany
DC Protein assay	Bio-Rad, Hercules, CA, USA
HSA ELISA	Assaypro, St. Charles, MO, USA
IL-6 ELISA	R+D Systems, Abingdon, UK
KC ELISA	R+D Systems, Abingdon, UK
MIP-2 ELISA	R+D Systems, Abingdon, UK
NO quantification assay	R+D Systems, Abingdon, UK
Procalcitonin ELISA	USCN Life Science, Wuhan, China
TNF ELISA	R+D Systems, Abingdon; UK

2.2.4 Buffers

Carbonate/bicarbonate buffer (pH 9.4)	2 mL 0.1 M Na_2CO_3, 8 mL 0.1 M $NaHCO_3$
Phosphate buffered saline (PBS) 10x	160 mM Na_2HPO_4, 40 mM NaH_2PO_4, 1.5 M NaCl
Potassium phosphate buffer 0.05 M	0.05 M KH_2PO_4, 0.1 M K_2HPO_4 (pH = 6)
Wash buffer for ELISA	0.05% Tween20 in PBS (pH = 7.2-7.4)

2.2.5 Equipment

Blood gas analyser ABL700	Radiometer, Kopenhagen, Denmark
Blood pressure transducer APT300	Harvard Apparatus, March-Hugstetten, Germany
Bio amplifier for ECG and lead wires	ADInstruments, Spechbach, Germany
Bridge amplifier for blood pressure	ADInstruments, Spechbach, Germany
Cold-light source	Streppel, Wermelskirchen-Tente, Germany
Cytospin centrifuge and equipment	Hereaus, Hanau, Germany
ELISA Reader GENios	Tecan, Männedorf, Switzerland
FlexiVent ventilator with module 1	SCIREQ, Montreal, Canada
Homeothermic blanket system	Harvard Apparatus, March-Hugstetten, Germany
Injection needles (Microlance)	Beckton Dickinson, Franklin Lakes, NJ, USA
Mass flow controller 0254	Brooks Instrument, Hatfield, PA, USA
Micro-Fine+Demi U-100 insulin syringes	Beckton Dickinson, Franklin Lakes, NJ, USA
Microscope Axio Lab	Zeiss, Jena, Germany
Microsprayer	Penn-Century Inc., Wyndmoor, PA, USA
MouseOx pulse oximeter	Starr Life Sciences Corp., Oakmont, PA, USA
Oximeter pod with SpO_2 tail wrap	ADInstruments, Spechbach, Germany
PE-10 tubing	Beckton Dickinson, Franklin Lakes, NJ, USA
PowerLab 8/30 data acquisition system	ADInstruments, Spechbach, Germany
Precision Infusion pump 11 Plus	Harvard Apparatus, March-Hugstetten, Germany
Pulse oximeter	ADInstruments, Spechbach, Germany
Surgical micro instruments	Fine science tools, North Vancouver, BC, Canada
Sutures	Pearsall's, Taunton, UK
Thermal mass flow meters	Brooks Instrument, Hatfield, PA, USA
Tygon tubing (0.25 mm inner diameter)	Novodirect, Kehl am Rhein, Germany
Vaporizer + Filter for Isoflurane	Harvard Apparatus, March-Hugstetten, Germany

2.2.6 Software

AxioVision	Zeiss,Jena, Germany
FlexiVent 5.2	SCIREQ, Montreal, Canada
GraphPad Prism 5.0	GraphPad Prism, La Jolla, CA, USA
JMP 7.0	SAS Institute, Cary, NC, USA
LabChart 7.0.2	ADInstruments, Spechbach, Germany
SAS 9.1	SAS Institute, Cary, NC, USA

2.3 Anaesthesia

2.3.1 Ketamine and xylazine

In the first experiments, the sedative and analgesic drug ketamine [120 mg/kg], which binds amongst others to the glutamate-NMDA-receptor-complex, together with the α-agonist xylazine [25 mg/kg], a combination commonly used in rodents, was used for anaesthesia. After few experiments only, this combination was found to be inappropriate. These drugs do not suppress the CO_2-induced breathing reflex so that hypercapnic mice breathe spontaneously during ventilation. Hypercapnia can be caused by extreme ventilation settings or impaired gas exchange so that this condition appears commonly in models of acute lung injury. Since measurement of lung functions with the flexiVent ventilator, which was used in this study, requires complete oppression of spontaneous breathing, anaesthesia allowing spontaneous breathing was unsuitable for the present study. A further disadvantage was that xylazin induced severe bradycardia leading to lethal circulatory failure after about four hours. This limited the duration of the experiments, which were planned for at least six hours, strongly. Bradycardia could have been antagonised by the vagolytic drug atropine, which was considered as unsuitable because of its versatile pharmacological effects, which could have influenced the outcome of the lung injury.

2.3.2 Isoflurane

Next, the volatile anaesthetic isoflurane, which was given in concentrations of 1-3% with a vaporizer via the tracheal line after induction of anaesthesia with ketamine and xylazine, was tested. Isoflurane was chosen because it is routinely used for anaesthesia in patients and it was one aim to establish a setup that resembles the clinical situation as close as possible. This drug turned out to be inappropriate for experimental usage in the present setup. Again spontaneous breathing impaired the measurement of lung functions. Moreover, it seemed very likely that inhaled isoflurane, which has anti-inflammatory properties, could have influenced the outcome of the lung injury models. Therefore it was necessary to find other more appropriate drugs for long-term anaesthesia.

2.3.3 Pentobarbital sodium and fentanyl

Anaesthesia with the barbiturate pentobarbital sodium for sedation and the opioid fentanyl as analgetic component proved to be adequate for deep sedation and oppression of the breathing reflex, which were required for measurement of lung mechanics. A further advantage was the inhibition of CO_2 chemoreceptors in the brain by pentobarbital sodium, which prevented the breathing reflex also in hypercapnic animals. Under barbiturates the breathing reflex is solely activated by hypoxia. Therefore it was important to apply not more

than maximally 30% of oxygen to mice that were anaesthetized, but not yet connected to the ventilator. The additional oxygen was delivered by a gas mixing device and was applied to the mouse via a small mask that was placed over the snout. Anaesthesia was initiated with an intra-peritoneal injection of pentobarbital sodium [75 mg/kg] and fentanyl [40 µg/kg]. Sedated mice were placed in supine position and 50 µL of 1% Xylazin was injected subcutaneously above the larynx for local anaesthesia. This reduced the application rate of pentobarbital sodium. Anaesthesia was maintained with pentobarbital sodium [20 mg/kg] via an intra-peritoneal catheter, made of a 30 gauge needle and a thin Tygon tubing, every 30 to 60 minutes. The fractionated administration of the barbiturate resulted in stable cardiovascular parameters. The disadvantage of pentobarbital is the narrow therapeutic index, which comprises a risk of lethal overdosing. A further advantage is that pentobarbital and fentanyl do not interfere with inflammatory pathways.

2.4 Tracheotomy

After verifying sufficient sedation by checking the paw withdrawal reflex, the fur on the throat of the mouse was disinfected with an ethanol-free iodide solution and opened with a longitudinal cut above the trachea. The left and right *musculi sternocleidomastoidei* were pulled apart to expose the trachea. The muscule strand surrounding the trachea (*musculus sternohyoidus*) was cut open and a suture was pulled around the trachea to form a loose ligature. The trachea was opened by a small cut through which a 20-gauge cannula was inserted and fixed by tightening the ligature. The cannula was coupled with a short piece of plastic tubing that served as adaptor for connection to the ventilator. The length of this adaptor was varied to increase dead space, if necessary.

2.5 Mechanical ventilation and measurement of lung functions

After tracheotomy, mice were ventilated with the flexiVent ventilator, a computer controlled piston-stroke ventilator that facilitates the measurement of lung mechanics by the low frequency FOT. The ventilator operates volume controlled and is equipped with a piston that moves in a closed glass cylinder, and two magnetically controlled valves (Fig. 2.1). The inspiratory valve was connected to the gas mixing device and opened during the inspiration period. A Y-Piece connected the tracheal cannula with the inspiratory valve and the expiratory valve via inflexible tubing. The expiration valve opened after closure of the inspiration valve to allow the release of the inhaled gas. A PEEP trap, in form of a simple water column which could be varied as necessary, was attached to the expiratory valve. The tubing connecting the Y-piece with the expiratory valve was interrupted by a pressure transducer (P1). A second pressure transducer (P2) was located behind the expiratory valve.

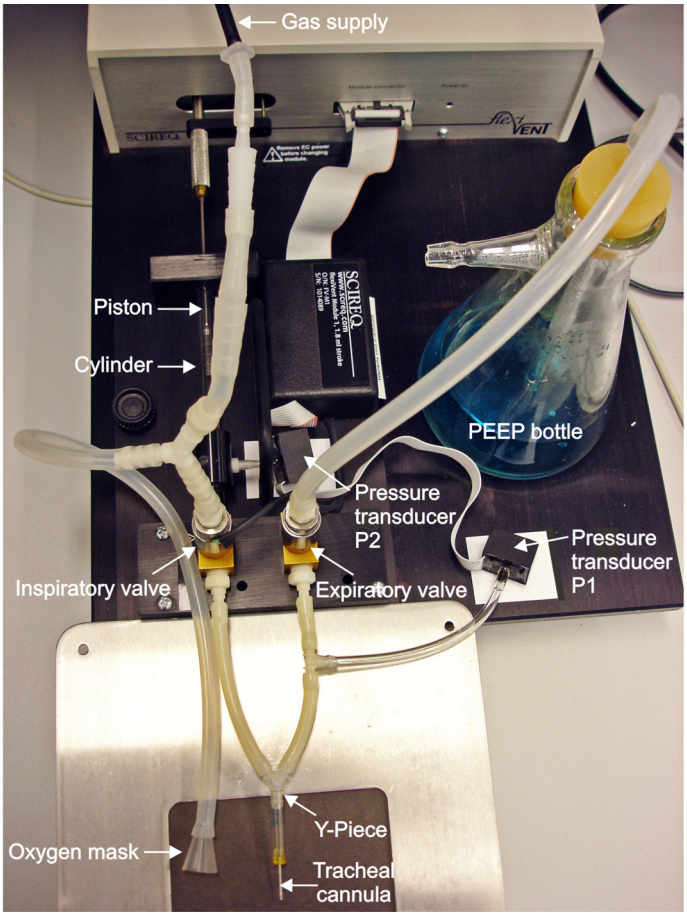

Fig. 2.1: Ventilation setup. Ventilation was performed with a computer-controlled piston stroke ventilator. Mice were connected to the ventilator with a tracheal cannula attached to a Y-piece, which facilitated the connection to the inspiratory and the expiratory valve. The gas supply was coupled to the inspiratory valve with a tubing that carried one open end, used as oxygen mask, for overpressure relief. A PEEP trap was attached to the expiratory valve. The ventilator was equipped with two pressure transducers (P1 and P2), allowing flow measurement. P1 was located at the cylinder, in which the piston moved, and P2 in the expiration branch.

The flexiVent measures the volume displaced by the piston and the pressure in the cylinder from which the mechanical load presented by the lungs of the mouse is calculated. Calibration of the system prior to each experiment allowed subtracting the load of the ventilator and the tubing from the load of the lungs facilitating accurate calculation of lung mechanics. The measurement of lung mechanics with the flexiVent is based on the FOT, which interrupts the ventilation mode and induces a low frequency oscillatory waveform to the respiratory system. Two different types of oscillatory measurements were performed with the flexiVent: firstly, a perturbation that included one single-frequency sinusoidal waveform, from which the dynamic resistance (R) and compliance (C) were calculated according to the single compartment model; secondly, a multi-frequency oscillation waveform for measurement of the input impedance at different frequencies. Fitting the constant phase model to the impedance allowed differentiating between the mechanics of the central airways and the periphery of the lung. The resulting parameters were: airway resistance (R_{aw}), tissue elastance (H) and tissue damping (G). Ventilation settings are described in chapter 2.7.

2.6 Monitoring of physiological parameters

In order to monitor the general health condition of the mice, several physiological parameters were measured during ventilation. Fig. 2.2 shows an overview of a mouse connected to the ventilator and several measuring instruments, which are explained in detail below.

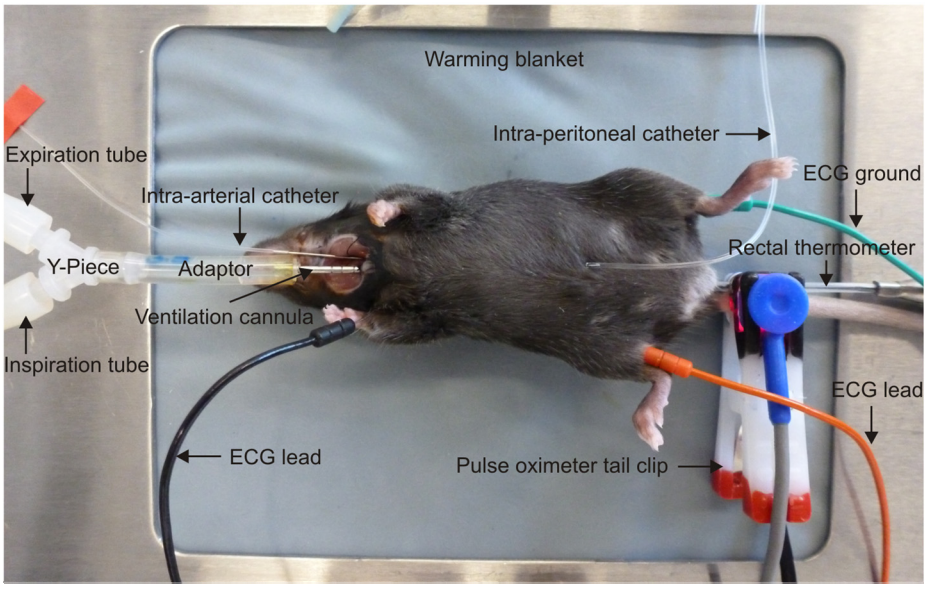

Fig. 2.2: Overview: mouse during physiological monitoring. The mouse was positioned on a body-temperature controlled heating blanket. Body temperature was measured with a rectal probe. A clip with a photosensor for pulse oximetry was attached to the tail. ECG leads were inserted with thin needles subcutaneously at the paws. A catheter was placed intra-peritoneally for maintenance of anaesthesia. A further catheter was inserted into the carotid artery for blood pressure measurement and fluid supply. The mouse was ventilated via an intra-tracheal cannula to which an exchangeable adaptor was coupled, with which dead space was varied.

2.6.1 Body temperature

Measurement and regulation of body temperature was started immediately after sedation by using a homeothermic blanket system in order to avoid hypothermia. The system comprises a heated blanket, on which the mouse was placed, a rectal thermometer, to determine the temperature of the mouse, and a temperature control system on which the set-point value for the body temperature was adjusted to 37°C. The control system turns on the heating of the blanket whenever the measured body temperature is below the set-point. In cases of hypothermia below 36°C the mouse was additionally warmed by an infrared light to achieve a quicker stabilisation of the body temperature.

2.6.2 Pulse oximetry

Oxygen saturation was measured with the MouseOx pulse oximeter. The measurement was performed with a clip placed on the upper end of the tail. The clip comprises a red and an infrared light and as well as a photo sensor. The absorption of light by haemoglobin changes upon binding of oxygen, so that the oxygenation level is reflected by the absorption of light. In arteries, the light absorption measured by the oximeter oscillates with the cardiac pulse. Thereby, not only oxygenation, but also the heart rate can be determined by this device. The MouseOx is designed to detect the high-frequency pulse in mice, which is the precondition for a reliable measurement. Measurement of oxygen saturation with an oximeter pod designed for subjects (ADInstruments, Spechbach,Germany) with a slower pulse failed. Oxygenation was monitored throughout the ventilation experiments.

2.6.3 Electrocardiogram and heart frequency

Electrocardiogram (ECG) was derived from two thin needles, which were used as leads, in the paws of the mouse. A third needle was used as ground wire. The needles were connected to an bio amplifier and the Powerlab data acquisition system, which was used to monitor and record the cardiovascular parameters. Heart rate was calculated from the ECG by the LabChart software, which runs the Powerlab system. ECG and heart rate were used to evaluate the depth of anaesthesia.

2.6.4 Invasive blood pressure measurement

For the invasive blood pressure measurement, a catheter was built by connecting one end of a 15 cm long polyethylene-10 tubing to the blunt end of a dismantled 27 gauge injection needle and the other end to the sharp side of a complete 27 gauge injection cannula. The needle shield of the cannula was coupled on a three-way valve, which was also connected to an infusion pump and a pressure transducer (APT300). The whole system was filled with

either 0.9% NaCl, in the ventilation and TNF model, or Ringer's buffer, in the acid model. The pressure transducer was connected to a bridge amplifier, which was part of the Powerlab data acquisition system. About 1 cm of the common carotid artery was exposed below the bifurcation into internal and external carotid artery by carefully dissecting the overlying and surrounding connective tissue. A thin suture (USP 7-0) was passed under the artery and a ligature was placed directly below the bifurcation (Fig. 2.3A). A vascular micro clamp was positioned 1 cm proximally from the ligature to occlude the vessel temporarily (Fig. 2.3B). A second thread was placed around the artery. Then an incision was made with micro scissors through which the catheter was inserted before it was fixated with the second thread (Fig. 2.3C). The micro clamp was removed and the infusion pump was started at a rate of 200 µL/h. The infusion kept the catheter free of blood and supplied the animal with fluid. Mean arterial pressure was measured every 10 minutes by closing the three-way valve in direction of the infusion by which the valve directed to the pressure transducer was opened.

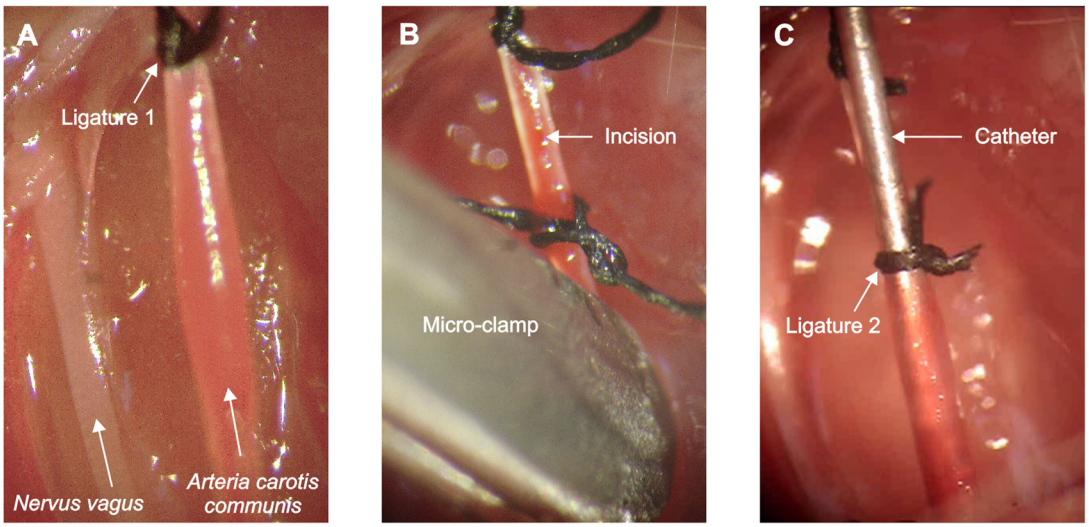

Fig. 2.3: Insertion of the intra-arterial catheter. A. The right carotid artery was exposed and ligature 1 was positioned in cranial direction. **B.** A vascular clamp occluded the blood flow temporarily, while a small incision was made. **C.** The catheter was inserted and fixated with a ligature 2.

2.6.5 Injection of albumin for determination of microvascular permeability

Either 1 mg bovine serum albumin (BSA) or human serum albumin (HSA) was injected i.v. during ventilation in all mice. In the ventilation experiments, mice received BSA in 100 µL NaCl 90 min prior to exsanguination. In the TNF experiments, BSA was injected in 140 µL volume 300 min before the end of the experiment, either together with zVAD-fmk or alone. A later injection with additional fluid would have manipulated the experimental design in this model. In the acid study, BSA was replaced by HSA, which was injected again 90 min before exsanguination. Albumin levels were quantified using commercially available ELISA kits. The albumin influx was calculated as follows: $albumin_{BAL}$ / $albumin_{Serum}$ x 1000.

2.6.6 Exsanguination and blood gas analysis

After ventilation, mice were sacrificed by exsanguination via the carotid artery by removing the arterial catheter. 55 µL of blood were collected immediately, before the death of the experimental animal, with a heparinised capillary for analysis of pO_2, pCO_2, pH, HCO_3^- and standard base excess (SBE) in a blood gas analyzer. This measurement was essential for evaluation of the quality of gas exchange in the ventilated mice. Blood gas analysis from anaesthetized control mice was not representative due to reduced breathing activity and was therefore omitted. The remaining blood, about 1 mL in most cases, was collected in a heparinised tube. The blood samples were centrifuged for 10 min at 3500 rpm to separate the blood cells from the plasma, which was collected and snap frozen for quantification of cytokines, albumin and other mediators, depending on the model.

2.7 Mouse models

2.7.1 The ventilation model

For the ventilation model, mice were anaesthetised as described in chapter 2.3 and then ventilated for six hours either with low tidal volume ($lowV_T$) of 8 mL/kg and a frequency (f) of 180 min^{-1} or high tidal volume ($highV_T$) of 16 mL/kg and f = 90 min^{-1}, so that both groups received the same minute volume. The $highV_T$ group was ventilated with 3% CO_2 to maintain normocapnia without further decreasing ventilation frequency or increasing dead space. The fraction of inspired oxygen (FiO_2) was 0.5 in this model. One RM with 30 cmH_2O pressure and six seconds duration was performed after onset of ventilation to open airspaces and standardise lung volume. Resistance, compliance and impedance of the lung were measured during single and multi-frequency oscillation waveforms every ten minutes. In this model, two independent series of experiments were performed and analysed separately. The first series of experiments was performed with a PEEP of 2 cmH_2O. Repeated RM of 1 s duration and 30 cmH_2O peak pressure were applied every five minutes (RM5) in one $lowV_T$ ($lowV_T$RM5) and one $highV_T$ group ($highV_T$RM5) or every 60 minutes (RM60) in one $lowV_T$ group ($lowV_T$RM60). One $lowV_T$ and one $highV_T$ group were ventilated without RM ($lowV_T$noRM and $highV_T$noRM). One group of anaesthetised unventilated mice served as control. In order to investigate the effects of a higher PEEP, a second series of experiments was performed later, in which mice were ventilated with a low V_T and a PEEP of 6 cmH_2O. With these settings, RM were performed every five minutes (PEEP6_RM5), every 60 minutes (PEEP6_RM60) or not at all (PEEP6_noRM). An overview over the experimental groups is given in Table 2.1 below.

Table 2.1: Experimental groups in the ventilation model

	Low PEEP (2 cmH_2O)					Moderate PEEP (6 cmH_2O)		
	$LowV_T$ RM5	**$HighV_T$ RM5**	**$LowV_T$ noRM**	**$HighV_T$ noRM**	**$LowV_T$ RM60**	**PEEP6 _RM5**	**PEEP6 _noRM**	**PEEP6 _RM60**
V_T [ml/kg]	8	16	8	16	8	8	8	8
f [min^{-1}]	180	90	180	90	180	180	180	180
PEEP [cmH_2O]	2	2	2	2	2	6	6	6
RM/h	12	12	-	-	1	12	-	1
FiO_2	0.5	0.5	0.5	0.5	0.5	0.5	0.5	0.5
CO_2 [%]	0	3	0	3	0	0	0	0

V_T: tidal volume, f: breathing frequency, PEEP: positive end-expiratory pressure, RM: recruitment manoeuvre of 1 s and 30 cmH_2O pressure, FiO_2: fraction of inspired oxygen, lowV_T: low tidal volume, highV_T: high tidal volume, RM5: one recruitment manoeuvre every five minutes, noRM: no recruitment manoeuvres, RM60: one recruitment manoeuvre every 60 minutes, PEEP6: PEEP = 6 cmH_2O.

2.7.2 The TNF model

All mice were ventilated for 30 min to gain stable baseline lung functions. $ASM^{-/-}$ and wt mice received 50 µg of murine TNF in 100 µL of 0.9% NaCl i.v. 45 min after onset of ventilation. In addition, half of the animals were treated with two i.v. dosages of the general caspase inhibitor Carbobenzoxy-valyl-alanyl-aspartyl-[O-methyl]-fluoromethylketone (zVAD-fmk). 250 µg zVAD-fmk were given in 100 µL of 0.9% NaCl after 30 min of ventilation and 100 µg zVAD-fmk together with 1 mg BSA (for analysis of microvascular permeability) in 140 µL of 0.9% NaCl after 60 min of ventilation. Mice that were not treated with TNF and/or zVAD-fmk received comparable volumes of NaCl. All i.v. injections were placed in the tail veins. Mice were ventilated for further six hours after injection of TNF, resulting in 405 min total ventilation time. The experimental design is depicted in Fig. 2.4 below.

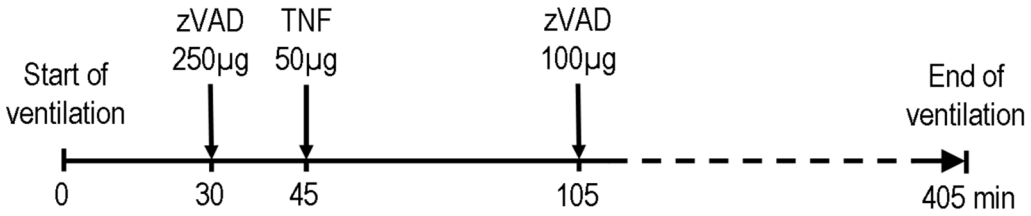

Fig. 2.4: Experimental design in the TNF model. TNF was injected 45 min after onset of ventilation to ensure stable physiological base line values. Mice were then ventilated for further 6 h. Half of the TNF-treated mice received one dose of the caspase inhibitor zVAD-fmk 15 min before and one 60 min after TNF treatment. All injections were administered into the tail vain.

Experimental groups, as listed in Table 2.2, were named as follows: mice treated with TNF, but not zVAD-fmk: $ASM^{-/-}$-zVAD and wt-zVAD; mice treated with both, TNF and zVAD-fmk: $ASM^{-/-}$+zVAD and wt+zVAD; one group of $ASM^{-/-}$ mice was ventilated without being treated

with TNF or zVAD-fmk to investigate only the influence of the ASM-deficiency on the ventilated lung: $ASM^{-/-}$-sham. In all groups in this model, ventilation settings were as follows: V_T = 8 mL/kg, f = 180 min^{-1}, one RM every 5 min, PEEP = 2 cmH_2O and FiO_2 = 0.3.

Table 2.2: Experimental groups in the TNF model

	wt-zVAD	wt+zVAD	$ASM^{-/-}$-zVAD	$ASM^{-/-}$+zVAD	$ASM^{-/-}$-sham
ASM expression	+	+	-	-	-
TNF injection	+	+	+	+	-
zVAD-fmk injection	-	+	-	+	-
Ventilation	405 min	405 min	405 min	405 min	405 min

ASM: acid sphingomyelinase, TNF: Tumor necrosis factor, zVAD-fmk: Carbobenzoxy-valyl-alanyl-aspartyl-[O-methyl]- fluoromethylketone, Ventilation: mechanical ventilation with 8 mL/kg tidal volume, f = 180 min^{-1}, one RM every 5 min, FiO_2 = 0.3 and PEEP = 2 cmH_2O.

2.7.3 The acid model

For acid instillation, 0.3% NaCl was titrated with HCl to a pH of either 1.5 or 1.8. 0.3% NaCl was used to gain a higher osmolarity, which is better comparable to the osmolarity of the gastric content than water. Mice were anaesthetised and tracheotomised as described above. After tracheotomy, mice were brought in an upright position. For the intratracheal (i.t.) instillation of acid, a commercially available device, the microspayer, was used. The microsprayer is a high pressure syringe connected to a very thin cannula that is suitable for intubation of mice. For technical reasons mice were not intubated, but the cannula of the microsprayer was inserted through the tracheal cannula and was positioned about 3 mm above the bronchial bifurcation instead. The microsprayer is constructed to produce an aerosol, when the piston is lowered very quickly. In this study, application of acid as an aerosol did not induce lung injury. Therefore the acid was applied by lowering the piston slowly, whereby a continuous thin stream was ejected by the microsprayer. In this way a volume of 50 µL acid [2.5 mL/kg] were injected into the lungs. Control mice received the same volume of 0.9% NaCl. After instillation, the microsprayer was removed and the mouse was placed upright in one hand of the operator. Then the mouse was carefully shaken up and down five times to force the acid into the lungs. The mouse was connected to the ventilator immediately and two long RM (P = 30 cmH_2O, duration: 6 s) were performed before onset of ventilation. Ventilation was performed with V_T = 16mL/kg, f = 90 min^{-1}, one RM every 5 min, PEEP = 2 cmH_2O and FiO_2 = 0.3. No additional CO_2 was administered in this model, because acid-treated mice showed increased pCO_2 levels due to impaired gas exchange. Control mice, treated with NaCl, were ventilated with additional dead space, increased by 3.5 cm, to avoid hypocapnia. Experimental groups are shown in Table 2.3. Two independent series of experiments were performed under differential conditions: firstly, the

severe acid model with acid pH = 1.5 over 5 h of ventilation and secondly the moderate acid model with acid pH = 1.8 over a period of 5 h 30 min ventilation. Therapeutical interventions were single dosages of either the glucocorticoid dexamethasone [1mg/kg] or the alkaloid quinine [20mg/kg], each given iv in 100 µL of Ringer's buffer directly after onset of ventilation. Control groups received the same volume of Ringer's buffer without drug.

Table 2.3: Experimental groups in the acid model

	Severe acid model pH = 1.5			**Moderate acid model pH = 1.8**			
	SA	**SAD**	**$NaCl_{5h}$**	**MA**	**MAD**	**MAQ**	**$NaCl_{5.5h}$**
Instillation i.t.	Acid	Acid	NaCl	Acid	Acid	Acid	NaCl
Ringer's i.v.	+	-	+	+	-	-	+
Dexa i.v.	-	+	-	-	+	-	-
Quinine i.v.	-	-	-	-	-	+	-
FiO_2	0.3	0.3	0.3	0.3	0.3	0.3	0.3
Ventilation	5 h	5 h	5 h	5.5 h	5.5 h	5.5 h	5.5h

SA: severe acid (pH 1.5), MA: moderate acid (pH 1.8); Instillation i.t.: 50 µL hydrochloric acid or 0.9 % NaCl administered intratracheally; Ringer's i.v.: 100 µL Ringer's buffer injected into tail vein; Dexa i.v.: 1 mg/kg dexamethasone injected intravenously; Quinine iv: 20 mg/kg intravenously; FiO_2: fraction of inspired oxygen; Ventilation: V_T = 16 mL/kg, f = 90 min^{-1}, PEEP = 2 cmH_2O and one recruitment manoeuvre every 5 min.

2.8 Mouse lung preparation

2.8.1 Preparation in the ventilation and TNF model

After thoracotomy, lungs were perfused free of blood. Therefore the left ventricle was opened with a cut and the needle of a 27 gauge venous catheter, which was connected to a burette filled with ice-cold PBS, was inserted into the pulmonary vein above the right atrium. The burette, which was fixed to a stand, was filled to a level of 20 cm height, so that all lungs were perfused with a pressure of 20 cmH_2O until the tissue became almost white. Then thymus and heart were removed, before the lungs were resected carefully from the thorax and transferred to a culture dish for further preparation. Next, the left lung was transiently disconnected by positioning a micro clamp on the left main bronchus. The right lung was then subjected to bronchoalveolar lavage (BAL), by instilling two times 300 µL ice-cold NaCl with a syringe via the tracheal tubing. About 550 µL BAL fluid was retrieved from each mouse. Following lavage, the right lung was separated by a ligature, cut off and snap frozen in liquid nitrogen for storage at -80°C. Thereafter, the micro clamp was carefully taken off the left bronchus and the left lung was filled with 4% buffered formalin using a hydrostatic pressure of 20 cmH_2O to facilitate adequate filling of the alveoli without damaging the tissue.

The filled left lung was closed with a ligature and placed in a Falcon tube containing 4% formalin for fixation. After fixation for three days at room temperature, lungs were embedded in paraffin for histopathological processing. Finally, the BAL fluid was centrifuged for 10 min at 3500 rpm. The cell pellet was transferred to a cytospin preparation (2.9.1). The supernatant was snap frozen for later quantification of total protein, cytokine and BSA levels as described in chapter 2.10.1 and 2.10.2.

2.8.2 Preparation in the acid model

Perfusion and resection of the whole lung were performed as described in the chapter above (2.8.1). Then the right lung was occluded with a micro clamp on the right bronchus, before the left lung was lavaged by instilling two times 200 µL ice-cold NaCl, whereof about 350µL were retrieved from each mouse. BAL samples were treated as in the other models. After ligature of the left bronchus, the left lung was removed. Continuing with the right lung, the upper right lobe was separated from the lower lobes by a ligature. The lower lobes were removed and immediately frozen in liquid nitrogen. The upper lobe was filled with 4% formalin and prepared for histopathology as described above.

2.9 Cytospin and Histopathology

2.9.1 Cytospin preparation

For the cytospin preparation, a microscopic slide was placed in a metal holder and covered with a filter containing two circular holes. Then an acryl glass container with two holes was placed on top of the filter so that the holes of the container were positioned above the holes of the filter and the filter was tightly fixed on the slide. The cell pellets retrieved from the centrifuged BAL fluid samples were resuspended in 150 µL RPMI medium. Each cell suspension was pipetted into a 1 mL pipette tip, before the filled tip was inserted into one of the holes of the container. The whole construction was placed in a centrifuge and centrifuged for 5 min at 300 rpm to enable the cells, which were held back in the tip by capillary forces, to be attached to the slide by centrifugal force. The cells on the slide were dried by room air followed by a modified Giemsa stain (Diff-Quick). Slides were mounted for preservation until evaluation by differential leukocyte count at 200x magnification.

2.9.2 Preparation of tissue slices from paraffin embedded mouse lungs

Tissue slices were cut with a microtome. Mouse lungs embedded in paraffin blocks were placed in the microtome and slices of 1 µm thickness were prepared. The slices were transferred into a water bath with lukewarm water and were then mounted on Poly-L-Lysin

(0.1%) coated microscope slides. The specimens were dried over night at 37°C before further processing.

2.9.3 Haematoxylin-Eosin (HE) staining

The HE staining of the lung slices was performed by first incubating the slides for 10 min in Mayer's-Haemalaun solution for a blue staining of the cell nuclei. After rinsing the slides with water, they were incubated for 10 min in tap water to blue the stain. For the counter stain of the cytoplasm the slides were incubated for 5 min in a 1% solution of the acidic red Eosin. Slides were again rinsed with water and then dehydrated by shortly dipping them in 70%, 96% and twice in 100% alcohol. Finally, slides were transferred to xylene and then mounted with mounting media and cover slips.

2.9.4 Histopathological scoring

The lung injury scoring system recently published in the official ATS workshop report on features and measurements of experimental lung injury was adopted [34] is briefly summarised in Table 2.4 depicted below. The score ranges from 0 to 1. A score of 0 indicates that no injury occurred, whereas 1 is the maximal injury.

Table 2.4: Histopathological scoring system

	Score per field		
Parameter	0	1	2
A. Neutrophils in the alveolar space	none	1-5	> 5
B. Neutrophils in the interstitial space	none	1-5	> 5
C. Hyaline membranes	none	1	> 1
D. Proteinaceous debris filling in the airspaces	none	1	> 1
E. Alveolar septal thickening	< 2x	2x-4x	> 4x

From each mouse lung, 10 pictures from different regions were taken at 200-fold magnification. The injury score was calculated by: Score = [(20 x A) + (14 x B) + (7 x C) + (7 x D) + (2 x E)] / (number of fields x 100).

2.10 Biochemical methods

2.10.1 Protein quantification

Total protein levels of the BAL fluid were measured using the DC protein assay from Bio-Rad. This method is based on the Lowry protein assay, which consists of two steps. The first step is the Biuret reaction, during which peptide bonds form violet complexes with Cu^{2+}-ions in alkaline solution. In the second step, Cu^{2+} is reduced to Cu^{+}, which then reduces the Folin-Ciocalteau reagent, inducing a further colour reaction and thereby increasing the sensitivity

of the assay. The DC assay returns stable results after 15 min of incubation. Absorbance was read at 550 nm. Protein concentrations were determined using a BSA standard curve.

2.10.2 Enzyme-linked immunosorbent assays

The following mediators were quantified using commercially available enzyme-linked immunosorbent assays (ELISA): the pro-inflammatory cytokines interleukin-6 (IL-6) and TNF, the chemokines keratinocyte-derived chemokine (KC) and macrophage inflammatory protein-2 (MIP-2) and the sepsis marker procalcitonin (PCT). Also BSA and HSA were detected with ELISA. Due to the limited sample volume from mice, all proteins listed above, except of PCT, were measured in diluted samples. BAL samples were diluted 1:4 and plasma samples 1:10. The assays were performed according to the manufacturer's protocols. All kits are listed in chapter 2.2.3.

2.10.3 Cell death detection assay

The cell death detection assay allowed quantification of apoptosis and necrosis via detection of mono- and oligonuceosomes by sandwich ELISA. For the assay, 30 mg of homogenized frozen lung tissue were lysed with a buffer included in the kit. The assay was performed according to the manufacturer's instructions and absorbance was read at 405 nm. The lysis buffer was measured as blank, which was subtracted from the results. Cell death was calculated as % per mg lung tissue relative to a 100% positive control.

2.10.4 Nitric oxide quantification assay

The gaseous signalling molecule nitric oxide (NO) is highly instable *in vivo* and is rapidly converted into the more stable metabolites nitrite (NO_2^-) and nitrate (NO_3^-). In the present study, an assay was used that measures total NO in blood plasma samples. Therefore, endogenous nitrate was converted to nitrite by nitrate reductase. Then the total nitrite was quantified as a chromophoric azo-derivative of the Griess reagent by reading the absorbance at 550 nm.

2.10.5 Acid sphingomyelinase activity assay

ASM activity was determined by using 14C-labelled sphingomyelin. For all samples, 10 µg protein diluted to 10 µL was incubated at 37°C for 2 h with 40 µL substrate (73 nmol 14C-labelled sphingomyelin + 400 nmol sphingomyelin). Lipids were separated by chloroform / methanol extraction. 4 mL scintillation liquid was added and radioactivity was counted in a β-counter.

2.11 Statistical analysis

Statistical analyses of time courses, i.e. lung mechanics, BP and HF, were analysed with the mixed model procedure followed by correction for false discovery rate (FDR) in the ventilation and acid model. To evaluate lung mechanics from the groups lowV_TRM60 and PEEP6_RM60 in a linear model, one time point every 60 minutes before and one after RM were analysed separately, resulting in two separate linear slopes (lowV_TRM60a and PEEP6_RM60a: before RM, lowV_TRM60b and PEEP6_RM60b: after RM). In the TNF model, lung mechanics, HF and BP were analysed using Two-Way Analysis of Variance to analyse the influence of genotype and drug-treatment as independent factors. Analyses of all other parametric data were carried out with One-Way Analysis of Variance, followed by t-test and FDR correction or the Tukey-test. BoxCox transformation was performed to achieve homoscedasticity, when suitable. Percentage data were transformed using the arcsine transformation. The Bartlett test was used to check for equal variances. Normal distribution was validated with the Shapiro-Wilk test. Non-parametric data, except of survival curves, were analysed with the Kruskall-Wallis test followed by Dunn's post-test. Survival curves were compared with the Kaplan-Meier estimator. Correlation was evaluated with Pearson's correlation coefficient. Cluster analysis was performed with JMP 9 using the method 'average' with standardised data. Data in figures are shown as mean + standard error of the mean (SEM). P-values ≤ 0.05 were considered as significant. Statistical analyses were carried out with GraphPad Prism 5.0, JMP 7, JMP 9 or SAS 9.1 software.

3 Results

3.1 The ventilation model with low PEEP (2 cmH_2O)

3.1.1 Lung mechanics

The first series of ventilation experiments was performed at a PEEP = 2 cmH_2O. This low PEEP level is commonly used in animal studies that aim to study VILI and is regarded as minimally protective (see Table 1.2). Ventilation with 8 mL/kg and no RM (low$V_T$noRM) caused a continuous decrease of pulmonary compliance (C) over more than two hours that reached a plateau at approximately 30% of the physiological baseline value (Fig. 3.1). Within this time pulmonary resistance (R) nearly tripled. Resistance and compliance showed less dramatic trends in mice ventilated with 16 mL/kg and no RM (high$V_T$noRM). In this group C plateaued earlier (60 min) at about 60% of the baseline value and R increased to a lesser degree (~25%). R and C differed significantly between the low$V_T$noRM and the high$V_T$noRM group (R: $p < 0.01$; C: $p < 0.001$). Respiratory input impedance revealed major alterations in the periphery of the lung. Tissue damping (G) and tissue elastance (H) were elevated in both high$V_T$noRM and low$V_T$noRM mice, reaching significantly higher values in the low$V_T$noRM group (G: $p < 0.01$; H: $p < 0.001$). In the latter group, airway resistance (R_{aw}) was increased as well. The increase in G, H and R_{aw} indicates that low V_T ventilation without RM leads to closure of peripheral areas of the lung and causes a small degree of airway constriction. In consequence, hysteresivity (G/H = η) decreased slightly over time, but was in a comparable range in all groups.

These findings indicate that ventilation without RM leads to impaired lung functions, which stabilise within two hours, though at a low level. Therefore the effect of repetitive RM (30 cmH_2O) every 5 min was examined. In both the lowV_TRM5 and the highV_TRM5 group, lung mechanics stayed in a physiological range and remained unchanged during the whole experiment. Depending on the different V_T, C and H differed reciprocally between low- and highV_T groups ($p < 0.05$). The stability of the lung mechanics demonstrates that application of deep inflations of 1 s duration and 30 cmH_2O are sufficient to prevent the deterioration of lung functions in healthy mouse lungs ventilated with 2 cmH_2O PEEP and moderate V_T.

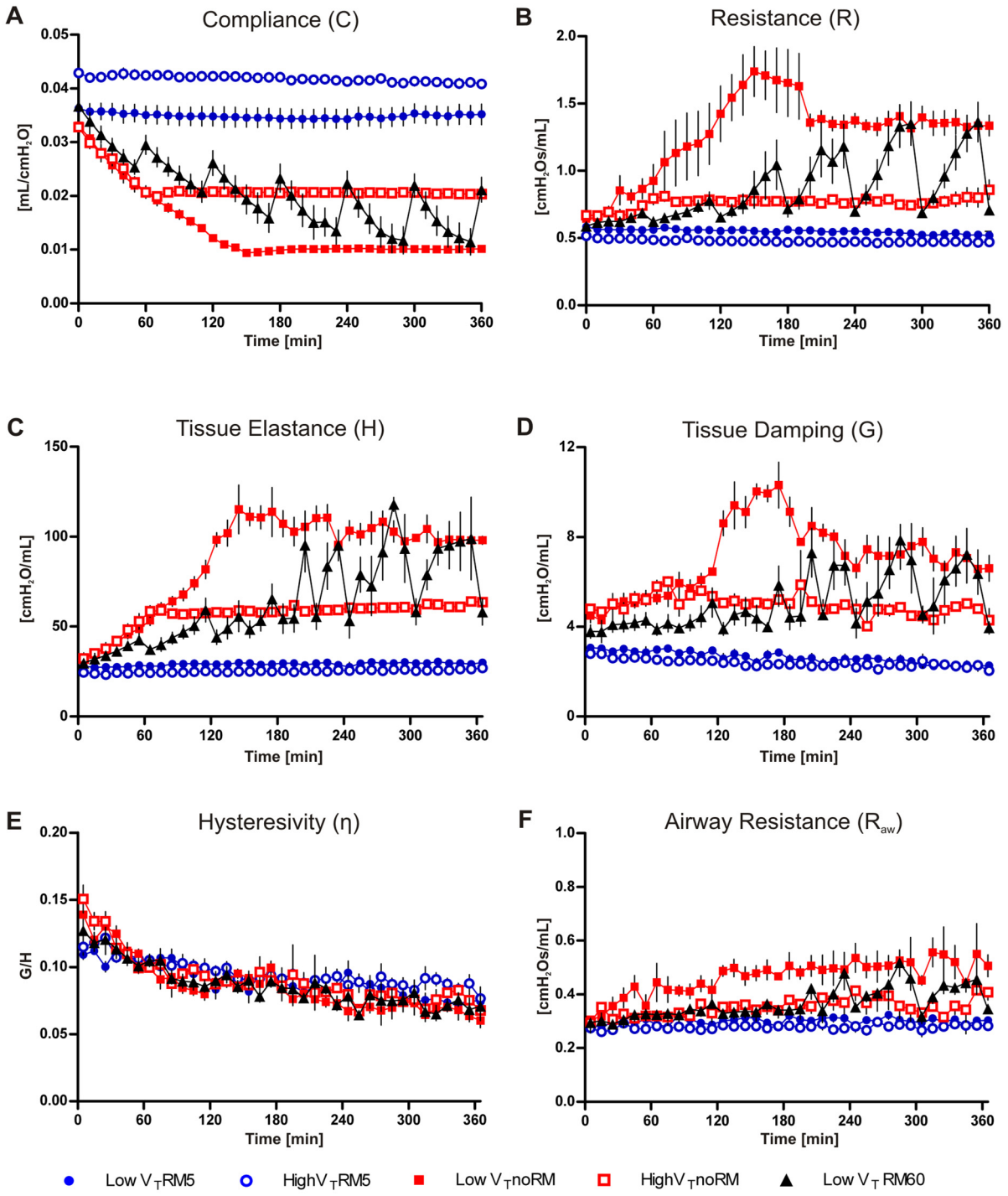

Fig. 3.1: Lung mechanics with PEEP = 2 cmH_2O. Mice were ventilated for six hours with low V_T = 8 mL/kg or high V_T = 16 mL/kg, PEEP = 2 cmH_2O and RM every five minutes (RM5), every 60 minutes (RM60) or without RM (noRM). Lung mechanics were measured every ten minutes by the forced oscillation technique. ($lowV_TRM5$: n=6, $highV_TRM5$: n=6, $lowV_TnoRM$: n=5, $highV_TnoRM$: n=4, $lowV_TRM60$: n=5). P-value ranges for group comparisons are shown in Table 6.1 in the supplement.

Further, it was examined whether it would suffice to apply RM only every 60 min instead of every 5 min. This was studied in the low V_T group (lowV_TRM60) only. In this group, respiratory conditions were instable. R and C worsened comparable to the low$V_T$noRM group, but improved significantly after each RM. These alterations were reflected in changes in G and H. However, even though each RM was beneficial, after six hours tissue elastance had increased permanently, indicating that one deep inflation per hour is not sufficient to maintain lung volume at baseline values. This is illustrated by the finding that H ($p < 0.001$), R, C, G (all $p < 0.01$) and R_{aw} ($p < 0.05$) were significantly different between the lowV_TRM60 and the lowV_TRM5 group.

3.1.2 Heart frequency, mean arterial pressure and oxygen saturation

Anaesthesia with pentobarbital sodium resulted in reduced heart frequency (300-400 min^{-1}) and mean blood pressure (50-60 mmHg), compared to average data of unsedated mice [148]. ECG (data not shown), Heart frequency (HF) and mean arterial pressure (MAP) remained unchanged throughout ventilation and were not significantly different between the groups (Fig. 3.2). This demonstrates that ventilation and recruitment strategy did not affect the circulation. The fluid support with 200 µL NaCl per hour in all groups was adequate to keep blood pressure stable. A small peak in HF was caused at the time-point of i.v. BSA injection (270 min). Oxygen saturation, measured by pulse oximetry, was over 90% in all mice at all times. Oxygen saturation served only as control parameter during the experiments, because this parameter is generally prone to interference. For evaluation of gas exchange, the more accurate arterial pO_2, measured by blood gas analysis, was used.

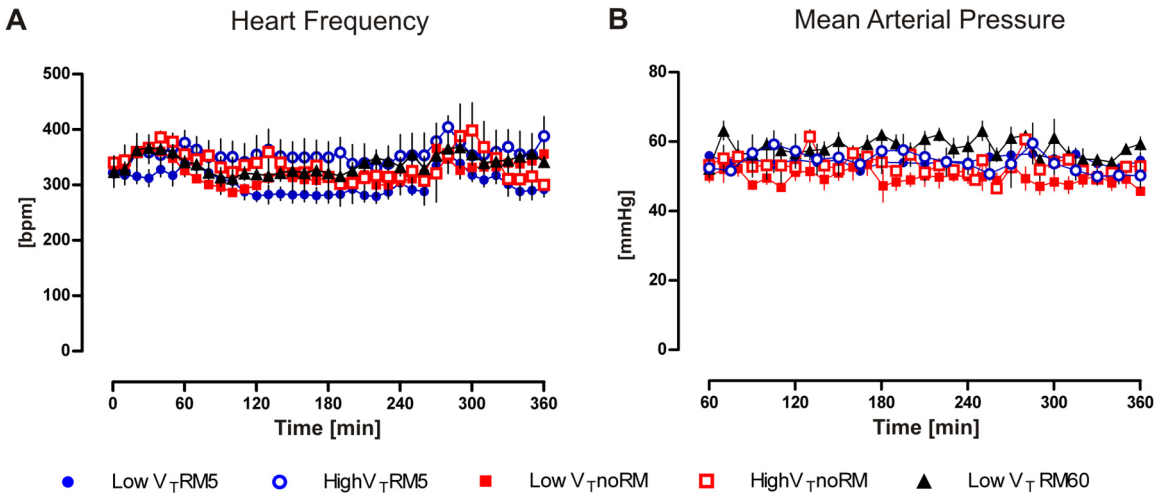

Fig. 3.2: Heart frequency and mean arterial pressure. Electrocardiogram (ECG) was recorded permanently beginning with onset of ventilation. **A.** Heart frequency (HF) was calculated simultaneously from the ECG and is displayed in beats per minute (bpm). **B.** Mean arterial blood pressure (BP) was measured via a catheter in the carotid artery. (lowV_TRM5 n=6, highV_TRM5 n=6, low$V_T$noRM n=5, high$V_T$noRM n=4, lowV_TRM60 n=5).

3.1.3 Blood gas analysis

Blood gas analyses revealed that infusion of saline and application of 3% CO_2 in the high V_T groups were adequate to keep the acid-base status stable and that ventilation resulted in normocapnia in the lowV_TRM5 and highV_TRM5 group, with pCO_2 levels ranging from 35 to 40 mmHg (Table 3.1). The pO_2/FiO_2 ratio was between 530 and 620 mmHg in both RM5 groups and in the high$V_T$noRM group (Fig. 3.3A). Most mice ventilated with high$V_T$noRM had physiological pCO_2 levels after six hours. The pO_2/FiO_2 ratio was decreased significantly to ~200 mmHg in the low$V_T$noRM group, indicating acute respiratory failure. In this group, impaired gas exchange was further indicated by an increase in pCO_2 levels to about 60 mmHg (Fig. 3.3B), leading to respiratory acidosis with a mean pH of 7.22. Mice in the lowV_TRM60 group showed very heterogeneous pO_2/FiO_2 ratios between 260 and 570 mmHg and markedly increased pCO_2 levels as well as hypercapnic acidosis. HCO_3^- and standard base excess were only slightly reduced and did not indicate metabolic imbalance.

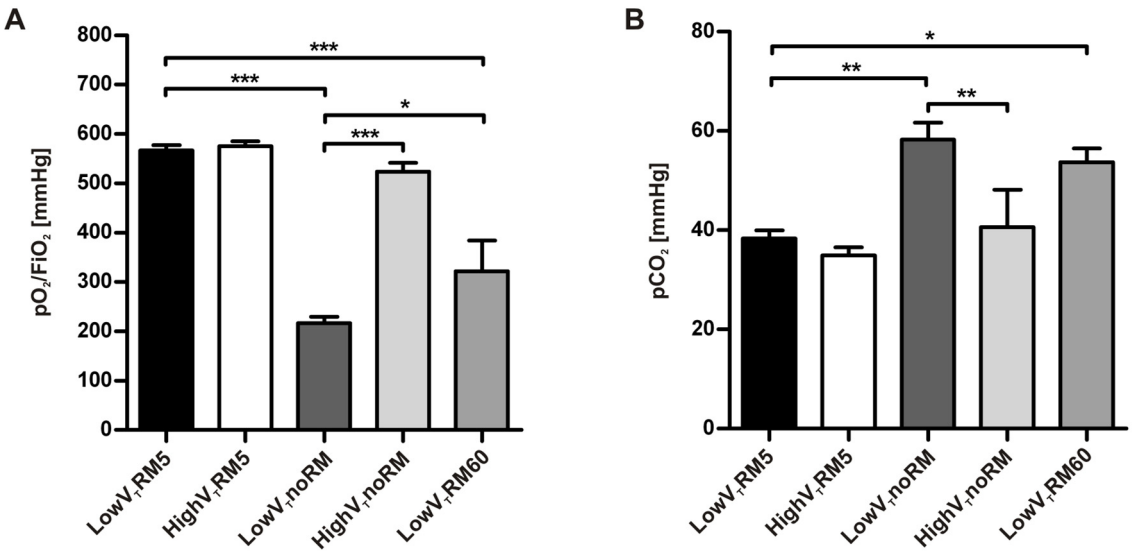

Fig. 3.3: Blood gas results with PEEP = 2 cmH_2O. Arterial blood was analysed after six hours of ventilation. **A.** The pO_2/FiO_2 ratio was calculated, FiO_2 was 0.5. **B.** Comparison of pCO_2 levels. (lowV_TRM5 n=6, highV_TRM5 n=6, low$V_T$noRM n=5, high$V_T$noRM n=4, lowV_TRM60 n=5). * $p \leq 0.05$, ** $p \leq 0.01$, *** $p \leq 0.001$.

Table 3.1: Blood gas results in the ventilation model with PEEP = 2 cmH_2O

	LowV_TRM5	**HighV_TRM5**	**Low$V_T$noRM**	**High$V_T$noRM**	**LowV_TRM60**
pO_2 [mmHg]	283.5 ± 13.4	287.7± 12.7	108.6 ± 13.6	261.8 ± 17.8	205.5 ± 72.4
pCO_2 [mmHg]	38.4 ± 3.9	34.9 ± 4.0	58.3 ± 7.61	40.6 ± 15.1	50.1 ± 9.4
pH	7.33 ± 0.03	7.36 ± 0.04	7.22 ± 0.03	7.32 ± 0.08	7.28 ± 0.05
HCO_3^- [mmol/L]	19.5 ± 1.6	19.2 ± 1.6	23.6 ± 2.3	19.7 ± 3.4	21.8 ± 1.9
SBE [mmol/L]	- 6.0 ± 1.6	- 5.5 ± 1.7	- 3.5 ± 2.1	- 5.4 ± 2.3	- 3.5 ± 1.6

Blood gas analyses from arterial blood after 6 h of mechanical ventilation with PEEP = 2 cmH_2O. Data are shown as mean ± standard deviation. SBE: standard base excess, lowV_T: low tidal volume, highV_T: high tidal volume, RM5: one recruitment manoeuvre every five minutes, noRM: no recruitment manoeuvres, RM60: one recruitment manoeuvre every 60 minutes.

3.1.4 Pulmonary microvascular permeability

Total protein levels were increased in all ventilated mice, compared to unventilated controls. Protein levels were highest in the groups without RM (Fig. 3.4A). The BSA BAL/plasma ratio confirmed that ventilation augmented microvascular permeability in the lung, particularly when inspiratory pressures were high, as in the groups ventilated without repetitive recruitment (Fig. 3.4B).

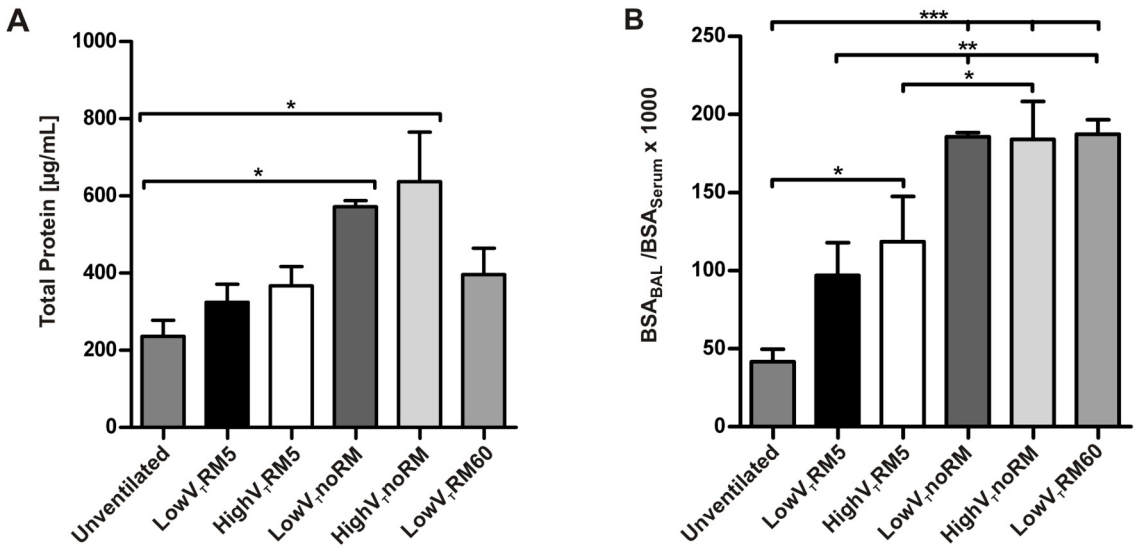

Fig. 3.4: Total protein levels and protein leakage with PEEP = 2 cmH_2O. A. Total protein levels were measured with a Lowry protein quantification assay. (Unventilated n=5, lowV_TRM5 n=6, highV_TRM5 n=6, low$V_T$noRM n=4, high$V_T$noRM n=4, lowV_TRM60 n=5). **B.** BSA was quantified in BAL and serum by ELISA and the ratio was calculated. (Unventilated n=5, lowV_TRM5 n=5, highV_TRM5 n=5, low$V_T$noRM n=4, high$V_T$noRM n=4, lowV_TRM60 n=5). * $p \leq 0.05$, ** $p \leq 0.01$, *** $p \leq 0.001$.

3.1.5 Pro-inflammatory mediators

Interleukin-6 (IL-6) and Keratinocyte-derived chemokine (KC) were elevated in the BAL fluid and blood serum from all ventilated mice (Fig. 3.5A, B, E, F). BAL fluid from mice ventilated with lowV_TRM5 showed a less dramatic increase in these pro-inflammatory cytokines. In both RM5 groups serum levels of IL-6 and KC were clearly lower than in all other ventilation groups. Interestingly, Interferon-γ induced protein (IP-10) and TNF were not significantly increased in the BAL from ventilated mice, compared to unventilated controls (Fig. 3.5C, D).

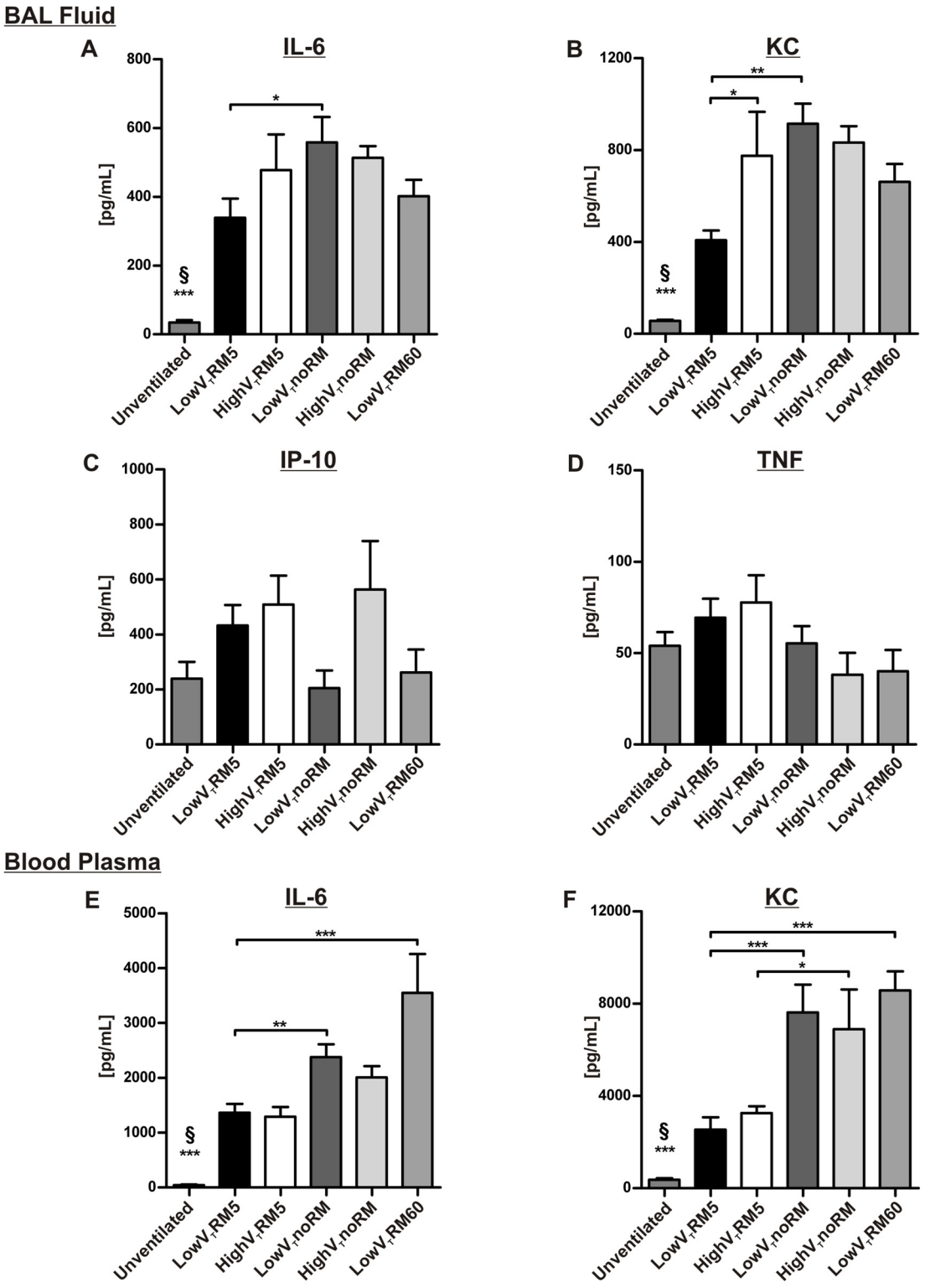

Fig. 3.5: Pro-inflammatory mediators with PEEP = 2 cmH_2O. The Cytokines IL-6, IP-10 and TNF as well as the chemokine KC were quantified in blood plasma or BAL supernatant with commercial ELISA kits after six hours of ventilation and in unventilated mice. (Unventilated n=5, lowV_TRM5 n=6, highV_TRM5 n=6, low$V_T$noRM n=4 in BAL and n=5 in serum, high$V_T$noRM n=4, lowV_TRM60 n=5). * $p \leq 0.05$, ** $p \leq 0.01$, *** $p \leq 0.001$, § *** $p \leq 0.001$ versus all other groups.

3.1.6 Neutrophil recruitment into the alveolar space

The only cell types found in BAL fluid of unventilated control mice were monocytes and macrophages. In contrast, all samples from ventilated mice also contained neutrophils (Fig. 3.6). Numbers of neutrophils were highest in mice ventilated with high V_T. Considerably less neutrophils were recruited to alveoli of lowV_T mice, whereof the group lowV_TRM5 had the lowest neutrophil count.

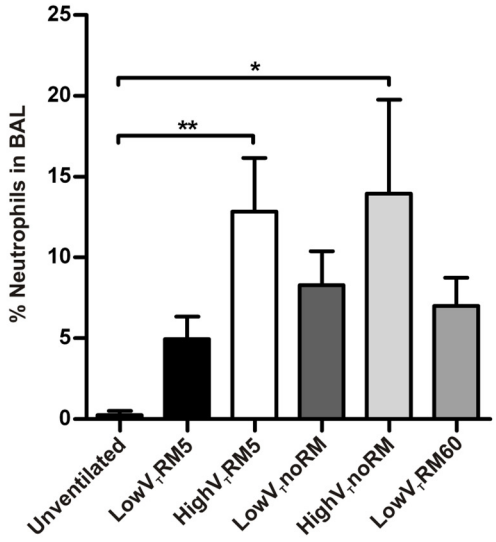

Fig. 3.6: Neutrophils in the BAL fluid with PEEP = 2 cmH_2O. BAL fluid was subjected to cytospin preparation, followed by modified Giemsa staining. 400 cells were counted from each preparation and the percentage of neutrophils was calculated. (Unventilated n=5, lowV_TRM5 n=5, highV_TRM5 n=5, low$V_T$noRM n=4, high$V_T$noRM n=4, lowV_TRM60 n=5). * $p \leq 0.05$, ** $p \leq 0.01$.

3.1.7 Lung histopathology

Examination of HE-stained lung sections showed that only mild lung injury was induced by the ventilation strategies applied (Fig. 3.7). This was supported by the employed lung injury score, theoretically ranging from zero to maximally one, which was below 0.4 in all subjects. Nonetheless, histopathological alterations were present in all ventilated lungs and were most pronounced in mice ventilated with high V_T (Fig. 3.8). In almost all ventilated lungs, interstitial neutrophils were present and in some sections alveolar septae were thickened. In mice ventilated with high V_T, also intra-alveolar neutrophils were observed. This is in line with the results from the differential cell count in the BAL fluid, where highest neutrophil numbers were counted in the high V_T groups. Neither hyaline membranes nor proteinaceous debris were observed in any sections, further demonstrating that the ventilation strategies used in this study induced only moderate injury in the healthy lungs.

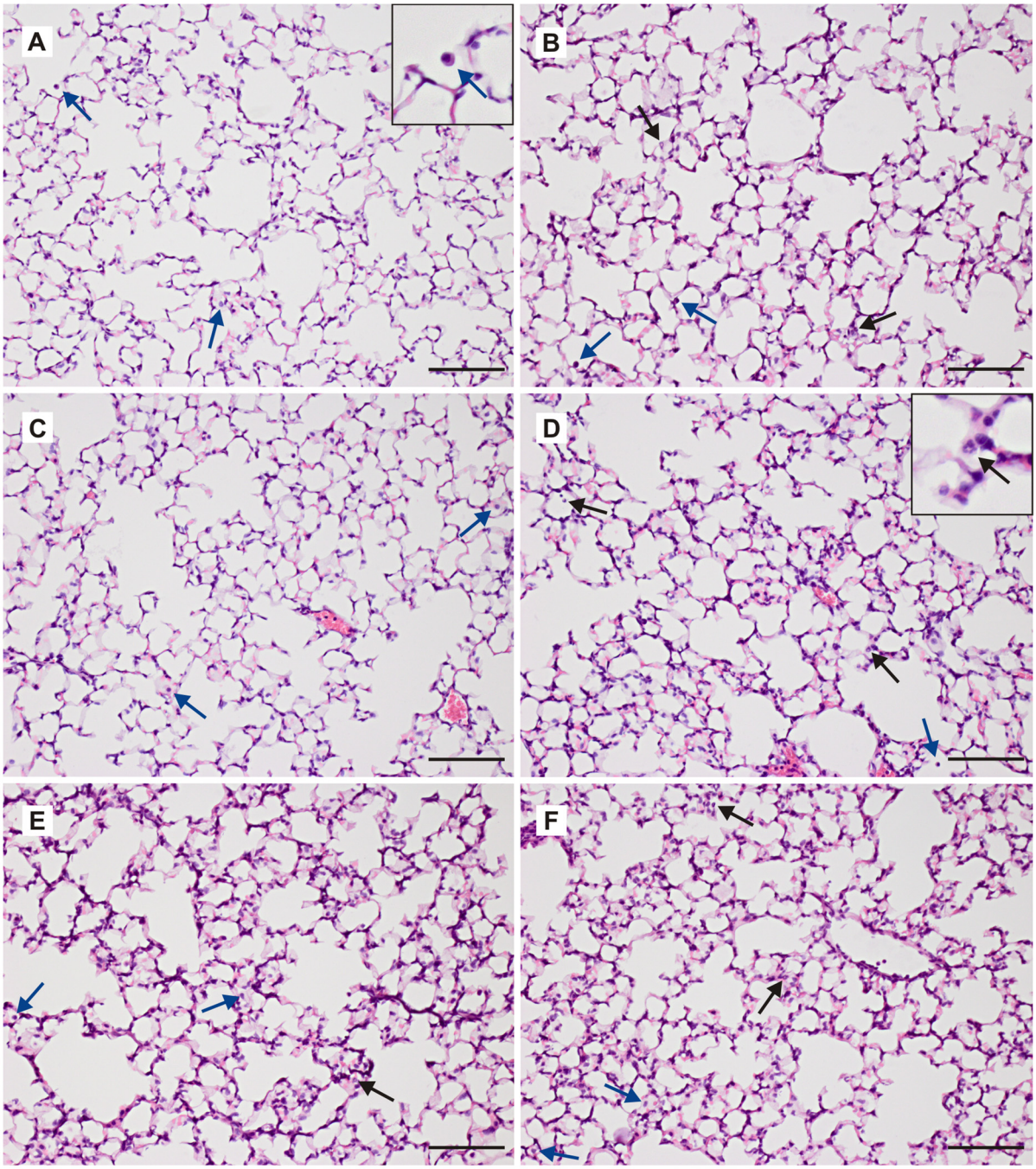

Fig. 3.7: Lung histopathology with PEEP = 2 cmH_2O. Representative HE-stained lung sections from: **A**. unventilated control, **B**. lowV_TRM60, **C.** lowV_TRM5, **D.** highV_TRM5, **E.** low$V_T$noRM and **F.** high$V_T$noRM mice. Black arrows indicate neutrophils; blue arrows indicate intra-alveolar monocytes and macrophages, scale bars 100 µm; magnification 200x. Insets in A and D contain enlarged images of exemplary leukocytes.

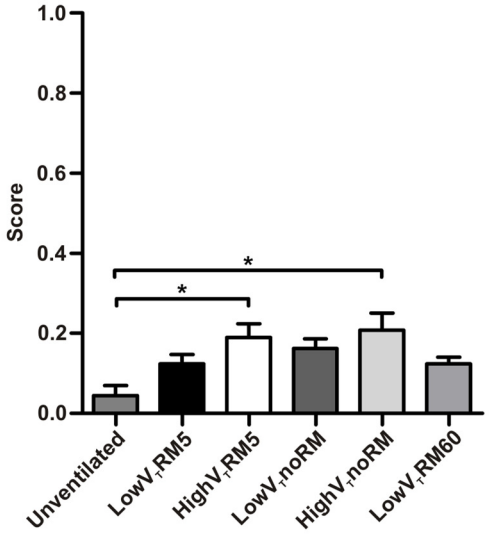

Fig. 3.8: Histopathological scoring with PEEP = 2 cmH_2O. Lungs were scored with an injury scoring system suggested by Matute-Bello et al. [34]. 10 fields per lung were evaluated according to the following criteria: A) neutrophils in the alveolar space, B) neutrophils in the interstitial space, C) hyaline membranes, D) proteinaceous debris in the airspaces, E) alveolar septal thickening. The score was calculated as follows: Score = [(20 x A) + (14 x B) + (7 x C) + (7 x D) + (2 x E)] / (number of fields x 100). (Unventilated n=5, lowV_TRM5 n=5, highV_TRM5 n=5, low$V_T$noRM n=4, high$V_T$noRM n=4, lowV_TRM60 n=5). * $p \leq 0.05$.

3.2 The ventilation model with moderate PEEP (6 cmH_2O)

3.2.1 Lung mechanics

In the second series of experiments the ventilation strategies RM5, noRM and RM60 were applied to mice ventilated with low V_T and a PEEP of 6 cmH_2O, to find out whether the impairment of lung mechanics during ventilation with noRM and RM60 could be prevented by a higher PEEP (Fig. 3.9). Ventilation with RM5 at a PEEP of 6 cmH_2O (PEEP6_RM5) showed stable lung functions. Ventilation without RM (PEEP6_noRM) resulted, notwithstanding the increased PEEP, in a strong decrease in C during the first 180 min of ventilation until a plateau was reached at about 30% of the initial C. Correspondingly R, G and H increased and finally doubled in this group. Also ventilation with RM60 (PEEP6_RM60) did not suffice to keep lung functions entirely stable at a PEEP of 6 cmH_2O. Although the decrease in C between the RM was relatively moderate, the initial C was not maintained over six hours. R, in contrast, returned to the initial value after each RM. In line with this, lung impedance measurements revealed a moderate increase in H, but not in G after six hours. All three groups differed significantly from each other regarding C, R, H and G, except from the parameters measured in the PEEP6_RM60 group directly after the RM. R_{aw} and η were not different between the groups and R_{aw} remained at baseline in all experiments (data not shown). These results indicate that an elevation of PEEP, although it helps to stabilise lung mechanics, is not sufficient to replace repetitive RM.

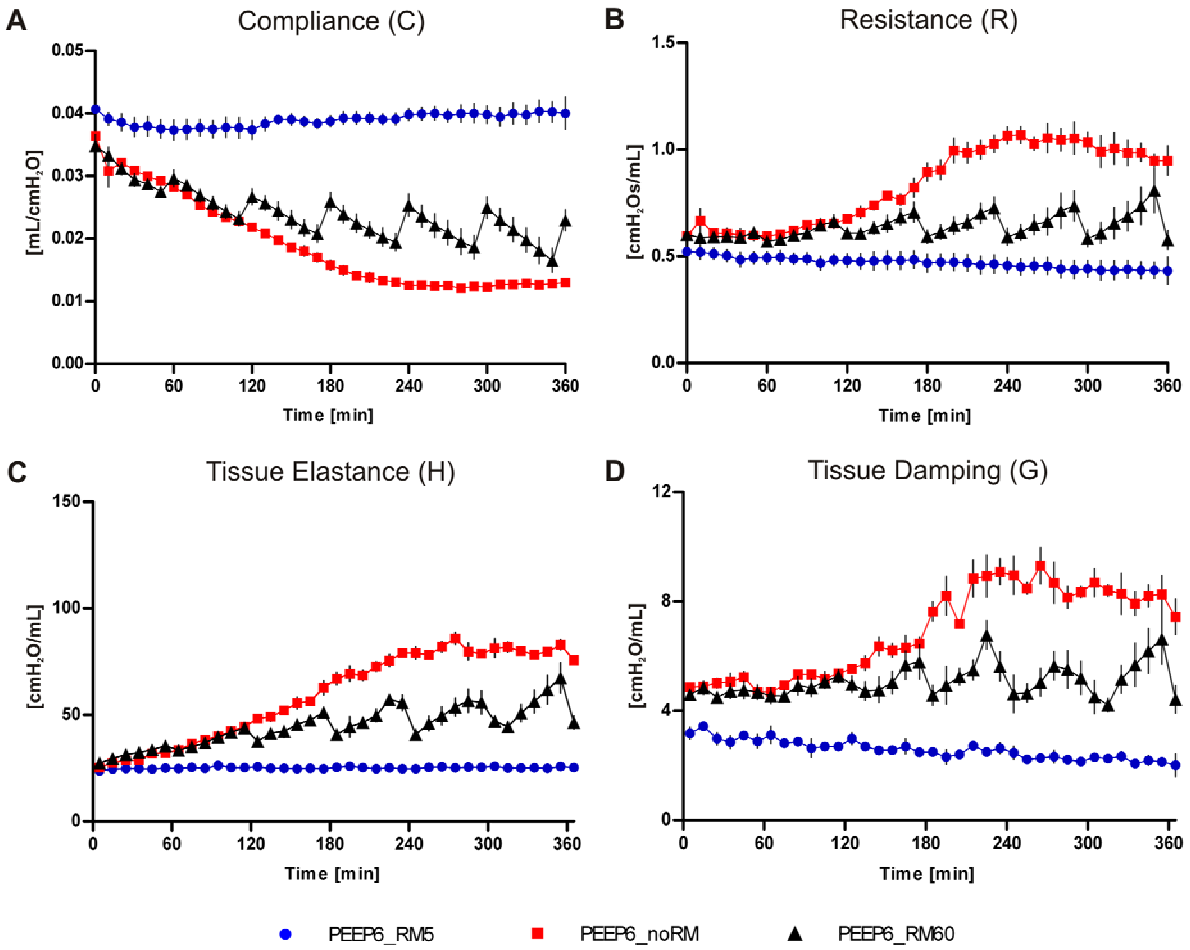

Fig. 3.9: Lung mechanics with PEEP = 6 cmH_2O. Mice were ventilated for six hours with low V_T = 8 mL/kg, PEEP = 6 cmH_2O and RM every five minutes (RM5), every 60 minutes (RM60) or without RM (noRM). Lung mechanics were measured with the forced oscillation technique every ten minutes. (n = 4 in all groups). Please see Table 6.2 in the supplement for p-value ranges of group comparisons.

3.2.2 Blood gas analysis

One aim of the second series of ventilation experiments was to investigate whether a higher PEEP can prevent the worsening of gas exchange in mice ventilated at a PEEP = 2 cmH_2O and RM60 or noRM. The pO_2/FiO_2 ratio was around 500 mmHg in the PEEP6_RM60 group and around 400 mmHg in the PEEP6_noRM group (Fig. 3.10). Both groups differed significantly from the control group PEEP6_RM5, which showed unimpaired gas exchange with a pO_2/FiO_2 ratio of about 600 mmHg This further demonstrates that regular RM are necessary even with a PEEP of 6 cmH_2O. In accordance, pCO_2 levels were significantly elevated in the groups PEEP6_RM60 and PEEP6_noRM, compared to the control group.

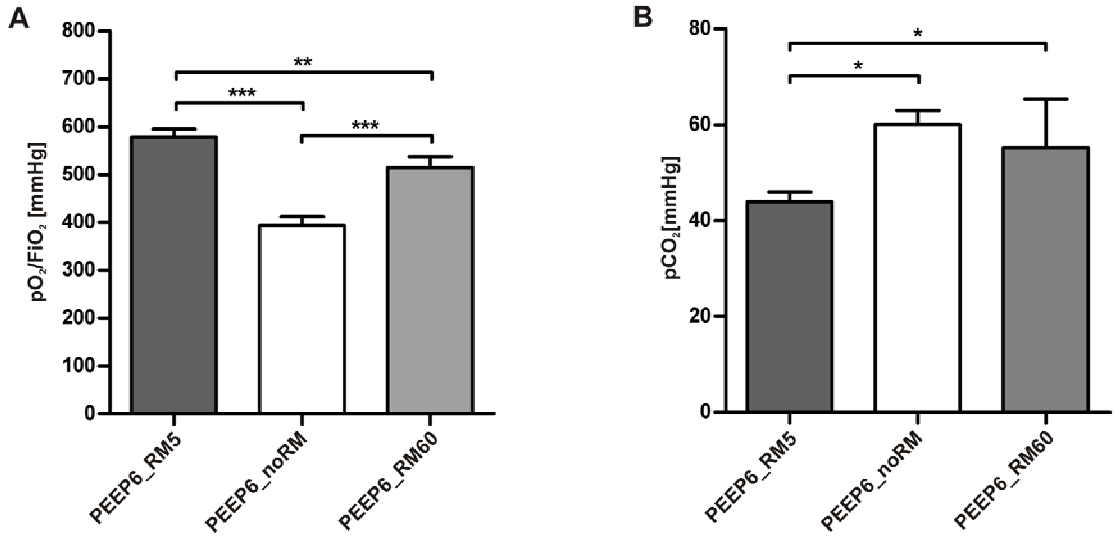

Fig. 3.10: Blood gas results with PEEP = 6 cmH_2O. Arterial blood was analysed after six hours of ventilation. **A.** The pO_2/FiO_2 ratio was calculated with $FiO_2 = 0.5$. **B.** Comparison of pCO_2 levels (n = 4 in all groups). ** $p \leq 0.01$, *** $p \leq 0.001$.

3.2.3 Pro-inflammatory mediators

In the second set of experiments IL-6 and KC levels in the BAL fluid were highest in the PEEP6_noRM group, followed by the PEEP6_RM5 group (Fig. 3.11A, B). Both mediators were lowest in the PEEP6_noRM group. IL-6 in the blood serum was not significantly different between these three groups (Fig. 3.11C). KC levels were highest in the group ventilated without RM, but differed only slightly between the groups ventilated with RM5 and RM60 (Fig. 3.11D). These results indicate that a higher PEEP helps preventing the release of pro-inflammatory mediators induced by formation of atelectasis.

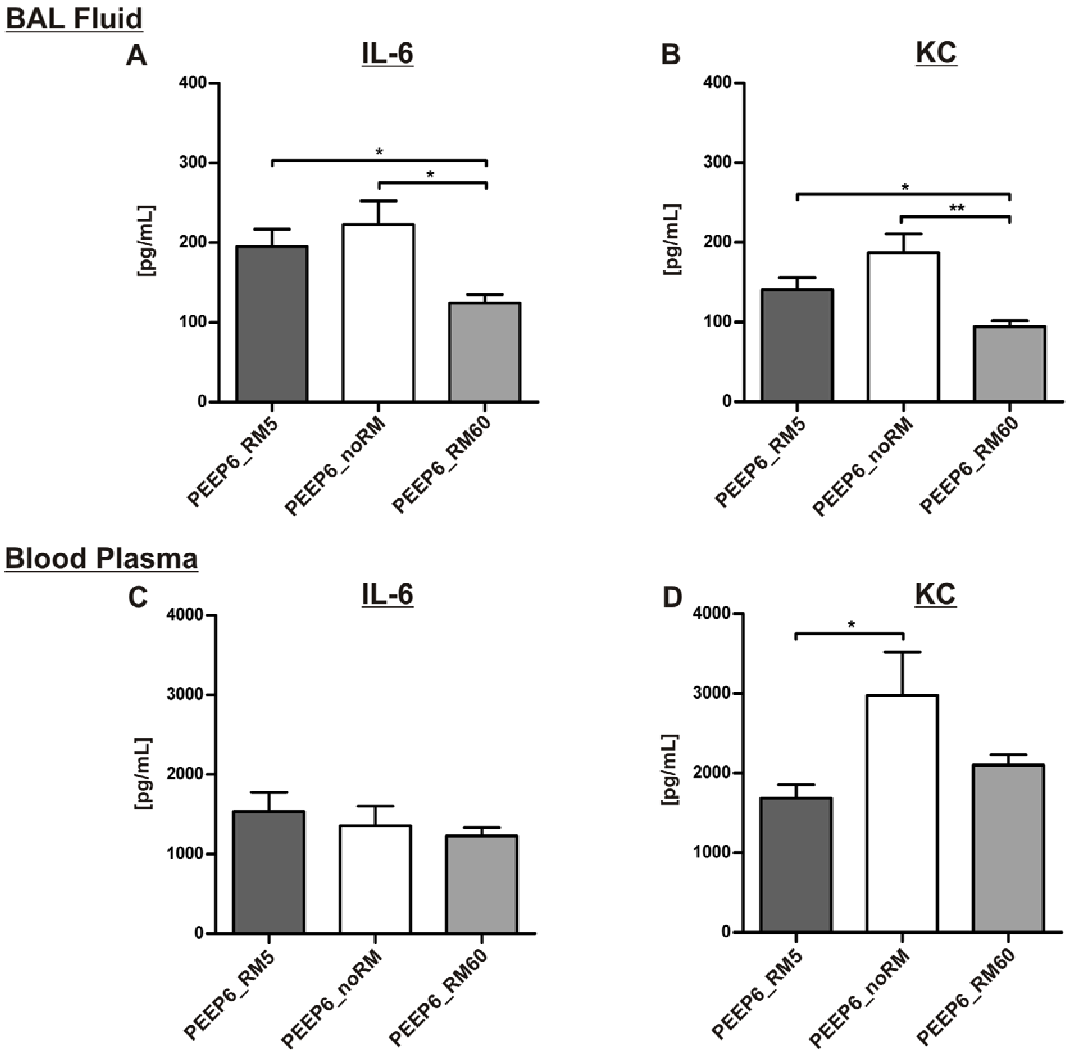

Fig. 3.11: Pro-inflammatory mediators with PEEP = 6 cmH_2O. The cytokine IL-6 and the chemokine KC were quantified after 6 h of ventilation in the blood plasma or BAL supernatant by ELISA. (n = 4 in all groups). * $p \leq 0.05$, ** $p \leq 0.01$.

3.2.4 Neutrophil quantification in the BAL fluid

In the second part of the study, in which all mice were ventilated with low V_T, neutrophil numbers were clearly highest in the group PEEP6_noRM. Neutrophil counts were lower in the BAL fluid from PEEP6_RM5 mice and lowest in the PEEP6_RM60 group (Fig. 3.12).

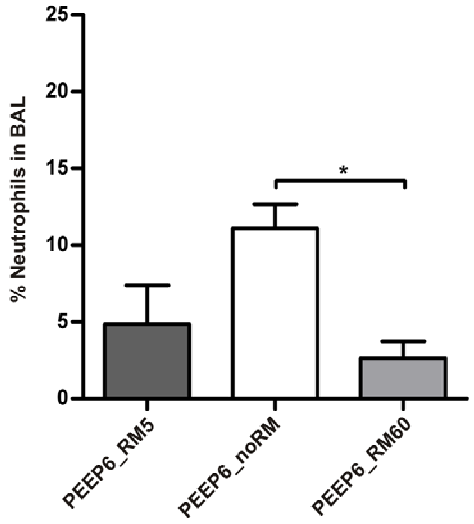

Fig. 3.12: Neutrophils in the BAL fluid with PEEP = 6 cmH_2O. Leukocytes were counted after cytospin preparation of the BAL fluid. From each preparation 400 cells were counted and percentage of neutrophils was calculated. (n = 4 in all groups). * $p \leq 0.05$.

3.3 The TNF model

3.3.1 Lung input impedance

Systemic application of TNF, 45 min after onset of ventilation, had no relevant influence on lung mechanics (Fig. 3.13).

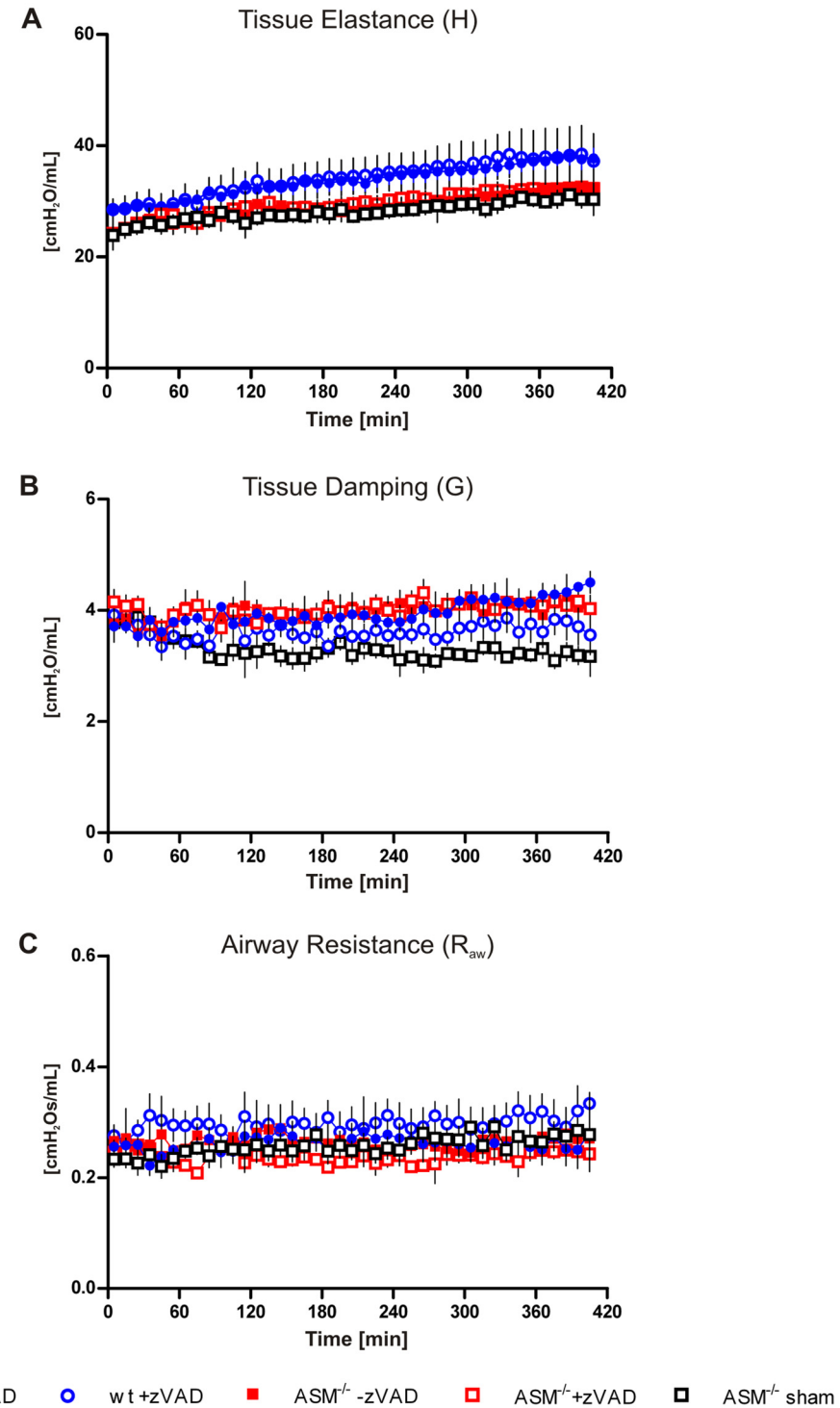

Fig. 3.13: Lung impedance in TNF-treated mice. Mice were ventilated with V_T = 8 mL/kg, f = 180 min^{-1}, PEEP = 2 cmH_2O and FiO_2 = 0.3. All groups, except from the group $ASM^{-/-}$sham, received 50 µg TNF i.v. 45 min after onset of ventilation. In addition, 250µg and 100µg zVad-fmk was given to the groups wt+zVAD and $ASM^{-/-}$ +zVAD at 30 min and 105 min of ventilation, respectively. (n=5 in all groups).

The caspase inhibitor zVAD-fmk had no influence on lung mechanics either. Pulmonary resistance and compliance stayed unchanged during the whole period of ventilation and are therefore not depicted. Also the more sensitive measurement of lung impedance revealed no noteworthy alterations. The central airways were not affected at all, shown by the measurement of Raw (Fig. 3.13A). The resistance in the periphery of the lung, given by G, was significantly different between TNF-treated and untreated mice ($p \leq 0.01$), but the difference was within a physiologically unimportant range (Fig. 3.13B). The tissue elastance H did not change after TNF treatment (Fig. 3.13C), although it differed basally between wt and $ASM^{-/-}$ mice ($p \leq 0.05$).

3.3.2 Gas exchange

Gas exchange was examined by measurement of the arterial pO_2 and pCO_2 after 405 min of ventilation. Two wt mice in each group died prior to exsanguination and could not be subjected to blood gas analysis. The Horovitz index was calculated from the pO_2 and the applied FiO_2 of 0.3 to evaluate the level of oxygenation (Fig. 3.14A). The index was between 500 and 600 mmHg in all subjects, thus being in the range of healthy lungs. The pCO_2 levels around 40 mmHg were in a normal range as well (Fig. 3.14B). In conclusion, the arterial blood gases showed no impairment of pulmonary gas exchange supporting the result of the impedance measurement that TNF had no influence on lung functions.

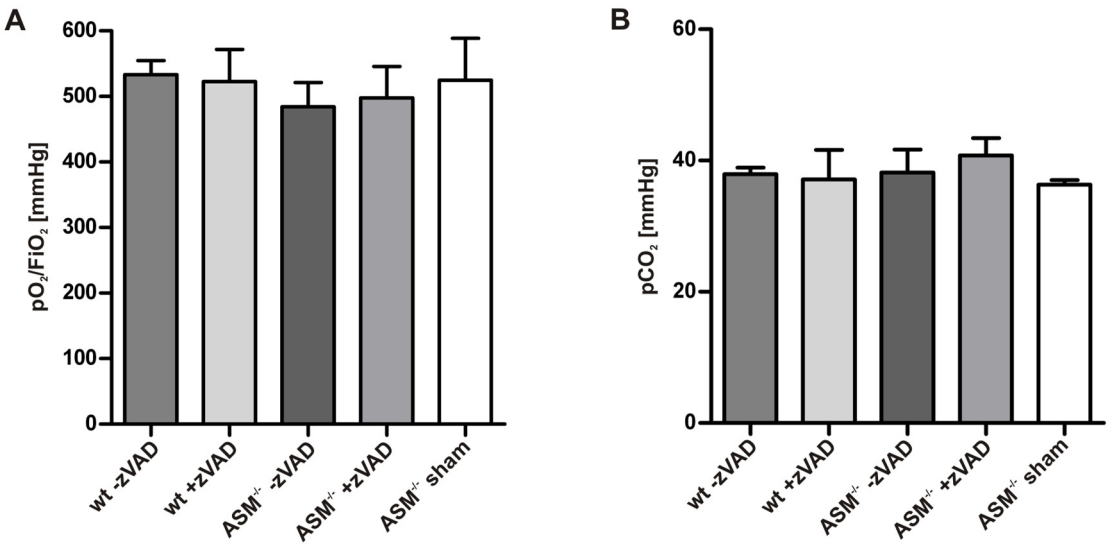

Fig. 3.14: Gas exchange in TNF-treated mice. Arterial pO_2 and pCO_2 were measured after 405 min of ventilation by blood gas analysis. **A.** The Horovitz index, calculated with $FiO_2 = 0.3$, was in a normal range in all subjects. **B.** The pCO_2 levels showed no impairment of gas exchange. All groups, except from the group $ASM^{-/-}$ sham, received 50 µg TNF i.v.. In addition, zVad-fmk was injected i.v. to the groups wt+zVAD and $ASM^{-/-}$+zVAD. (wt -zVAD n=3, wt +zVAD n=3, $ASM^{-/-}$ -zVAD n=5, $ASM^{-/-}$ +zVAD n=5, $ASM^{-/-}$ sham n=5).

3.3.3 Pro-inflammatory mediators

Quantification of pro-inflammatory mediators in the BAL fluid and blood serum was performed by ELISA. TNF was measured to ascertain how much of the 50 µg that had been injected i.v. was present in the circulation and in the lung. Fig. 3.15A shows that at least about 1000 ng/mL TNF were detectable in the plasma in all groups. In some mice in the group wt-zVAD, TNF plasma levels were higher. Of note, higher plasma TNF levels did not correlate with a reduced survival. No TNF was present in the plasma of the group ASM$^{-/-}$ sham. In the BAL, mean TNF levels ranged from around 600 to 1500 pg/mL in the TNF-treated groups (Fig. 3.15D). Compared to the ASM$^{-/-}$sham group, with a mean of 15 pg/mL, relatively high amounts of TNF were found in the alveoli of the TNF-treated groups.

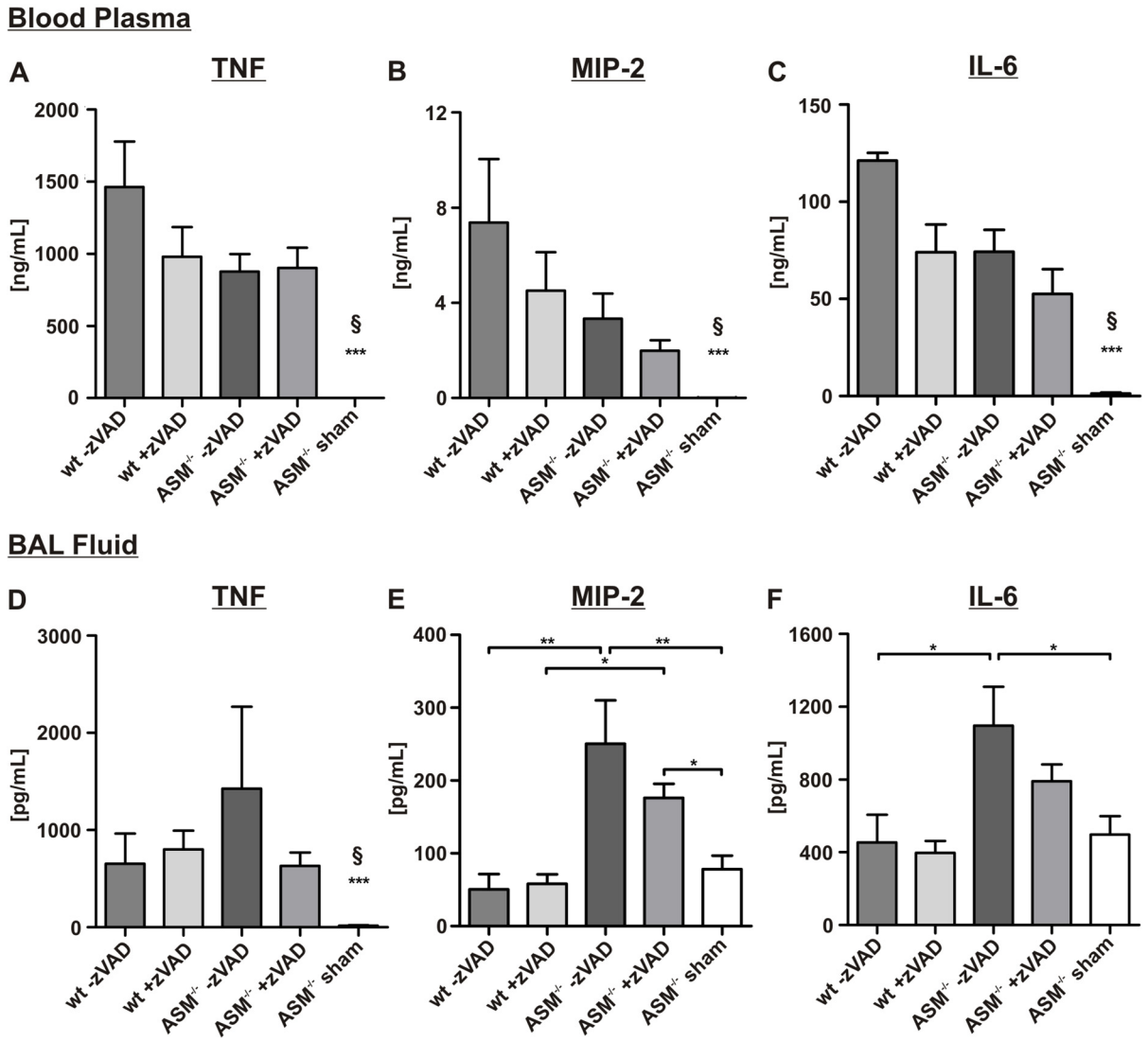

Fig. 3.15: Pro-inflammatory mediators in TNF-treated mice. The cytokines TNF and IL-6 and the chemokine MIP-2 were measured in the BAL fluid and blood plasma by ELISA after 405 min of ventilation. All groups, except from the group ASM$^{-/-}$sham, received 50 µg TNF i.v.. In addition, zVad-fmk was injected i.v. to the groups wt+zVAD and ASM$^{-/-}$+zVAD. (wt -zVAD n=4, wt +zVAD n=5, ASM$^{-/-}$ -zVAD n=5, ASM$^{-/-}$ +zVAD n=5, ASM$^{-/-}$ sham n=6). * $p \leq 0.05$, ** $p \leq 0.01$, § *** $p \leq 0.001$ versus all other groups.

High concentrations of the chemokine macrophage inflammatory protein-2 (MIP-2) were measured in the blood plasma of all groups six hours after TNF-injection, with higher levels in the wt than in the $ASM^{-/-}$ groups (Fig. 3.15B). In contrast, in the lungs MIP-2 was in a very low range (<300 pg/mL) only (Fig. 3.15E). MIP-2 concentrations were at least ten-fold higher in the plasma than in the lavage, indicating that the chemotactic gradient was directed towards the vascular side. Compared to the ventilated sham group, MIP-2 was slightly increased in the BAL of the groups $ASM^{-/-}$-zVAD and $ASM^{-/-}$+zVAD. This was also the case for the BAL IL-6 levels (Fig. 3.15F). Overall, alveolar IL-6 was in a normal range for ventilated mice in all groups and similar to the results shown in the lowV_TRM5 mice in the ventilation study (Fig. 3.5). In the plasma of the untreated sham group, the mean IL-6 was 1350 pg/mL Fig. 3.15C). This is also comparable to data from the first ventilation study. In the groups that were injected with TNF, IL-6 was strongly increased (>50 ng/mL).

3.3.4 Microvascular permeability

In the TNF model, permeability was assessed by an indirect and a direct method. The quantification of neutrophil numbers in the BAL, shown in Fig. 3.16A, served as indirect measure for permeability. Despite of the ventilation, only very few neutrophils had sequestered the lungs of wt mice (1-2%). Neutrophil counts were slightly higher in the groups ASM$^{-/-}$-zVAD (12%) and ASM$^{-/-}$+zVAD (6%). This result could be explained by the higher MIP-2 levels in these groups (Fig. 3.15D). Interestingly, about 45% of the leukocytes in the lungs of the group ASM$^{-/-}$sham were neutrophils, indicating that the phenotype of the ASM$^{-/-}$ mice included alterations in the lungs. The ratio of i.v. injected BSA quantified in the BAL and in the plasma was calculated as direct measure for permeability. The albumin ratio, depicted in (Fig. 3.16B), was < 1 in most of the TNF-treated mice. According to literature [130], this is a normal range for ventilated mice. The albumin data from the TNF model is not comparable to the ventilation study in this thesis, because a different BSA detection ELISA had to be used. The ASM$^{-/-}$sham group differed with a mean albumin ratio of 2.7. These results indicate that the microvascular permeability was not altered by TNF, but was increased per se in ASM$^{-/-}$ mice. Moreover, TNF-treatment seemed to have protected these mice from neutrophil recruitment and increased permeability, promoting the idea that the high systemic TNF-levels induced formation of a chemotactic gradient that was directed towards the vascular side.

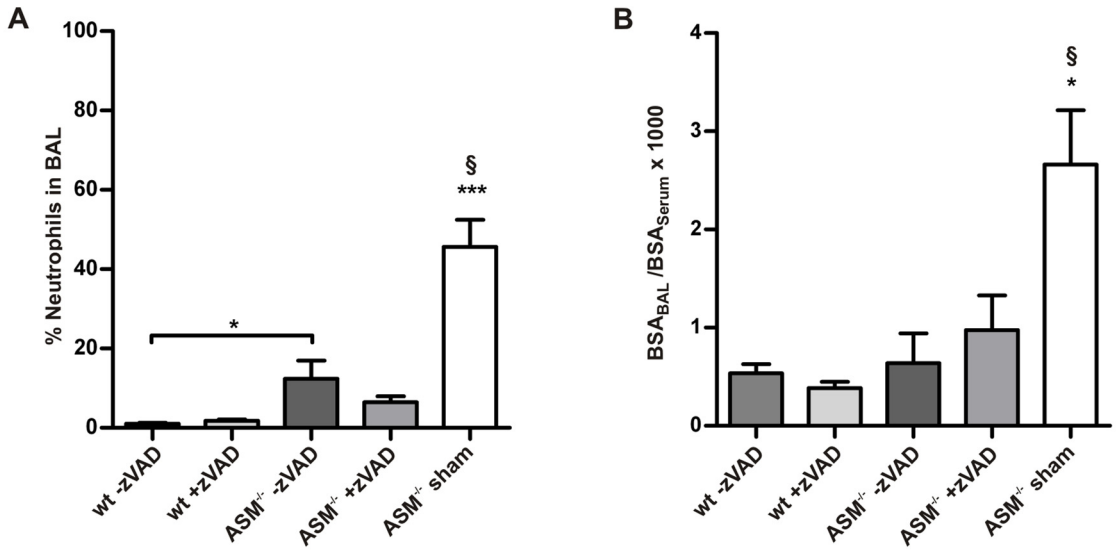

Fig. 3.16: Microvascular permeability in TNF-treated mice. A. Neutrophils in the BAL after cytospin preparation. The percentage of neutrophils from 400 total leukocytes was calculated. **B.** Albumin influx into the lungs shown as ratio of bovine serum albumin (BSA) quantified in the BAL and in the blood plasma. All groups, except from the group ASM$^{-/-}$sham, received 50 µg TNF i.v.. In addition, zVad-fmk was injected i.v. to the groups wt+zVAD and ASM$^{-/-}$+zVAD. (wt -zVAD n=5, wt +zVAD n=4, ASM$^{-/-}$ -zVAD n=4, ASM$^{-/-}$ +zVAD n=5, ASM$^{-/-}$ sham n=6). §* $p \leq 0.05$ versus all other groups, § *** $p \leq 0.001$ versus all other groups.

3.3.5 Lung histopathology

Histopathological examination revealed that the alveoli of ASM$^{-/-}$ mice contained enlarged lipid-storing macrophages, so called foamy cells. These cells were found in TNF-treated and untreated mice (Fig. 3.17B, C), demonstrating that their appearance was not induced by TNF. The lung injury score showed that no severe injury was present in any group, further indicating that the high systemic TNF levels did not harm the lungs. The only criterion according to the scoring system, found in all lungs, was recruitment of interstitial neutrophils.

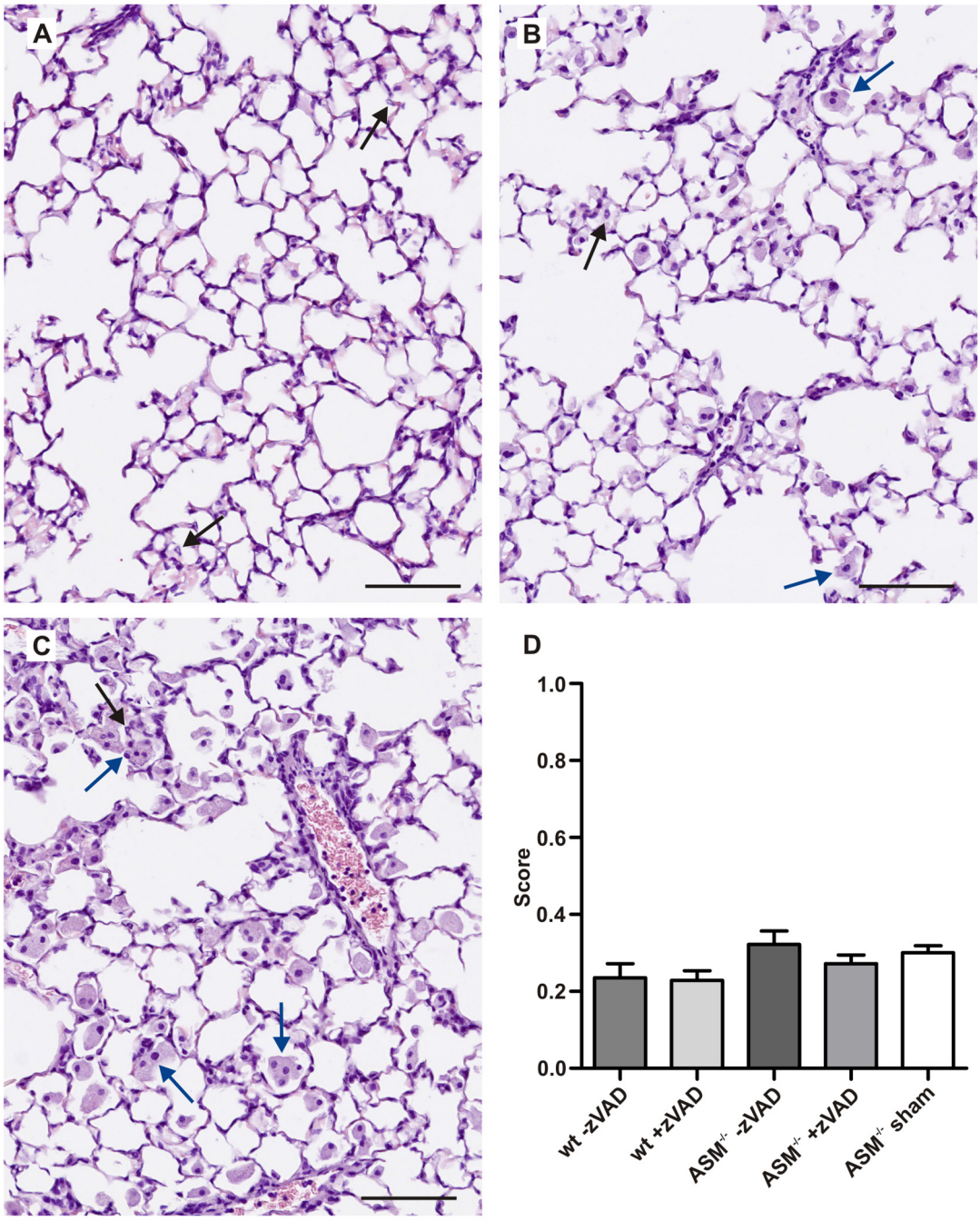

Fig. 3.17: Influence of TNF and ASM on lung histopathology. Representative HE-stained sections from: **A.** wt-zVAD, **B.** ASM$^{-/-}$-zVAD, **C.** ASM$^{-/-}$sham. Black arrows indicate neutrophils, blue arrows enlarged macrophages. Scale bars: 100 µm; magnification: 200x. **D.** The injury score was assessed as described in Fig. 3.8.

3.3.6 Cell death in the lung

Cell death is shown in Fig. 3.18 as relative percentage compared to a positive control that was assumed as 100%. Independent from TNF-treatment, relative cell death was about twice as high in all ASM-deficient groups compared to the wt groups. Of note, also the $ASM^{-/-}$sham mice revealed a higher level of cell death than the TNF-treated wt mice. The caspase-inhibitor zVAD-fmk showed a small, although not significant, inhibitory effect on relative cell death.

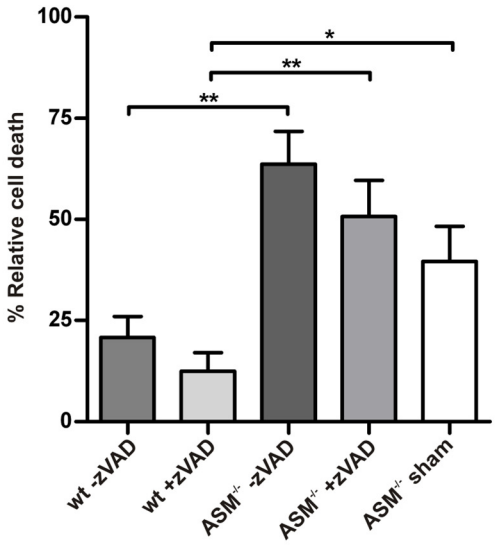

Fig. 3.18: Relative cell death in the lungs of TNF-treated mice. Cell death, including apoptosis and necrosis, was quantified in homogenised lung tissue with an ELISA that detects mono- and olignucleosomes. All groups, except from the group $ASM^{-/-}$sham, received 50 µg TNF i.v.. In addition, zVad-fmk was injected i.v. to the groups wt+zVAD and $ASM^{-/-}$+zVAD. (wt -zVAD n=5, wt +zVAD n=4, $ASM^{-/-}$ -zVAD n=5, $ASM^{-/-}$ +zVAD n=5, $ASM^{-/-}$ sham n=6). * $p \leq 0.05$, ** $p \leq 0.01$.

3.3.7 Arterial acid base status

Measurement of arterial pH and HCO_3^- revealed that all TNF-treated mice suffered from severe metabolic acidosis (Fig. 3.19). Acidosis is defined as an arterial blood pH < 7.3. The metabolic origination was further indicated by the fact that these mice were normocapnic, as shown above in Fig. 3.14B. One cause of metabolic acidosis is an impairment of the microcirculation as given during circulatory shock. The presence of metabolic acidosis after TNF-treatment indicates that TNF could have induced septic shock in this model.

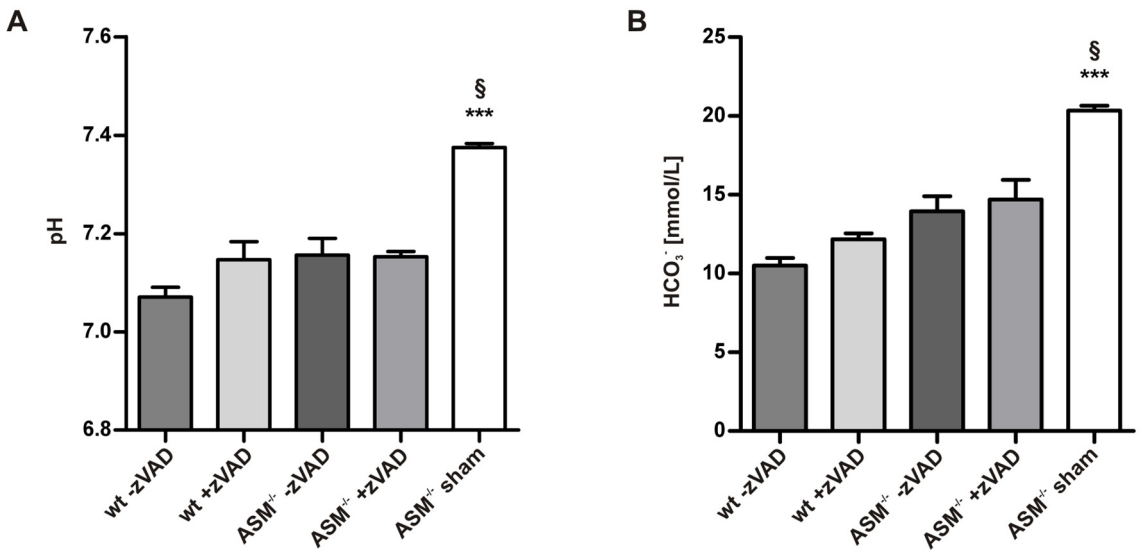

Fig. 3.19: Arterial pH and bicarbonate values in TNF-treated mice. The acid-base status was examined by blood gas analysis at the end of the experiment (405 min). Normal values in healthy mice are: pH = 7.37, bicarbonate (HCO_3^-) = 22 mmol/L. All groups, except from the group $ASM^{-/-}$sham, received 50 µg TNF i.v.. In addition, zVad-fmk was injected i.v. to the groups wt+zVAD and $ASM^{-/-}$+zVAD. (wt -zVAD n=3, wt +zVAD n=3, $ASM^{-/-}$ -zVAD n=5, $ASM^{-/-}$ +zVAD n=5, $ASM^{-/-}$ sham n=5). § *** $p \leq 0.001$ versus all other groups.

3.3.8 Procalcitonin plasma levels

The sepsis marker procalcitonin (PCT), measured in the blood plasma six hours after TNF injection, was in a range that indicates sepsis (>2000 ng/L) in all TNF-treated animals. No PCT was detectable in the control group $ASM^{-/-}$sham. These data support that the injected TNF dosage sufficed to induce sepsis.

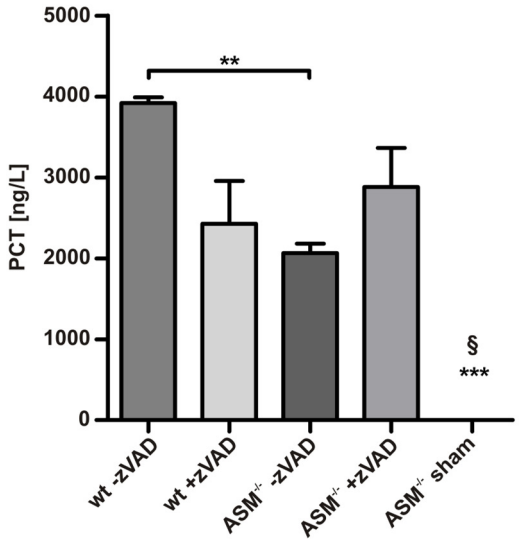

Fig. 3.20: Procalcitonin levels in TNF-treated mice. Procalcitonin (PCT) was quantified in the blood plasma with a commercial ELISA kit for mouse PCT. Levels above 2000 ng/L indicate sepsis. All groups, except from the group $ASM^{-/-}$sham, received 50 µg TNF i.v.. In addition, zVad-fmk was injected i.v. to the groups wt+zVAD and $ASM^{-/-}$+zVAD. (wt -zVAD n=4, wt +zVAD n=4, $ASM^{-/-}$ -zVAD n=5, $ASM^{-/-}$ +zVAD n=5, $ASM^{-/-}$ sham n=6). ** $p \leq 0.01$, § *** $p \leq 0.001$ versus all other groups.

3.3.9 Influence of TNF on the systemic circulation

TNF-treatment impaired the systemic circulation in wt, but not in ASM$^{-/-}$ mice. Fig. 3.21B shows that the MAP decreased strongly over time in both wt groups, reaching critically low values about four hours after TNF injection. MAP in ASM$^{-/-}$ mice stayed stable, indicating that these mice were protected from the cardiovascular effects. The HF, which was recorded independently from the MAP, ascended in all TNF treated groups, with a significantly higher increase in the groups wt-zVAD and wt+zVAD. Given the very low MAP in these groups the increase in HF can be interpreted as reflex tachycardia. The depression of the systemic circulation further supports that TNF induced septic shock.

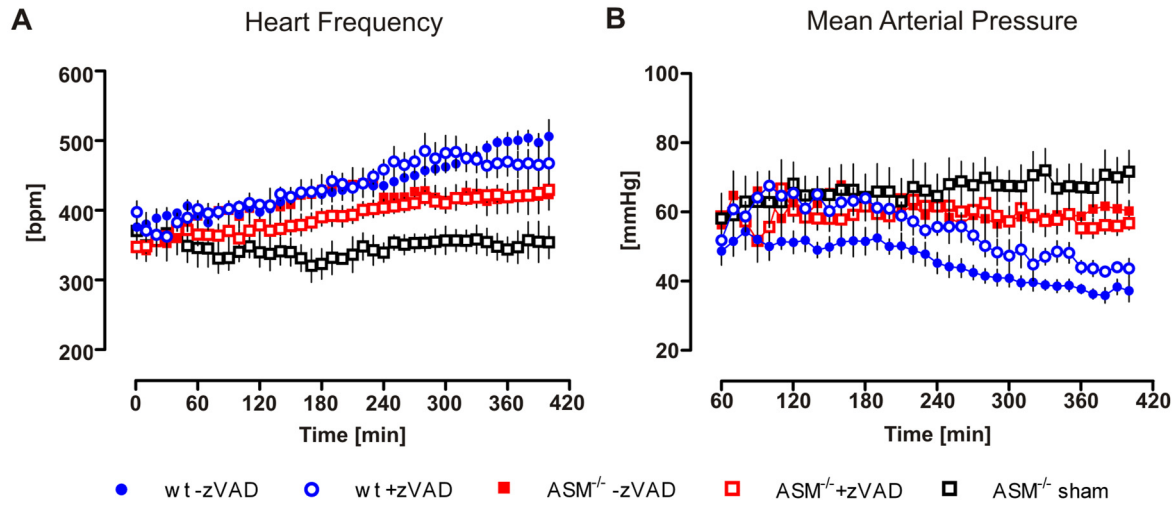

Fig. 3.21: Cardiovascular parameters after TNF-treatment. TNF was injected at 45 min to all groups, except from the group ASM$^{-/-}$sham. The groups wt+zVAD and ASM$^{-/-}$+zVAD additionally received 250µg and 100µg zVad-fmk at 30 min and 105 min of ventilation, respectively. **A.** The heart frequency (HF) was calculated from the electrocardiogram that was recorded permanently. **B.** Mean arterial pressure (MAP) was measured in the carotid artery. Due to the preparation time for the arterial catheter, pressure could not be measured from the beginning of the experiment. Cardiovascular parameters were analysed with two-way ANOVA. The influence of ASM-deficiency was highly significant with $p \leq 0.01$ for HF and $p \leq 0.001$ for MAP. TNF-treatment had a significant effect on HF with $p \leq 0.001$ (n=5 in all groups). Caspase-inhibition with zVAD-fmk had no significant influence.

3.3.10 Survival analysis of TNF-treated mice

The survival analysis was performed to investigate the influence of ASM-deficiency on the survival in TNF-treated mice (Fig. 3.22). None of the ASM$^{-/-}$ mice died during the experiment. In contrast, four of the wt mice died within the 405 min of ventilation, whereof two had received zVAD-fmk and two had not. The survival curves of the two strains differed significantly ($p < 0.05$), demonstrating that ASM-deficiency had a protective effect on TNF-induced lethality.

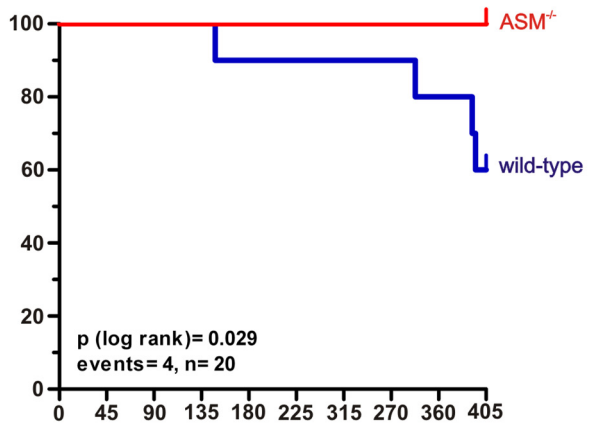

Fig. 3.22: Survival in TNF-treated mice. Survival was compared by univariate Kaplan-Meier analysis in TNF-treated wt and ASM$^{-/-}$ mice. The -zVAD and +zVAD treated groups of each strain were pooled, because zVAD-fmk had no influence on survival, resulting in n = 10 subjects in each group. The control group ASM$^{-/-}$sham was not included. All TNF-treated ASM$^{-/-}$ mice survived, whereas 4 wt mice (2 wt-zVAD and 2 wt+zVAD) died during the experiment. Vertical ticks indicate censored cases at 405 min.

3.3.11 Nitric oxide levels in the plasma

Quantification of nitric oxide (NO) levels, a gaseous signalling molecule with vasodilatative properties, showed only minor differences within the groups that had been treated with TNF. Neither the ASM-deficiency nor the caspase inhibition had a significant influence. Of note, only minor concentrations of NO were detected in the group ASM$^{-/-}$sham, indicating that TNF had induced the release of NO, which probably contributed to the development of shock. One limitation of this assay is that haemoglobin interferes with NO reduction, leading to decreased NO levels in haemolysed plasma samples [149]. Haemolysis can be induced by sepsis and was observed in several blood samples. Therefore, it cannot be excluded that differences between the groups were masked due to haemolysis.

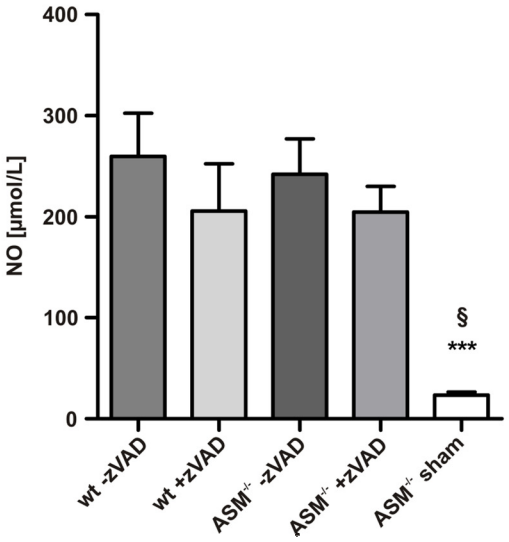

Fig. 3.23: Total nitric oxide (NO) in the plasma of TNF-treated mice. The stable NO metabolites nitrite and nitrate were quantified in the blood plasma, which was retrieved at the end of the experiment. All groups, except from the group $ASM^{-/-}$sham, received 50 µg TNF i.v.. In addition, zVad-fmk was injected i.v. to the groups wt+zVAD and $ASM^{-/-}$+zVAD. (wt -zVAD n=4, wt +zVAD n=4, $ASM^{-/-}$ -zVAD n=5, $ASM^{-/-}$ +zVAD n=5, $ASM^{-/-}$ sham n=6). § *** $p \leq 0.001$ versus all other groups.

3.3.12 Acid sphingomyelinase activity in the urine

The activity of ASM in the urine was measured as indirect proof for the genotypes of the examined mice. An activity level < 300 pmol/mg/h was regarded as zero level. Fig. 3.24 illustrates that no ASM activity was present in the $ASM^{-/-}$ mice in contrast to the wt mice, where ASM activity was detected in all subjects. The low activity range in the wt mice was possibly due to the freezing and thawing of the samples.

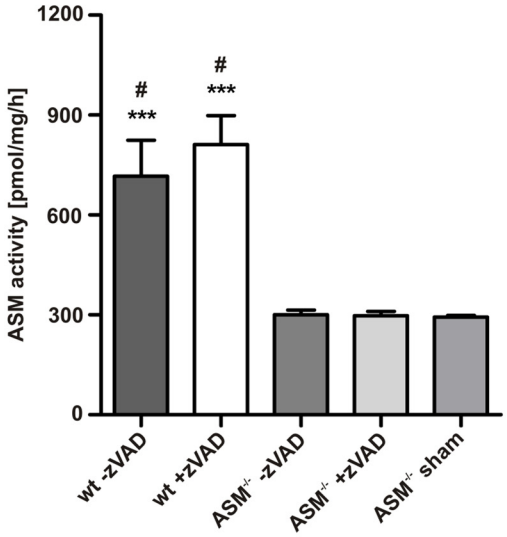

Fig. 3.24: ASM activity in the urine of TNF-treated mice. ASM activity was measured with radioactively labelled sphingomyelin as substrate. Activity levels ≤ 300 were regarded as zero level. All groups, except from the group $ASM^{-/-}$sham, received 50 µg TNF i.v.. In addition, zVad-fmk was injected i.v. to the groups wt+zVAD and $ASM^{-/-}$ +zVAD. (wt -zVAD n=5, wt +zVAD n=5, $ASM^{-/-}$ -zVAD n=5, $ASM^{-/-}$ +zVAD n=5, $ASM^{-/-}$ sham n=6). #*** $p \leq 0.001$ versus $ASM^{-/-}$ -zVAD, $ASM^{-/-}$ +zVAD and $ASM^{-/-}$ sham.

3.4 The severe acid model

3.4.1 Lung mechanics

Measurement of lung mechanics revealed that acid with pH 1.5 had a strong influence on the lung (Fig. 3.25).

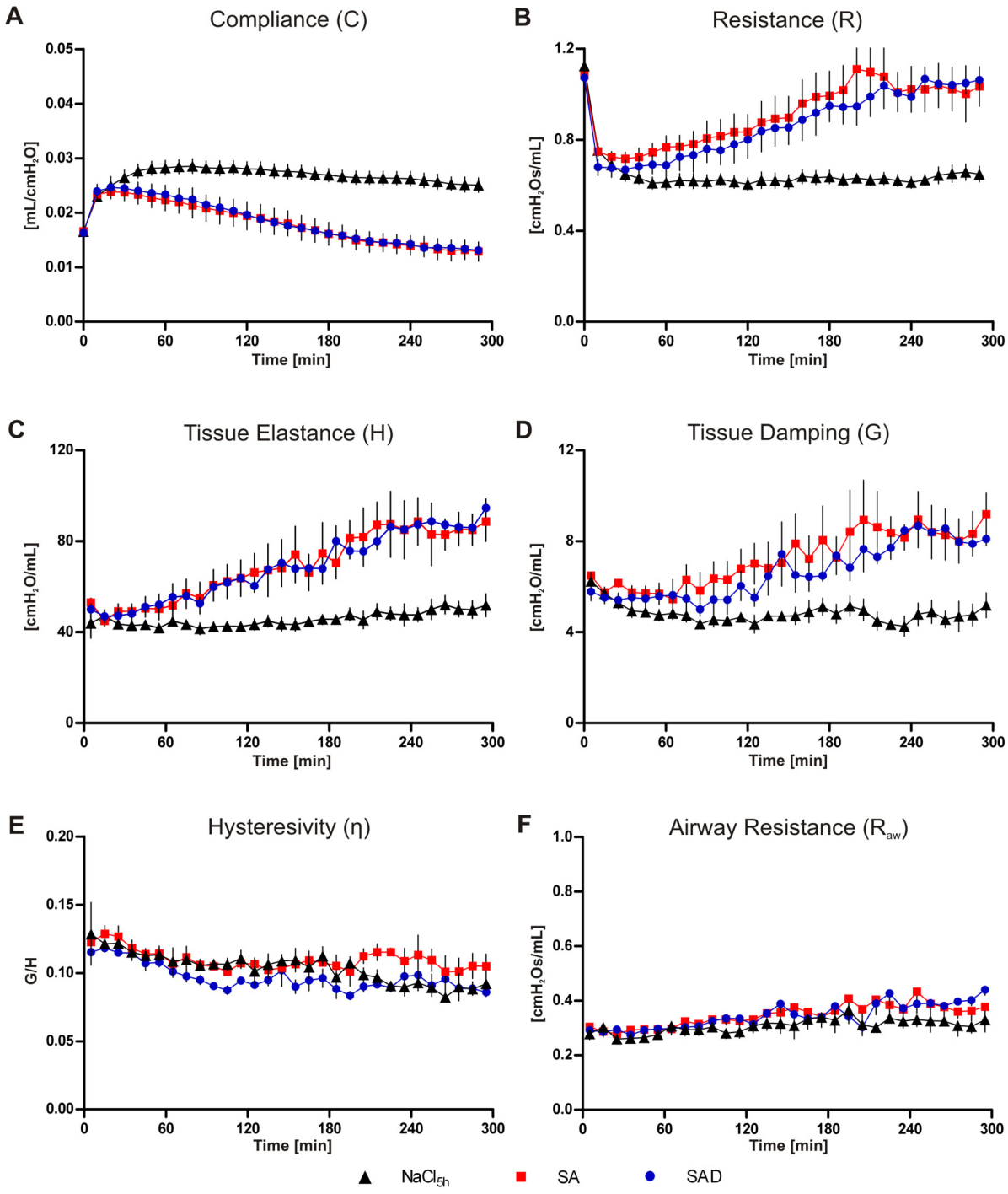

Fig. 3.25: Lung mechanics in the severe acid model. Mice were instilled i.t. with either 50 µL of acid pH 1.5 (SA) or 0.9% NaCl ($NaCl_{5h}$) and were ventilated for 300 min at V_T = 16 mL/kg, f = 90 min^{-1}, PEEP = 2 cmH_2O and FiO_2 = 0.3. One acid-instilled group was medicated with 1 mg/kg dexamethasone (SAD). Lung mechanics were measured using the forced oscillation technique. (n = 5 in all groups). Please see Table 6.3 in the supplement for p-value ranges of group comparisons.

C as well as R worsened permanently over time in the group SA (severe acid), reaching critical ranges with a compliance < 0.02 mL/cmH_2O and a resistance > 1.0 cmH_2Os/mL after about two hours. The NaCl-instilled control group ($NaCl_{5h}$) showed stable lung functions, demonstrating that the impairment of lung functions was not due to the amount of fluid that had been administered to the lungs. The third group in this study was treated with 1 mg/kg of the glucocorticoid dexamethasone (SAD) i.v.. Interestingly, this treatment had no influence on lung mechanics. The lung impedance measurement clarified that acid-instillation had strongly affected H and G, without influencing R_{aw}. H and G almost doubled during five hours in both acid-instilled groups SA and SAD and differed significantly from the group $NaCl_{5h}$ ($p \leq 0.001$). Notably, this was not reflected in a change in hysteresivity, which stayed almost unchanged in all three groups.

3.4.2 Cardiovascular parameters

HF and MAP were relatively stable in the acid and NaCl treated groups as shown in Fig. 3.26. The slight peak in both parameters at 230 min was due to the i.v. injection of HSA. Dexamethasone caused a small increase in MAP, which was accompanied by a higher urine production in the group SAD. However, the difference in MAP was not significant.

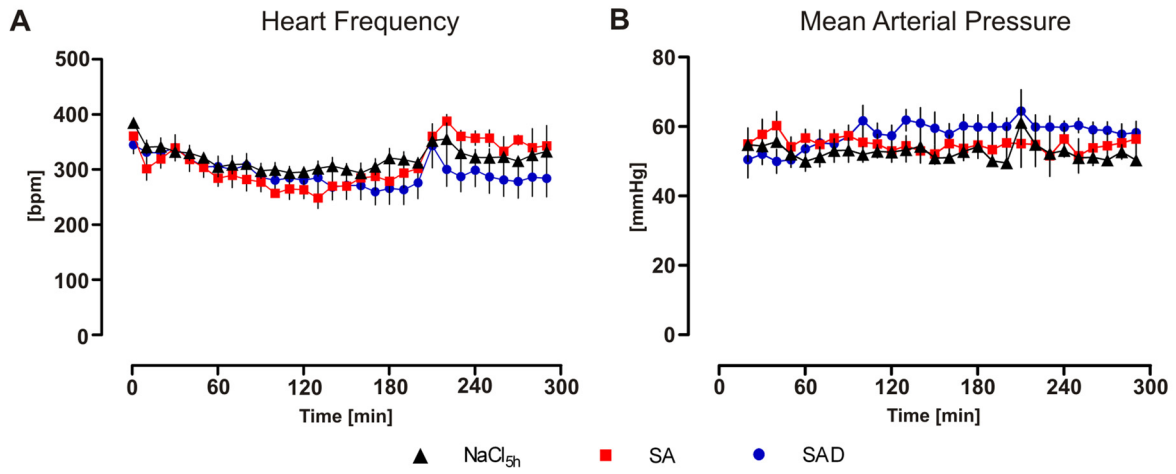

Fig. 3.26: Cardiovascular parameters in the severe acid model. A. Heart frequency (HF) and **B.** Mean arterial pressure (MAP) were recorded as described above (Fig. 3.21). $NaCl_{5h}$: NaCl-instilled control group, SA: acid-instilled group, SAD: acid-instilled group treated with dexamethasone. (n = 5 in all groups).

3.4.3 Oxygenation

The Horovitz index was between 400 and 500 mmHg in the $NaCl_{5h}$ control group (Fig. 3.27). According to the blood gas results in the ventilation study, the oxygenation index ranged between 500 and 600 mmHg in untreated lungs ventilated with 16 mL/kg. This indicates that application of 50 µL fluid caused a small impairment in gas exchange in the acid model. In both acid-instilled groups SA and SAD, oxygenation was strongly decreased to around 200 mmHg, demonstrating that the gas exchange in the lung was strongly impaired after application of acid with pH 1.5. Dexamethasone failed to improve oxygenation.

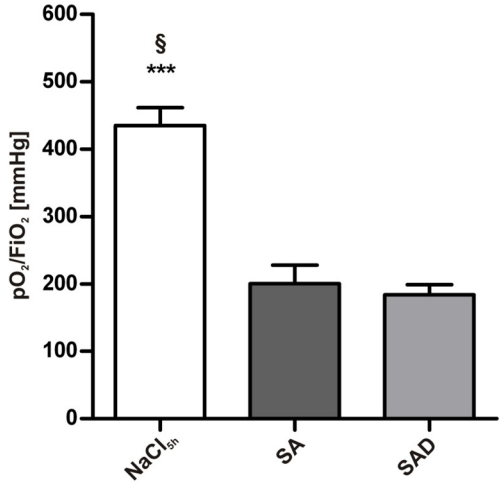

Fig. 3.27: Oxygenation in the severe acid model. The Horovitz index was calculated with the arterial $p0_2$ measured after 300 min of ventilation with $FiO_2 = 0.3$. $NaCl_{5h}$: NaCl-instilled control group, SA: acid-instilled group, SAD: acid-instilled group treated with dexamethasone. (n = 5 in all groups). § *** $p \leq 0.001$ versus all other groups.

3.4.4 Pro-inflammatory mediators

The cytokine IL-6 was strongly increased in the BAL fluid of the acid-treated SA mice, compared to the NaCl5h group (Fig. 3.28A). Plasma IL-6 levels were elevated as well, but to a lesser degree (Fig. 3.28D). In the BAL of the dexamethasone-treated group SAD, IL-6 was significantly lower than in the group SA, reaching the niveau of the control group NaCl5h. In the plasma of the group SAD, the IL-6 concentration was even lower than in the NaCl-treated control group. Acid-instillation caused also a clear increase of the chemokine KC in the BAL and in the plasma (Fig. 3.28B, E). This was not the case after dexamethasone injection. The susceptibility of the IL-6 and KC levels to dexamethasone treatment shows that the glucocorticoid had an anti-inflammatory effect and was actually effective. Interestingly, also TNF was markedly elevated in the BAL fluid after acid instillation (Fig. 3.28C). TNF levels were lower in the group SAD than in the group SA, though the difference was not significant.

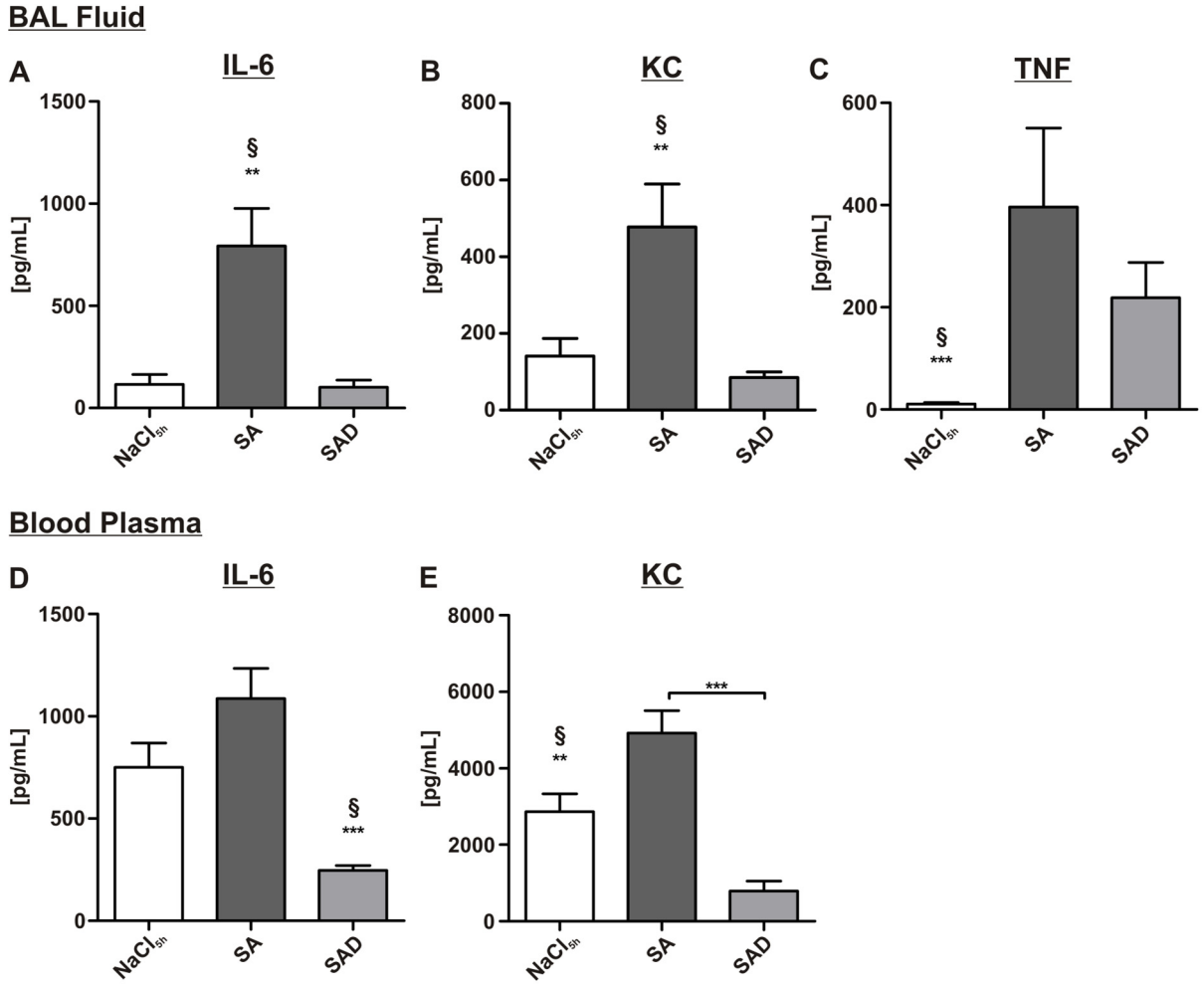

Fig. 3.28: Pro-inflammatory mediators in the severe acid model. The cytokines IL-6 and TNF and the chemokine KC were measured in the BAL fluid and blood plasma with ELISA after 300 min of ventilation. TNF was below the detection limit in the blood plasma. $NaCl_{5h}$: NaCl-instilled control group, SA: acid-instilled group, SAD: acid-instilled group treated with dexamethasone. (n = 5 in all groups). *** $p \leq 0.001$; § ** $p \leq 0.01$, § *** $p \leq 0.001$ versus all other groups.

3.4.5 Microvascular permeability

Microvascular permeability was strongly affected in the severe acid model. Neutrophil numbers were clearly increased in the acid-treated mice compared to the NaCl controls (Fig. 3.29). Correspondingly, also the albumin influx was at a very high level after acid-treatment. Dexamethasone significantly decreased these effects revealing a protective function on the acid-challenged alveolar-capillary barrier.

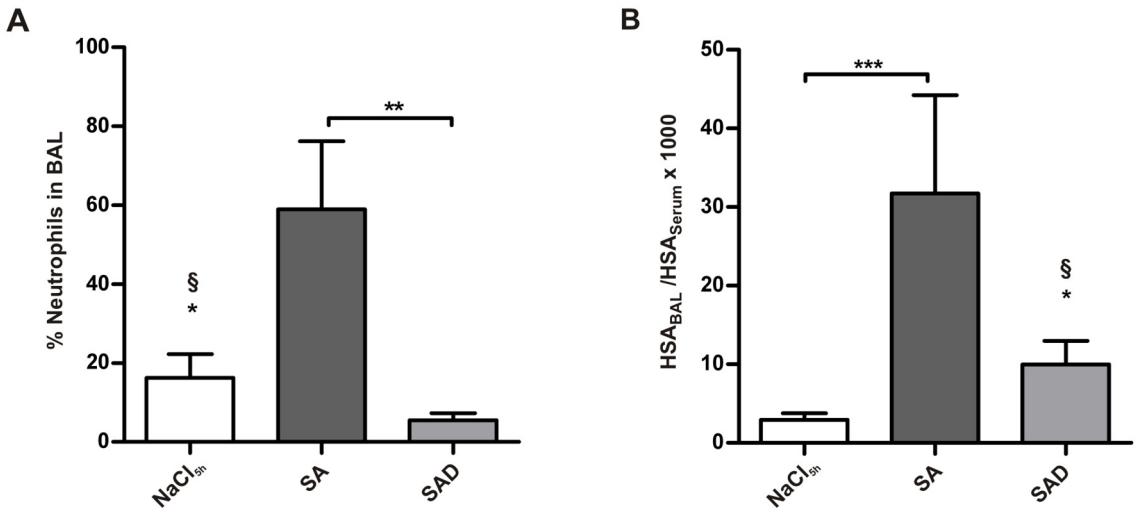

Fig. 3.29: Neutrophil counts and albumin influx in the severe acid model. A. Neutrophils were quantified in the BAL fluid after cytospin preparation and differential staining as described above Fig. 3.16. **B.** Albumin influx into the lungs shown as ratio of human serum albumin (HSA) quantified in the BAL and in the blood plasma. $NaCl_{5h}$: NaCl-instilled control group, SA: acid-instilled group, SAD: acid-instilled group treated with dexamethasone. (n = 5 in all groups). ** $p \leq 0.01$, *** $p \leq 0.001$, § * $p \leq 0.05$ versus all other groups.

3.4.6 Lung histopathology

Acid-induced lung injury was characterised mainly by accumulation of intra-alveolar and interstitial neutrophils. Moderate thickening of alveolar septae was only observed in some regions of the acid-treated lungs (Fig. 3.30A). Although dexamethasone failed to prevent physiological dysfunction, the lung injury score was significantly lower in the steroid-treated group (Fig. 3.30B, D). NaCl-instillation had no effect distinct from ventilation-induced alterations (Fig. 3.30C), which were alveolar septal thickening and neutrophil infiltration.

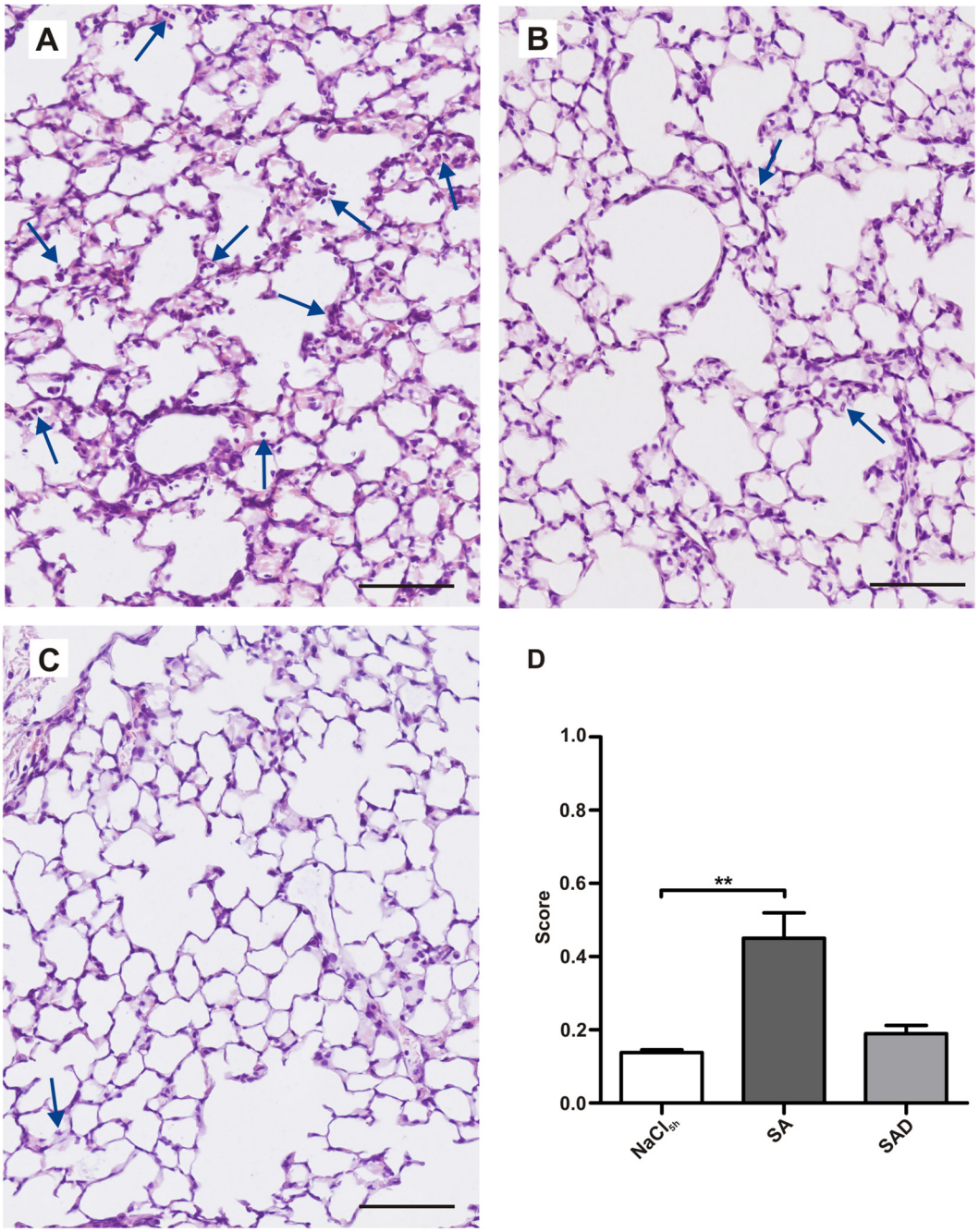

Fig. 3.30: Lung histopathology in the severe acid model. Representative HE-stained sections from: **A.** Acid instilled mouse (SA), **B.** Acid-instilled, dexamethasone-treated mouse (SAD), **C.** NaCl-instilled mouse ($NaCl_{5h}$). **D.** Lung injury score, determined as described above Fig. 3.8. Blue arrows indicate neutrophils, scale bars: 100 µm; magnification: 200x. ($NaCl_{5h}$ n=5, SA n=4, SAD n=5). ** $p \leq 0.01$.

3.5 The moderate acid model

3.5.1 Establishment of the moderate acid model

The strongly impaired lung functions and resulting hypoxemia, which were not susceptible to steroid therapy, indicated that the injury induced within 300 min with an acid of pH 1.5 was extremely severe. Therefore, the next approach was to establish an attenuated acid model. The only feasible method to achieve this was increasing the pH of the acid. As it is known from literature, acid-induced lung injury is pH-dependent and does not occur with a pH > 2.5 [63]. In consequence, the pH was increased only slightly to pH 1.8 in this thesis. As a result, the oxygenation was no longer significantly different from the NaCl-instilled control mice after 300 min of ventilation (data not shown). Since lung functions worsened continuously over time, the next step was to find the right point of time to terminate the experiment after onset of hypoxemia. The fact that blood gas measurements could not be performed during the experiments led to the question, what else could indicate whether hypoxemia was present. Analysis of data from 50 acid- or NaCl-instilled mice in this study revealed that the pulmonary compliance and the Horovitz ratio correlated well with each other ($p < 0.0001$) (Fig. 3.31). A compliance < 0.02 mL/cmH_2O was associated with an oxygenation index ≤ 300 mmHg, indicating lung injury. In consequence, mice were instilled with acid pH 1.8 and ventilated until the compliance was < 0.02 mL/cmH_2O. In preliminary experiments this was the case after 330 min. Thus, the second acid study was performed with acid pH 1.8 and a duration of 330 min.

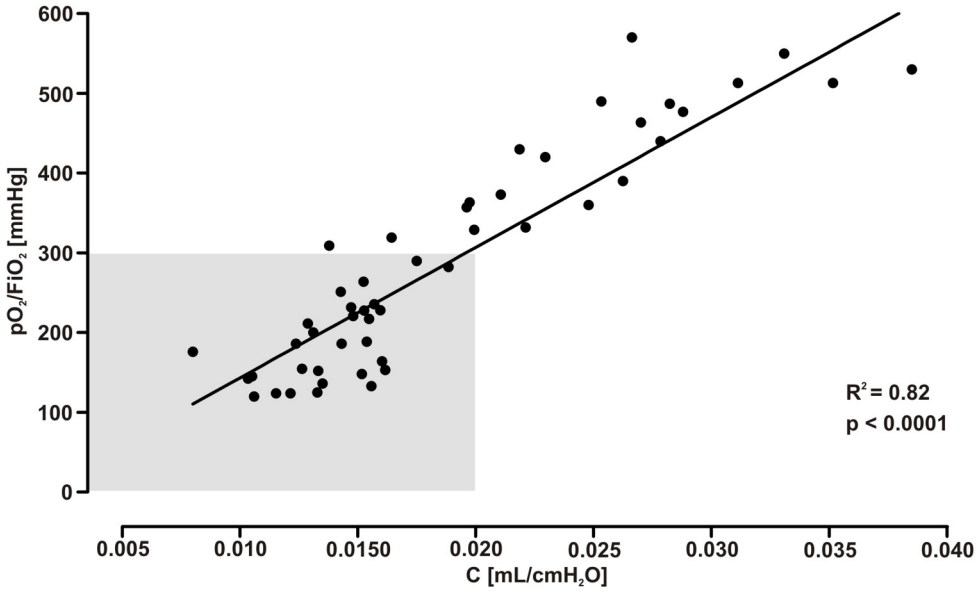

Fig. 3.31: Correlation of pulmonary compliance (C) with the Horovitz index (pO_2/FiO_2). Data were retrieved from mice (n = 50), which were instilled either with 50 µL of acid or 0.9% NaCl and were then ventilated for 5-6 h. The grey box indicates that a compliance < 0.02 mL/cmH_2O was associated with hypoxemia (pO_2/FiO_2 ≤ 300 mmHg). R^2: goodness of fit, Pearson's r = 0.91.

3.5.2 Lung mechanics

Instillation of acid with pH 1.8 resulted in impaired lung mechanics, although to a lesser extent than acid with pH 1.5, as depicted in Fig. 3.32.

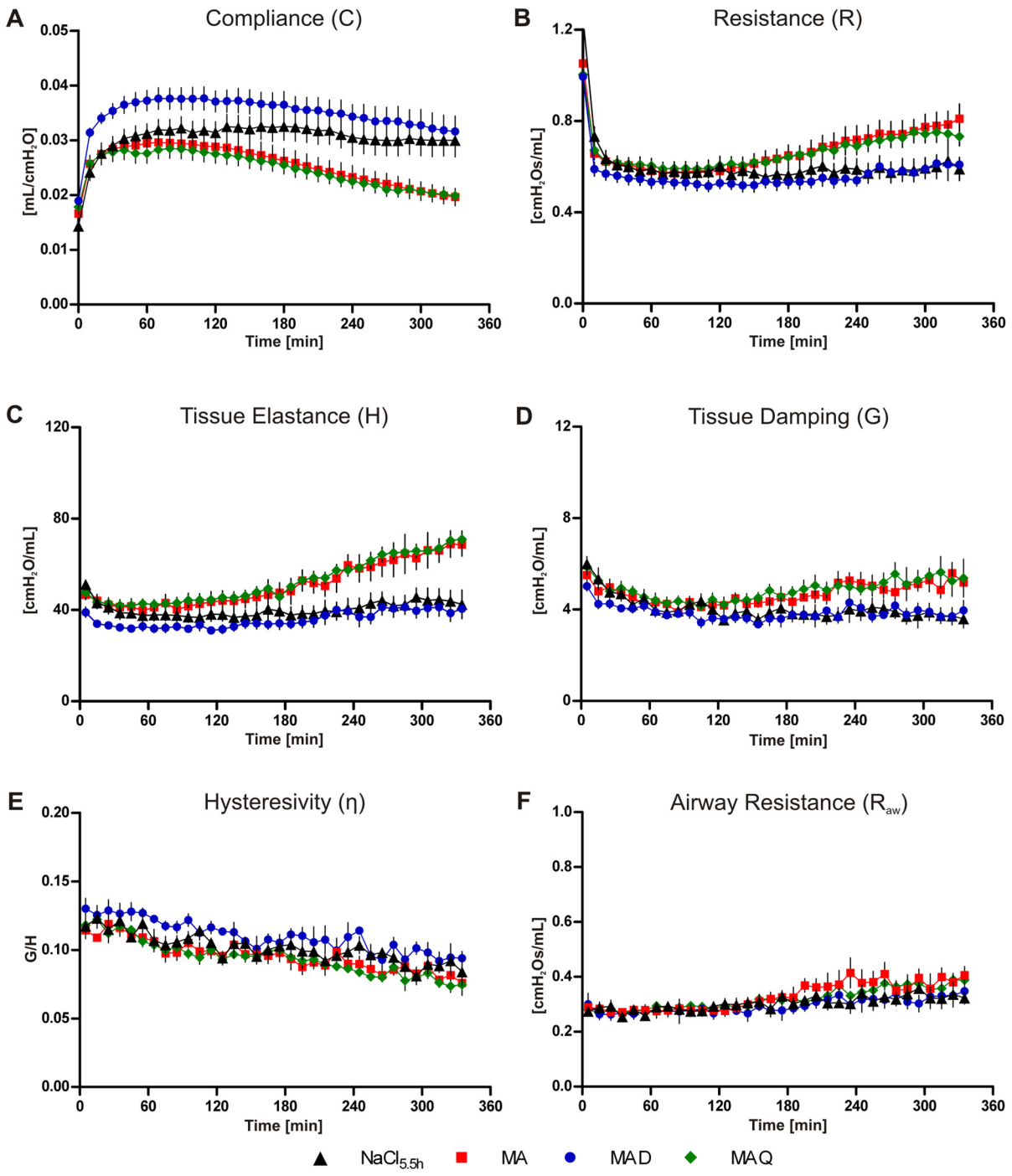

Fig. 3.32: Lung mechanics in the moderate acid model. Mice received 50 µl of 0.9% NaCl ($NaCl_{5.5h}$) or acid at pH 1.8 i.t. (MA) and were ventilated for 330 min at V_T = 16 mL/kg, f = 90 min^{-1}, PEEP = 2 cmH_2O and FiO_2 = 0.3. One group of acid-instilled mice was treated with 1 mg/kg dexamethasone (MAD) and one with 20 mg/kg Quinine (MAQ). Lung mechanics were assessed with the forced oscillation technique. ($NaCl_{5.5h}$ n=5, MA n=6, MAD n=5, MAQ n=6). Please see Table 6.4 in the supplement for p-value ranges of group comparisons.

In the acid-treated group MA, C was reduced to around 0.02 mL/cmH_2O after 330 min, so that experiments were terminated at this time point under the assumption that this compliance level correlated with a Horovitz index ≤ 300 mmHg. R increased continuously, but stayed below 1 cmH_2Os/mL. Impedance measurement showed that H increased by about 50% of the initial value, which is only half as much as in the severe model. Of note, the effect on G was only very small in this model. Further, hysteresivity and R_{aw} changed only in physiologically unimportant ranges. Interestingly, the treatment with dexamethasone successfully prevented the acid-induced alterations of lung mechanics. Although a very slight steady loss of C was recorded, all other parameters were comparable to the results in the $NaCl_{5.5h}$ group, which served as control and showed very stable lung functions. R, C, G and H in the $NaCl_{5.5h}$ and MAD group were significantly different from the group MA ($p < 0.01$). After the successful treatment with the glucocorticoid, a second therapeutical approach was tested using quinine. However this approach did not improve the loss of function due to acid-instillation. R as well as the tissue properties C, G and H were impaired in the group MAQ to the same degree as in the group MA.

3.5.3 Cardiovascular parameters

As already demonstrated in the severe acid model, HF and MAP were largely unaffected by acid-instillation (Fig. 3.33). HSA-injection at 240 min caused a small peak in HF and BP in some mice. Interestingly, dexamethasone increased the MAP significantly compared to the control group and the group MA, although this had no clear consequence for the HF.

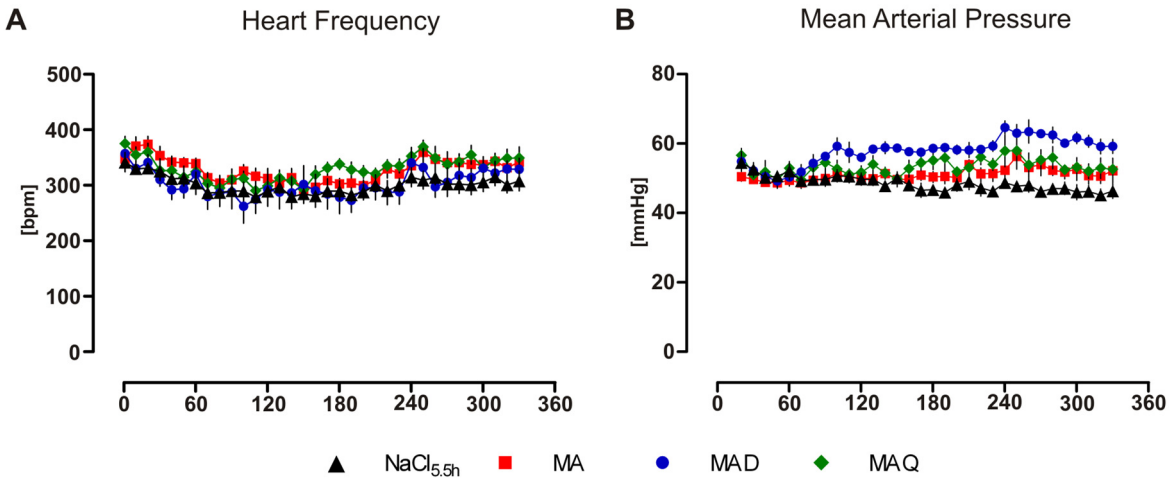

Fig. 3.33: Cardiovascular parameters in the moderate acid model. A. Heart frequency (HF) and **B.** mean arterial pressure (MAP) were recorded as described above (Fig. 3.21). $NaCl_{5.5h}$: NaCl-instilled control group, MA: acid-instilled group, MAD: acid-instilled group treated with dexamethasone, MAQ: acid-instilled group treated with quinine. Mixed model analysis revealed that the group MAD had a significantly increased MAP compared to the groups $NaCl_{5.5h}$ ($p \leq 0.001$) and MA ($p \leq 0.05$). ($NaCl_{5.5h}$ n=5, MA n=6, MAD n=5, MAQ n=6).

3.5.4 Oxygenation

The Horovitz index was around 300 mmHg in the acid-treated group MA after 330 min of ventilation, indicating that the approach of correlating compliance with oxygenation to evaluate onset of lung injury, had been successful (Fig. 3.34). Oxygenation was around 500 mmHg in the control group $NaCl_{5.5h}$ and thereby almost comparable to uninstilled lungs. The glucocorticoid therapy successfully improved oxygenation, which was in a comparable range in the group MAD and in the control group, whereas quinine was not effective.

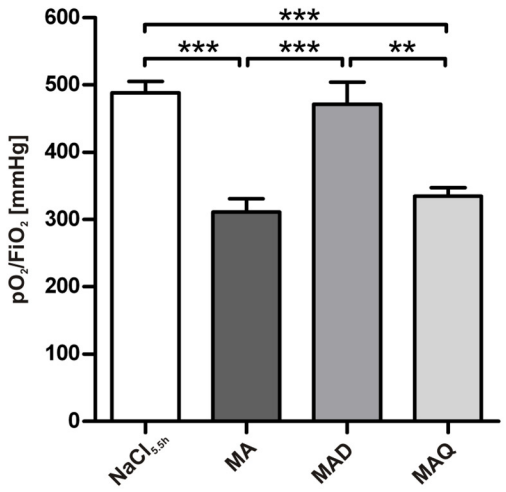

Fig. 3.34: Oxygenation in the moderate acid model. The Horovitz index was calculated with the arterial pO_2 measured after 330min of ventilation by blood gas analysis and FiO_2 = 0.3. $NaCl_{5.5h}$: NaCl-instilled control group, MA: acid-instilled group, MAD: acid-instilled group treated with dexamethasone, MAQ: acid-instilled group treated with quinine. ($NaCl_{5.5h}$ n=5, MA n=6, MAD n=5, MAQ n=6). ** $p \leq 0.01$, *** $p \leq 0.001$.

3.5.5 Pro-inflammatory mediators

The mediators IL-6, TNF and KC clearly responded to the acid challenge of the lungs, as indicated by the significant increase between the control group $NaCl_{5.5h}$ and the group MA (Fig. 3.35). This response was weaker than with acid pH 1.5 (Fig. 3.28), reflecting that the injury was attenuated with acid pH 1.8. TNF was again below the detection limit in the blood plasma of all groups. IL-6 and KC were increased in the acid-instilled group MA. IL-6 was in the same range as in the severe model, but the concentration of the chemokine KC was lower than before, showing that the systemic response to acid pH 1.8 was mitigated as well. The liberation of all three mediators in the lung was strongly reduced by dexamethasone to a level that was comparable to the control group. This effect was also observed in the plasma, where KC and IL-6 were decreased even below the concentrations detected in the $NaCl_{5.5h}$ group. Of note, quinine was not only ineffective in preventing the impairment of lung mechanics and oxygenation, but also in anticipating the inflammatory response. In the group MAQ, BAL and plasma levels of the quantified mediators were similar as in the group MA.

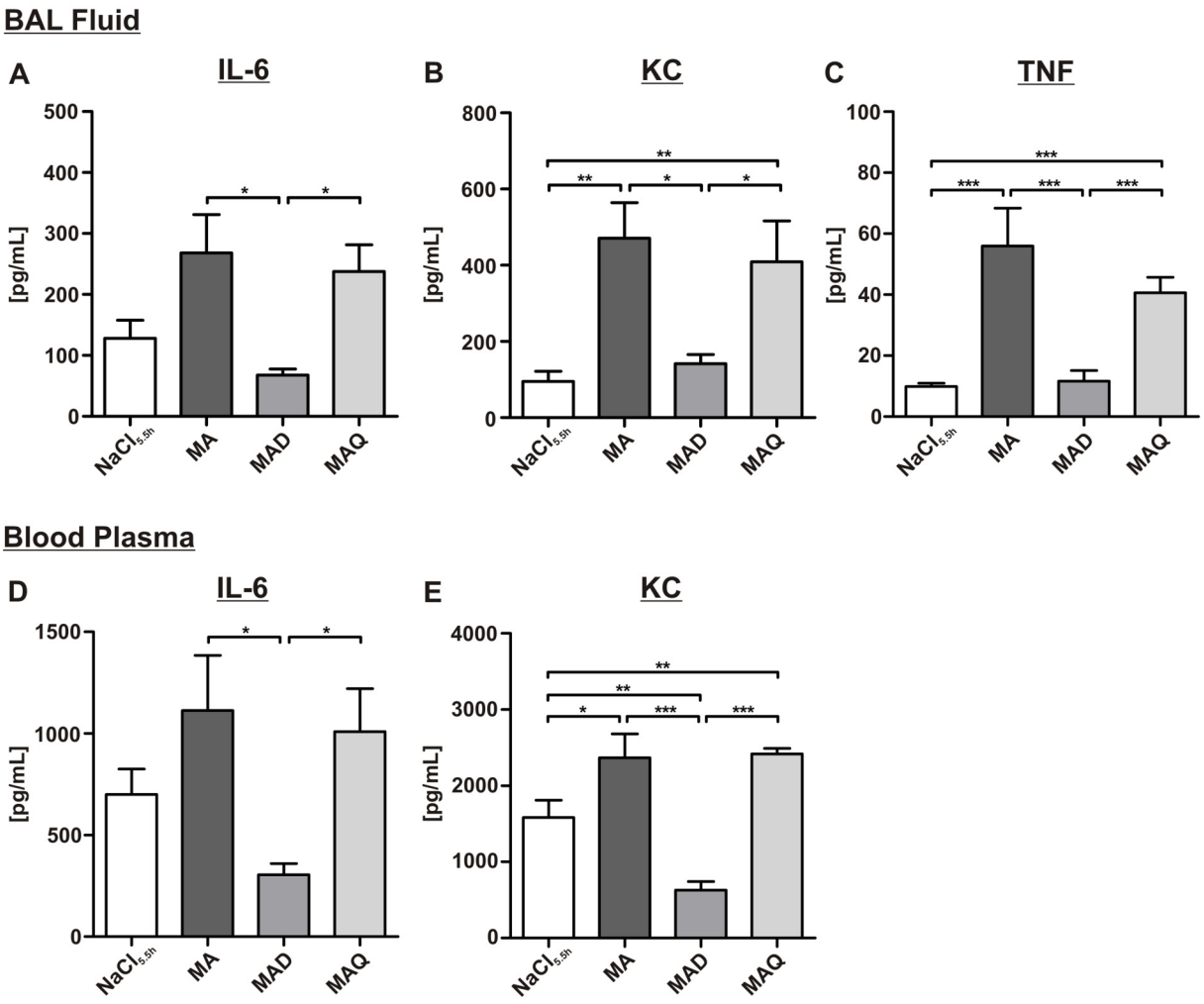

Fig. 3.35: Pro-inflammatory mediators in the moderate acid model. The cytokines IL-6 and TNF as well as the chemokine KC were quantified in the BAL fluid and blood plasma by ELISA after 330 min of ventilation. TNF was below the detection limit in the plasma. $NaCl_{5.5h}$: NaCl-instilled control group, MA: acid-instilled group, MAD: acid-instilled group treated with dexamethasone, MAQ: acid-instilled group treated with quinine. ($NaCl_{5.5h}$ n=5, MA n=6, MAD n=5, MAQ n=6). * $p \leq 0.05$,** $p \leq 0.01$, *** $p \leq 0.001$.

3.5.6 Microvascular permeability

No significant differences were observed concerning the number of neutrophils in the BAL between the groups in the moderate acid model (Fig. 3.36A). The small difference between the groups, MA, MAQ and $NaCl_{5.5h}$ is probably due to the moderate effect of acid with pH 1.8. In the group $NaCl_{5.5h}$ the number of intra-alveolar neutrophils was slightly higher in comparison to the control group $NaCl_{5h}$ in the severe model, which might be due to the longer period of ventilation. Nevertheless, the group MAD indicated clearly that dexamethasone had an inhibitory influence on neutrophil recruitment. The situation is much clearer regarding albumin influx (Fig. 3.36B). Acid with pH 1.8 strongly increased albumin leakage from a level between 1 and 2 in the control group, which can be regarded as normal for ventilated mice, to a mean index of around 8. Dexamethasone prevented albumin leakage successfully, whereas quinine revealed no protective effect.

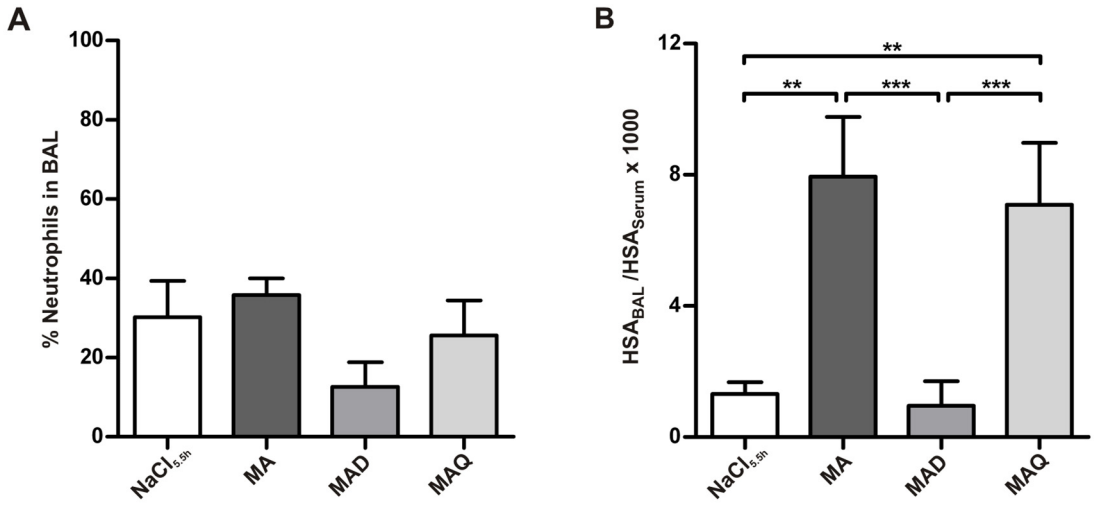

Fig. 3.36: Microvascular permeability in the moderate acid model. A. Neutrophil counts determined in the BAL as explained in Fig. 3.16. **B.** HSA was quantified in the BAL and plasma by ELISA to assess albumin leakage. $NaCl_{5.5h}$: NaCl-instilled group, MA: acid-instilled group, MAD: acid-instilled group treated with dexamethasone, MAQ: acid-instilled group treated with quinine. ($NaCl_{5.5h}$ n=5, MA n=6, MAD n=5, MAQ n=6). ** $p \leq 0.01$, *** $p \leq 0.001$.

3.5.7 Lung injury score

The lung injury score revealed that instillation of acid pH 1.8 induced only small histopathological changes, which did not result in significant differences between the groups (Fig. 3.37). The group MA received a slightly higher score than the group $NaCl_{5.5h}$, due to a higher number of neutrophils in the alveoli and the interstitial space. As also demonstrated by the cytospin preparation (Fig. 3.36A), the steroid-treated group MAD was protected from neutrophil sequestration, resulting in a slightly lower score than in the group MA. Finally, the score of the quinine-treated group MAQ was in the same range as the group MA, indicating that quinine had no protective effect.

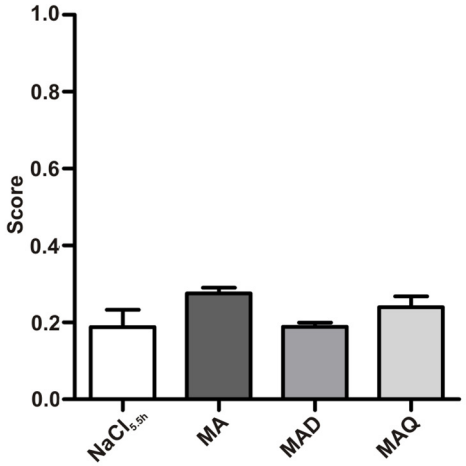

Fig. 3.37: Lung injury score in the moderate acid model. The injury score was determined as described above Fig. 3.8. $NaCl_{5.5h}$: NaCl-instilled group, MA: acid-instilled group, MAD: acid-instilled group treated with dexamethasone, MAQ: acid-instilled group treated with quinine. ($NaCl_{5.5h}$ n=3, MA n=5, MAD n=4, MAQ n=6).

3.6 Concluding cluster analysis

Finally, a cluster analysis was performed, in which the groups from the ventilation study at PEEP = 2 cmH_2O, the TNF study and both acid studies were included. The ventilation model at PEEP = 6 cmH_2O was excluded, because albumin leakage had not been assessed in this study and further because this series of experiments covered the same aspects of injury as the ventilation study at PEEP = 2 cmH_2O. A control group with idealised values for healthy mice was added, because oxygenation and elastance could not be assessed in unventilated control mice in the present setup. This analysis aimed to discover common features in the different injury models. The following criteria were analysed: albumin leakage as indicator of oedema, neutrophil recruitment as hallmark of pulmonary inflammation, hypoxemia and pulmonary elastance (H) as indicators of physiological dysfunction. To be able to compare albumin leakage, which had been assessed by different ELISA kits in the single studies, the leakage was categorised from low to high. Hypoxemia reflects the difference between an ideal oxygenation (600 mmHg) and the measured Horovitz index. The hierarchical clustering, which is depicted in Fig. 3.38, revealed four clusters: cluster I (green labelling) comprised all groups, in which the injury parameters were at a low levels, indicated by the green coloured fields. The colourless to pink fields indicate moderate alterations, which were also present in some groups in this cluster. Cluster II (red labelling) included the groups low$V_T$noRM, lowV_TRM60 and SAD. The red fields reflect a strong increase in hypoxemia and H in this cluster, whereas oedema and inflammation played only a minor role. This is not the case in cluster III (blue labelling), which consists of the groups MA and MAQ. Herein all four parameters were changed to a moderate degree. Cluster IV (black labelling) contains only the group SA, in which all criteria were increased severely. This cluster stands out from the other three clusters, which is also indicated by the very long distance to the other clusters in the dendogram. For each cluster a parallel plot is shown below, which further illustrates to which degree the single parameters were affected. In cluster I oedema played no role, whereas moderate hypoxemia, increased H or neutrophils were present in some groups. Cluster II is characterised by physiological dysfunction, with almost no inflammatory aspects. In the last two clusters all parameters were increased, whereof albumin leakage was affected to a lesser degree than the other injury criteria in cluster III. Notably, all parameters were highest in cluster IV. In addition, the four injury criteria were also clustered, showing that hypoxemia and H correlated very well with each other and also albumin leakage correlated with neutrophils counts.

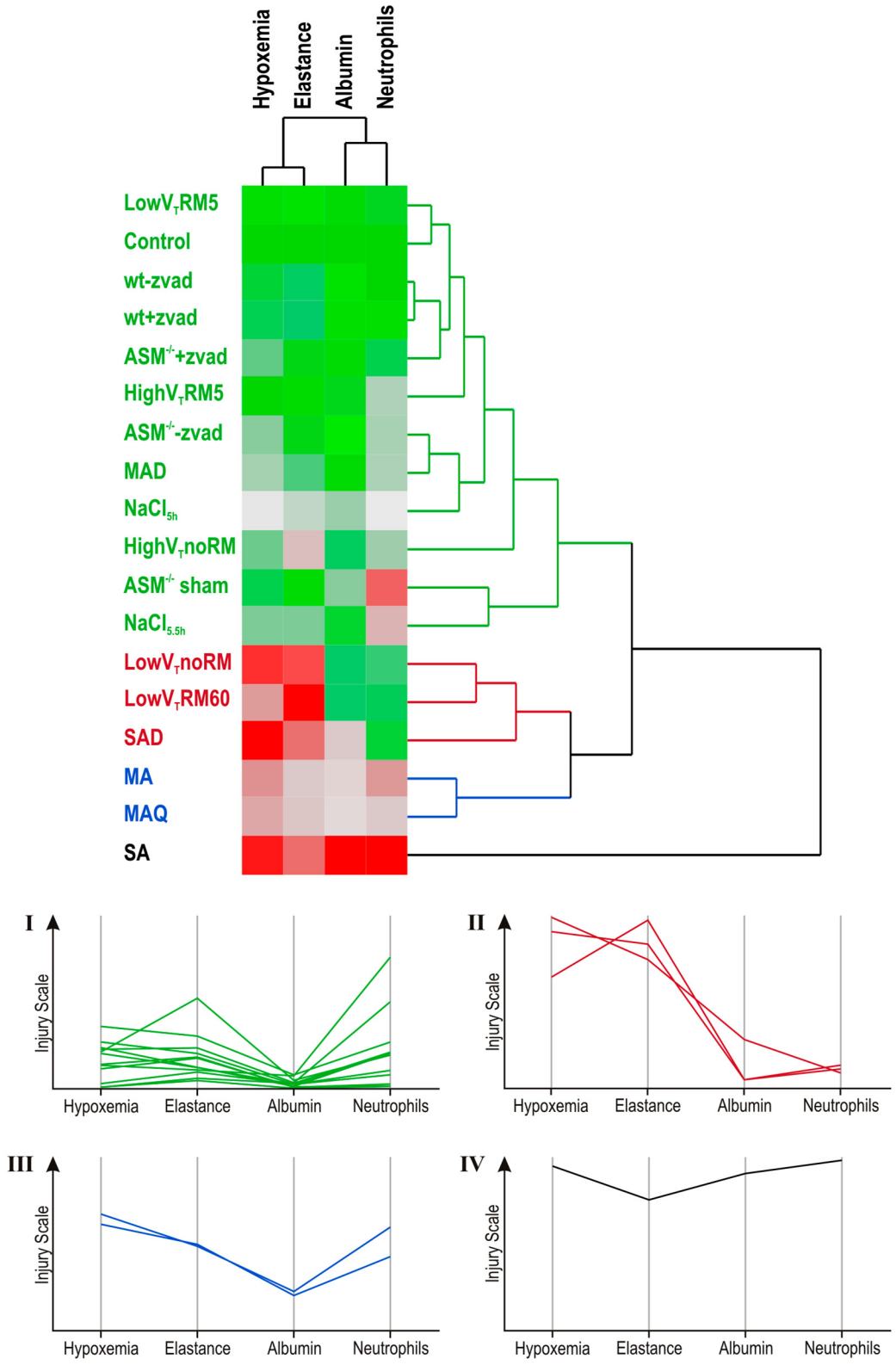

Fig. 3.38: Concluding cluster analysis. All groups from the ventilation study at PEEP = 2 cmH_2O, the TNF study and both acid studies were analysed. One control group with idealised data was added. Four parameters were examined: oxygenation, elastance, albumin leakage and neurophils in the lung. Green coloured fields indicate normal values, colourless and pink fields moderate alteration and red fields pathologically changed values. All green labelled groups are in cluster I, the red labelled groups low$V_T$noRM, lowV_TRM60 and SAD belong to cluster II and the blue groups MA and MAQ to cluster III. The group SA, labelled in black, stands alone as cluster IV. The dendogram reflects how similar groups are to each other. The connecting bars, which carry the colour of the corresponding cluster, become shorter with increasing similarity. The parallel plots below illustrate how strong each parameter was affected in each cluster. The numbers I-IV denote which cluster is shown in which plot.

4 Discussion

The present thesis comprises three approaches that have the potential to cause ALI, namely MV, sepsis and acid-instillation, and thereby covers a broad range of pathomechanisms that underlie this syndrome. Although the protective aspects of MV as a supportive strategy were in the focus in the first study, also injurious settings were examined. The effects of high V_T ventilation causing over-inflation of the lungs as well as low-volume injury (atelectotrauma) were under consideration. The second approach aimed to investigate extra-pulmonary ALI, caused by TNF-induced sepsis. Extra-pulmonary ALI differs from intra-pulmonary ALI regarding the severity of the disease and also the susceptibility to therapeutic interventions [30]. However, this approach did not induce lung injury, so that extra-pulmonary ALI could not be further examined. Finally intra-pulmonary lung injury in response to acid-instillation was investigated and served as model to examine the effectiveness of steroids in ALI, which is still under debate. The employment of different models of ALI takes into account that different insults do not necessarily cause the same type or degree of injury. Further, the discovery of pathomechanisms that are common in different models of ALI is a prerequisite for the development of adequate therapies, considering the widely varied aetiology of this disease [47].

4.1 The ventilation model

The first study focussed on MV under permanent monitoring of lung mechanics and vital functions to establish. VILI is the basis for the majority of lung injury models [46]. In addition, there is an increasing demand for MV of mice, not only in pulmonary research, but also in many other areas such as neurology [150], imaging [151] or cardiovascular research [152]. Monitoring of pulmonary and vital parameters is an essential prerequisite for correct interpretation of data from such models. Evidence of physiological dysfunction is one of the experimental criteria required to prove that ALI has occurred in animal models (Table 1.1). To date, most studies on intra-pulmonary ALI omitted the verification of physiological dysfunction [47]. Moreover, only a small number of ventilation studies included both, monitoring of lung mechanics and physiological key parameters, over several hours (Table 1.2).

4.1.1 The importance of recruitment manoeuvres in mechanical ventilation of mice

The present study indicates that the general notion according to which low V_T and sizable PEEP levels are preferable is – at least in healthy mice – only true when repetitive RM are applied. The effects of repetitive RM are not well established neither in experimental animals

nor in men, one reason being that trials that were performed under unequal conditions are difficult to compare [143]. To date, application of RM in patients with healthy lungs has been explored only sporadically [153], although there is some evidence that RM may support protective ventilation by improving oxygenation and lung mechanics, thereby allowing reduction of V_T [154,155]. Clinically, it has been shown that low V_T ventilation improves the outcome of patients with injured lungs [39], and also reduces inflammation in those with healthy lungs [156]. Taken together, it seems highly important to gain more information on the effects of repetitive 'sigh-like' RM during low V_T ventilation.

The ventilation experiments demonstrated that application of deep inflations of 1 s duration and 30 cmH_2O peak pressure in five minute intervals was sufficient to keep respiratory mechanics stable and thereby lung volume constant in low and high V_T ventilation, without increasing PEEP over 2 cmH_2O (Fig. 3.1). Initially a relatively low PEEP level was selected, because the same PEEP was planned to be used in the next studies, in which injurious insults were administered, and high PEEP levels are known to be protective (many VILI models use no PEEP at all). Since RM can be performed with varying duration, peak pressure and end-expiratory pressure [157], a very short type of RM was chosen, which was considered to be non-injurious to the lung and not to impair cardiac output. Accordingly, MAP and HF were stable, regardless of the ventilation strategy. Although MAP was in a low range due to anaesthesia with pentobarbital, so that small changes might have been masked, this did not result in reflex tachycardia or impairment of microcirculation, as the pH values indicate (Table 3.1). These stable cardiovascular conditions were also guaranteed by several supportive measures such as constant fluid support (200 µL/h), regular administration of pentobarbital via an intraperitoneal catheter, and an automated system to keep the body temperature constant. Further, it can be speculated that the low blood pressure is protective in this model, since oedema formation is generally aggravated by high blood pressure.

In order to keep blood gases stable, the low and high V_T groups had to be ventilated with different respiratory rates and, based on other studies [158], it cannot be completely ruled out that this might have affected the outcome of the study. The conditions were chosen to provide the same minute volume at both V_T. The supplementation of 3% CO_2 to the inhaled gas mixture in the high V_T groups was adequate to prevent hypocapnia, which otherwise would have occurred at a respiratory rate of 90 min^{-1} in the highV_TRM5 group. 3% CO_2 alone did not induce hypercapnia. Thus, a protective effect of hypercapnia during MV, which has been described in several studies [159,160], seems unlikely.

A pressure of 30 cmH_2O for each RM was necessary to maintain lung volume stable. In accordance with previous studies [127,129] RM with 25 cmH_2O peak pressure were not sufficient to avoid a loss of lung volume (data not shown). The double sigmoidal nature of the murine pressure volume curve [161] may explain the positive response to RM with 30 cmH_2O pressure. According to Zosky et al. [161], pressures above 20 cmH_2O induce fundamental changes in the murine lung, resulting in increased compliance. These changes are proposed to be either due to reopening of collapsed alveoli or to a secondary population of alveoli that are present but not aerated below a critical transpleural pressure [162]. In the present study, measurement of lung input impedance revealed that the alterations in pulmonary resistance and compliance in RM60 and noRM mice were predominantly due to changes in the periphery of the lung. Although significant differences in R_{aw} between RM5, RM60 and noRM mice ventilated at the same V_T were observed, this effect was rather small, indicating that bronchoconstriction of large airways is of minor importance to explain the present findings. The strong increase in G and H in mice ventilated without RM demonstrates a progressive loss in lung volume [16]. Increases in G reflect energy dissipation and are associated with an increase in tissue resistance and/or regional heterogeneity as result of peripheral airway constriction, whereas H reflects energy storage in lung tissues and represents lung stiffness [127]. The small decrease in η shows that H increased slightly stronger than G. Usually η ranges between 0.1 and 0.2, indicating that elastic and frictional energy is coupled in the structures of the lung [25]. The present data underline that impaired lung functions were not primarily due to heterogeneity caused by narrowing of small airways [163]. Thus narrowing of conductive airways played only a minor role in this model and it can be concluded that the loss of lung volume was mainly due to formation of atelectasis.

In fact, lung volume declined only to a certain threshold and a plateau phase was reached in all mice ventilated without RM. This supports the hypothesis that depending on the pressure applied to the lung some populations of alveoli are open and others closed [161]. The minimal lung volumes in the plateau phase differed according to the employed V_T, leading to the highest G and H values in the low$V_T$noRM group. Formation of atelectasis was more severe in low V_T than in high V_T ventilation, as shown elsewhere [128,129], indicating that low V_T ventilation without RM is injurious. These findings are in line with a previous work showing that low V_T ventilation augmented lung injury in isolated rat lungs, proposing that the degree of lung injury is dependent on the end-expiratory lung volume [164]. Ventilation with high V_T resulted in a higher C and thereby to some degree protected from the decline in lung volume. However, the application of one RM per hour was not sufficient to keep G and H entirely stable over six hours, demonstrating that the beneficial effect of recruitment is transient and formation of atelectasis is reversible only to a certain point. The present data

emphasise the importance of frequent deep inflations in mice in order to maintain lung functions in a physiological range.

Further evidence for the formation of atelectasis was given by blood gas analysis, which revealed impaired gas exchange in low$V_T$noRM and lowV_TRM60 mice (Fig. 3.3). The present study demonstrates that impairment of gas exchange, to a level that would fulfil the clinical definition for ARDS (Table 1.1), can be caused by a ventilation strategy that leads to derecruitment of lung volume. On the other hand, the data on lung histopathology, neutrophil count and BAL levels of pro-inflammatory cytokines indicate that inflammatory lung injury was not severe even in the low$V_T$noRM group. Notably, neutrophil counts and histopathological alterations (Fig. 3.6, 3.7, 3.8) did not correlate well with gas exchange and lung functions, further supporting the conclusion that atelectasis rather than inflammation was the major reason for the impaired gas exchange in the groups ventilated without sufficient RM. In fact, neutrophil infiltration was highest in the high V_T groups, suggesting ventilation-induced inflammation (biotrauma) as a mechanism.

Nonetheless, protein leakage, indicating increased microvascular permeability, another hallmark of VILI, was highest in those low V_T groups that developed atelectasis due to lacking adequate RM (noRM, RM60) (Fig. 3.4). Collapse of lung units is accompanied by an increase in vascular filtration pressure, leading to oedema formation, when vascular barrier functions are impaired [165]. This is in line with the observed alveolar septal thickening. Furthermore, microvascular leakage may also interfere with pulmonary surfactant, thus contributing to a reduction of compliance [166], which was clearly present in this model. Finally, in atelectatic lungs shear forces between closed and open alveoli may develop [37]. Taken together it can be concluded that a lack of RM may cause what has been termed atelectotrauma.

The present study demonstrates that repetitive RM are not only beneficial for lung functions, gas exchange and barrier function, but also reduce the liberation of pro-inflammatory cytokines (Fig. 3.5). This is an important finding, because in theory frequent deep inspirations might be a trigger for stretch-induced pro-inflammatory mediator release. IL-6 and KC were increased in the BAL and blood serum of all ventilated mice and it appears that ventilation will always cause mild inflammation in the lungs, both experimentally [132,133,167] and clinically [168,169]. The underlying mechanisms may be related to the surgery or mechanotransductive processes, i.e. stretch-activation of signalling cascades, or to increased vascular shear stress in those groups ventilated with higher positive pressures [170]. IL-6 and KC were significantly lower in the BAL fluid of lowV_TRM5 mice compared to

all other groups, demonstrating that this ventilation strategy was the most protective one. It is well established that protective ventilation, minimising overdistension and recruitment / derecruitment of the lung, attenuates cytokine liberation in the lung and circulation [171]. Interestingly, the blood serum of both V_T groups ventilated with RM5 contained significantly lower levels of IL-6 and KC than the corresponding groups ventilated with RM60 or noRM. This shows that the RM5 procedure was also protective at higher V_T. The high levels of IL-6 and KC in the BAL of highV_TRM5 mice indicate that the inflammatory response was initiated in the lung. Notably, neither levels of IP-10 nor of TNF - two cytokines that are frequently found in severe forms of ALI - were altered significantly in ventilated mice, compared to unventilated controls. The relatively high baseline values for TNF in unventilated mice are most likely due to the fact that BAL samples had to be diluted in order to gain enough volume for the assay. Concentrations were calculated by multiplication with the dilution factor, possibly leading to higher concentrations than actually present in the BAL. Nevertheless, all groups were analysed at the same time and cytokine levels were in the same range in all groups, allowing a comparison. IP-10 is proposed to play a role in development of ARDS and is further considered as a useful biomarker for lung disease [172,173]. TNF is considered as a mediator of pulmonary inflammation released by injurious ventilation [92,174]. The finding that these mediators remained unaltered by ventilation further suggests that lung injury was only moderate in the current model.

4.1.2 The role of positive end-expiratory pressure in mechanical ventilation of mice

This study aimed to define settings for ventilation under stable conditions and therefore a second set of experiments was performed with a PEEP of 6 cmH_2O, to address the question whether a higher PEEP could prevent the severe impairment of lung functions and the effects on oxygenation and inflammation, which were observed in the low$V_T$noRM and lowV_TRM60 groups ventilated with a PEEP of 2 cmH_2O. Lung mechanics and blood gas results revealed that a higher PEEP, even when combined with RM60, was not sufficient to prevent formation of atelectasis (Fig. 3.9). C decreased and R, G and H increased strongly during the first 180 min of the experiments in the PEEP6_noRM group before parameters reached a plateau. A previous study demonstrated that an increase in PEEP from 2 cmH_2O to 6 cmH_2O alone did not prevent an increase in R_{aw}, G and H during 150 min of ventilation, but was more effective during pressure controlled RM [127]. The present study shows that a combination of higher PEEP and short RM every 60 minutes does not suffice to prevent impairment of lung functions and oxygenation and that frequent RM are required, as with a PEEP of 2 cmH_2O. Of note, the increase in R_{aw}, which was observed in the groups low$V_T$noRM and lowV_TRM60 ventilated with a PEEP = 2 cmH_2O, was completely abolished

in all groups ventilated with a PEEP = 6 cmH_2O, indicating that a higher PEEP helps to prevent narrowing of large airways during MV.

It is well known that PEEP plays a critical role in preventing/reducing lung injury [147]. The combination of low V_T and high PEEP has already proved to be beneficial for the outcome of patients with ARDS [175]. Further, an experimental ventilation strategy using low V_T, PEEP and RM resulted in a better outcome in ARDS patient than a strategy without RM, although differences were not significant due to limitations of the trial [176]. Given the significance of biotrauma [177,178], it is an important question whether a ventilation strategy that combines high PEEP with RM attenuates pulmonary inflammation during low V_T. The second part of this ventilation study showed that differences in cytokine levels between mice ventilated with the same RM strategies were smaller with 6 cmH_2O than with 2 cmH_2O PEEP. IL-6 serum levels were even in a comparable range in all PEEP6 groups (Fig. 3.11). Interestingly, the highest IL-6 and KC BAL levels were detected in the PEEP6_noRM group. This correlates well with the neutrophil count that was also highest in this group. Thus, the application of RM appears to be beneficial with respect to pulmonary inflammation also at a PEEP of 6 cmH_2O.

4.2 The TNF model

The pro-inflammatory cytokine TNF is an important mediator in the development of several pulmonary diseases, including asthma, COPD and ALI [100]. In experimental studies, the effect of TNF on the lung was frequently examined *ex vivo* in isolated perfused lungs, where the systemic circulation and the immune system play no role [90,97,98,179] or *in vitro* on vascular endothelial cells alone [102], where TNF caused a disruption of the microvascular barrier. *In vivo* studies examined either the effect of TNF directly administered to the respiratory system, i.t. [180] or intra-nasally [89]. Only in two cases TNF was applied systemically, but as continuous infusion [93,94]. All these studies in the past focussed on oedema formation and the underlying mechanisms, but measurement of lung functions or oxygenation was not performed. The second part of the present thesis, in which the effects of high systemic TNF levels on the lung were studied, demonstrates that TNF alone does not suffice to induce lung injury *in vivo*.

4.2.1 The effects of high systemic TNF levels on the lung

Measurement of the input impedance of the lung revealed that i.v. injection of 50 µg murine TNF per mouse, a dosage that can be regarded as lethal, had no relevant influence on the tissue properties, indicated by G and H, or on the airways, indicated by R_{aw} (Fig. 3.13). Blood gas analysis further supported that TNF did not cause functional impairment of the lung,

since gas exchange was in the range of healthy mice in all groups despite of the TNF-application. This surprising finding led to the question, whether the injected TNF had actually arrived in the lung. Due to its physiological function, the blood turnover in the lung is very high so that i.v. injected substances reach the lung very quickly. Quantification of TNF via ELISA showed that in fact high levels (~1 ng/mL) were detectable in the BAL fluid and even 10^3-fold higher concentrations (~1 µg/mL) in the blood plasma (Fig. 3.15). Interestingly, the very high plasma levels of TNF were mirrored by high plasma levels of the cytokine IL-6 and the neutrophil-attracting chemokine MIP-2. Both mediators were only moderately increased in the lung and particularly MIP-2 levels were very low in the BAL fluid. This finding indicates that the chemotactic gradient was directed towards the vascular side in TNF-treated mice. The observation that neutrophil counts were not increased by TNF, but in a range that can be regarded as normal for ventilated mice, as shown in the first study, further supports this hypothesis. Furthermore, microvascular permeability, assessed by quantification of BSA-influx over the alveolar-capillary barrier, was not increased by TNF compared to literature values [130]. Unfortunately, the permeability index measured in the TNF study could not be directly compared to the index assessed in the previous ventilation study, because a different ELISA kit had to be used for BSA quantification. Finally the histopathological scoring confirmed that the high concentration of circulating TNF did not generate neutrophilia or any other pathological alteration within the given time frame of 6 h.

This is in contrast to the findings observed in models, where TNF was administered directly to the lungs and triggered neutrophil recruitment and oedema formation [89,180]. The role of TNF in oedema formation is well established [73], posing the question, why the integrity of the alveolar-capillary barrier had not been affected in the current investigation. As mentioned above, the high amount of circulating TNF seemed to have directed the chemotactic gradient towards the vascular side, whereby the neutrophils were possibly held back in the circulation instead of sequestering the lung. TNF-induced oedema was shown to be neutrophil-dependent [90,98,181] and furthermore it was demonstrated that TNF-related oedema requires interaction of the integrin complex CD11/CD18, which is located on the neutrophils, and the endothelial receptor ICAM-1 [97]. This allows the conclusion that the lack of neutrophils in the lungs possibly prevented oedema formation in this study. Although TNF sufficed to cause endothelial damage without neutrophils in cell culture experiments [182,183], it has to be taken into account that around 40 cell types interact with each other in the lung, so that the *in vivo* situation cannot be compared exactly to *in vitro* conditions. In contrast to the findings in the current investigation, a study in sheep, which were infused with 0.01 mg/kg human recombinant TNF for 30 min, resulted in a pathophysiology comparable to endotoxin-induced lung injury, including hypoxemia and increased pulmonary microvascular

permeability [93]. In sheep, leukocyte numbers in the circulation were reduced in response to TNF treatment, indicating that TNF enhances neutrophil adherence to the endothelium and thereby promotes accumulation of neutrophils in the lung, as it is also the case for endotoxin [93]. As there are parallels between TNF- and endotoxin-induced lung injury, probably species differences in the mononuclear phagocyte system, which play a role in endotoxin-induced lung injury, have to be taken into account, when comparing the effects of TNF on the lungs of sheep and mice. Interestingly, species that possess pulmonary intravascular macrophages (PIM) such as sheep localise endotoxin from the blood to the lung, but species without PIM, such as rodents, localise endotoxin to other organs that contain intravascular macrophages e.g. liver or spleen [46]. The effect of systemically applied endotoxin is therefore only moderate in mice compared to sheep, suggesting that the same may be true for TNF. Of note, the i.v. infusion of TNF (0.1 mg/kg/day) in rats over 5 days had an effect on the lung, resulting in an increase in lung weight by 38%, although no direct effect on membrane permeability was observed [94]. The potency of TNF in this study can probably be assigned to the long period of infusion, which discerns this investigation from other experimental approaches. The influence of continuously high TNF levels on pulmonary inflammation was further demonstrated in mice overexpressing TNF in type II pneumocytes. These mice developed pulmonary inflammation and emphysema within a few weeks only [184]. The time limitation in the present study might be one reason, why the lung was not affected by TNF. It would certainly be interesting to examine whether other organs such as the kidney, the liver or the spleen were affected.

There is also evidence that TNF has a less injurious effect on healthy than on pre-damaged lungs. In isolated perfused rodent lungs, TNF failed to induce lung injury in un-injured lungs, whereas microvascular permeability was aggravated by TNF in ischemic or endotoxin-challenged lungs [90,179]. Even the i.t. application of 500 ng TNF into healthy rat lungs *in vivo* induced only moderate recruitment of neutrophils and microvascular leakage within 5 h [180]. These findings suggest that TNF has a stronger injurious effect when inflammation is ongoing and other mediators are also active. In line with this consideration, TNF was shown to exacerbate pulmonary inflammation by inhibiting the clearance of apoptotic cells by alveolar macrophages [185]. In models of intra-pulmonary lung injury, including endotoxin-induced lung injury and VILI, blocking of TNF activity by antibodies, repression of TNF generation or inhibition of the p55 receptor attenuated lung injury, showing that TNF plays a role in the pathophysiology of ALI in injured lungs [57,91,92,181,186]. The critical role for TNF in inflammatory respiratory diseases is further shown by the ongoing investigation of anti-TNF therapies in clinical trials with asthma and COPD patients (source: NIH ClinicalTrials.gov).

Finally, the dual role of TNF in pulmonary oedema has to be also taken into account in the current study [73]. The protective properties of the lectin-like TNF domain, which promotes alveolar fluid clearance, might have been beneficial in the situation given in this model, where TNF was increased in the lung, but to a lesser degree than in the vasculature.

4.2.2 The role of acid sphingomyelinase (ASM) in lung injury

The present study also aimed to elucidate the role of ASM in the lung, by including $ASM^{-/-}$ mice. The background for this investigation is the well-known role of ASM in the pathophysiology of ALI. Several mechanisms were proposed, by which the promotion of pulmonary oedema is linked to ASM activity [99], particularly also when TNF is present [109,111]. Further, it is well established, that TNF activates ASM [107,117,187], which was a further reason for the examination of $ASM^{-/-}$ mice in this approach.

The present model turned out to be not suitable to further elucidate the role of ASM in ALI, as no significant lung injury was induced by the high TNF dosage, as described above in detail (chapter 4.2). Interestingly, some parameters indicated that $ASM^{-/-}$ mice were affected stronger by TNF-treatment than the wt mice. BAL cytokine levels were higher in the TNF-treated group $ASM^{-/-}$-zVAD than in the corresponding wt group wt-zVAD (Fig. 3.15). Also neutrophil counts were higher in the group $ASM^{-/-}$-zVAD than in the group wt-zVAD, although this was not reflected by a significant difference in microvascular permeability (Fig. 3.16). This is contrary to previous studies on intra-pulmonary lung injury, in which ASM-deficiency or pharmacological inhibition of ASM were protective [118,119,188]. As mentioned above, TNF plays a pivotal role in injured lungs. The course of disease in type B NPD patients shows that general ASM-deficiency is actually not protective, but causes progressive lung injury [124]. Also in the mouse model of NPD, the lungs are a site of the characteristic lipid storage phenomenon. Lipid storage is most severe in the monocyte-macrophage system, leading to accumulation of mononuclear cells (foamy cells) filled with cytoplasmatic lipid inclusions, which are responsible for alveolar congestion [189]. Although only young $ASM^{-/-}$ mice under 12 weeks age were included in this study, in order to avoid an influence of lipid storage, histopathological examination of the lungs revealed that the accumulation of foamy cells had already begun (Fig. 3.17), suggesting that these lungs were slightly more susceptible to increased TNF levels than the healthy lungs of wt mice. In this context it has to be pointed out that the group $ASM^{-/-}$sham, which received no pharmacological treatment, revealed the most obvious signs of alveolar-capillary barrier disruption, with an extremely high number of alveolar neutrophils and a strongly increased albumin leakage. In fact, TNF-treatment had actually evolved a protective effect in $ASM^{-/-}$ mice, further promoting the hypothesis that TNF had directed the chemotactic gradient towards the vascular side.

4.2.3 Cardiovascular effects of TNF

The LD_{100} of murine TNF ranges between 15-50 µg in mice [78,117,190]. The TNF-induced lethality is possibly due to severe cardiovascular depression, as described in detail below. In preliminary experiments, the C57BL/6x129/SvEv hybrid mice, which were used in this study, were found to be relatively resistant to TNF so that 50 µg per mouse (~ 2 mg/kg) were administered here. The present setup proved to be adequate to avoid lethal cardiovascular decompensation during the 6 h of ventilation after TNF injection in most mice.

Blood gas analysis elucidated that TNF-treated mice suffered from severe metabolic acidosis, a sign of impaired microcirculation, as it occurs in sepsis. As body temperature and breathing rate were manipulated in the current setup, parameters which are determined clinically as evidence of sepsis, the sepsis marker procalcitonin (PCT) was quantified to verify that sepsis was induced by TNF. The pro-hormone PCT correlates with the severity of sepsis and is activated in response to infections by the release of cytokines including TNF. Therefore PCT has also been termed a hormokine [191]. Although no injurious effect on the lung could be assigned to the high TNF levels, the high PCT levels > 2000 ng/L indicated that sepsis was induced by TNF within 6 h and that the high systemic TNF dose resulted in a pathophysiological reaction similar to that occurring with endotoxin.

The role of TNF in sepsis has been addressed also in clinical trials, where inhibition of TNF resulted in reduced mortality [80,83,84]. On the other hand, the clinical use of TNF as a drug in cancer-therapy has been considered, but was found to be limited by its toxicity. In clinical trials, which examined the systemic application of TNF, hypotension was characterised as the dose-limiting factor [192]. In fact, progressive hypotension as well as tachycardia were observed also in this study, although only four mice died during the experiment due to the supportive strategies, which included fluid support, regulation of body temperature and ventilation. The observed cardiovascular decompensation can be regarded as manifestation of sepsis [193], allowing the conclusion that TNF actually induced sepsis in this study.

4.2.4 The role of ASM in TNF-induced sepsis

The present study demonstrated that $ASM^{-/-}$ mice were protected from cardiovascular depression and mortality in TNF-induced shock, indicating an important role of ASM in the pathogenesis of septic shock. This is in line with the finding that increased ASM levels correlated with the development of sepsis in patients, where ASM is regarded as potential therapeutic target [114]. Interestingly, $ASM^{-/-}$ mice were shown to be also resistant to endotoxin-induced mortality in an earlier approach [117]. Furthermore, the mechanisms of TNF- and endotoxin-induced shock were largely identical in that study. A lethal dose of TNF

had the same effects as a lethal dose of endotoxin, causing ceramide generation within 1 h, followed by endothelial apoptosis beginning after 6 h and lethality from 10 h onward, suggesting that endotoxic shock derives from ceramide-induced widespread microvascular endothelial apoptosis, from which $ASM^{-/-}$ mice are protected. However, the cardiovascular effects in TNF-induced shock were not addressed in that context [117].

A potential mechanism by which ASM could be involved in promotion of cardiac decompensation in response to TNF is the activation of NO synthases by ceramide, leading to NO liberation and vasodilatation, as it was already shown for the neutral sphingomyelinase and eNOS [110,111]. The role of NO in the development of hypovolaemic shock is well established [194,195]. To address the hypothesis that reduced NO liberation was responsible for the protection from mortality in $ASM^{-/-}$ mice in this study total NO was quantified. However, the measurement revealed no differences between TNF-treated wt and $ASM^{-/-}$ mice, although NO was clearly increased by TNF (Fig. 3.23). From this result, a participation of ASM in NO liberation can not be concluded. To validate the loss of ASM enzyme activity in the $ASM^{-/-}$ groups, ASM activity was assessed in the urine, whereby it was proved that the ASM was defective (Fig. 3.24). It has to be taken into account that NO quantification can be affected by haemolysis, as already mentioned in the results. Haemoglobin was shown to interfere with NO reduction, leading to reduced NO levels in haemolysed plasma samples [149]. Of note, haemolysis was present particularly in plasma samples of wt mice, indicating that the suggested NO activating pathway cannot be excluded completely. The role of NO in TNF-induced shock has been already examined in previous animal models, where inhibition of NO reversed hypotension, but did not protect from TNF-induced organ damage and lethality. It has been suggested that NO mediates not only vasodilatation, but also protective effects [190,196]. This is further strengthened by a clinical trial on a NO synthase inhibitor in septic patients, which had to be stopped, because mortality was significantly increased in the treatment group [197], leading to the conclusion that the mechanism by which ASM mediates TNF-induced lethality has to be investigated further in the future.

4.2.5 The role of ASM in caspase-independent apoptosis

Caspase-inhibition was originally considered as a potential therapeutic way of reducing apoptosis, which contributes to many diseases [78]. In murine models, treatment with zVAD-fmk protected from TNF-induced liver injury and apoptosis [198] and also TNF-induced enterocyte apoptosis was reduced by caspase-inhibition [199]. In consequence, a further study aimed to investigate the mechanisms of systemic toxicity of lethal TNF concentrations under caspase-inhibition. Surprisingly, caspase-inhibition by zVAD-fmk enhanced TNF-induced toxicity by caspase-independent pathways [78]. Also in cell culture experiments, an

increased sensitivity to TNF-induced programmed cell death was found in response to zVAD-fmk [200]. Further, degradation of ceramide and inhibition of ASM resulted in increased cell survival after TNF-treatment [125], indicating that ASM played a role in TNF-induced cell death. In a study addressing the effects of TNF on the liver in $ASM^{-/-}$mice, these were shown to be protected from hepatocellular cell death [201]. The present study investigated for the first time the role of ASM TNF-induced caspase-independent cell death in the lung.

Application of the general caspase-inhibitor zVAD-fmk had no relevant influence on TNF-treated wt or $ASM^{-/-}$ mice in this study. Interestingly, neither the cardiovascular parameters nor mortality were affected by caspase-inhibition, although a strong accelerating effect on mortality had been demonstrated in the study by Cauwels et al. [78]. In that study, increased TNF-toxicity after caspase-inhibition was shown to originate from an increase in phospholipase 2 (PLA2), which is regulated by caspases. The PLA2 causes oxidative stress when producing arachidonic acid, the precursor of prostaglandins and leukotrienes. It is very likely that not only the generation of ROS, but also the production of pro-inflammatory leukotrienes and prostaglandins played a role. The direct inhibition of 5-lipoxygenase, which produces leukotrienes, but not the inhibition of cyclooxygenases, which produce prostaglandins, improved survival. Nevertheless, the fever inducing prostaglandin PGE_2 was shown to be induced strongly in response to systemic TNF application in sheep [93] and body temperature was not assessed in the study by Cauwels et al.. Therefore in the present study, the stabilisation of body temperature may have played a particularly important role, as it prevented hypothermia that corresponds with fever in mice and might have prevented a more rapid death of zVAD-fmk-treated mice. Furthermore, the high fluid support given by the permanent intra-arterial infusion of 200 µL/h 0.9% NaCl plus the i.v. injections of 340 µL volume in total may have masked potential effects of zVAD-fmk on the systemic circulation. In conclusion, the supportive strategies, which were necessary to investigate the effects of a lethal TNF dose *in vivo* over a time frame of 6 h might have been responsible for the inefficacy of caspase-inhibtion.

Unselective caspase inhibition affects not only the induction of cell death but also inflammation. The activation of the pro-inflammatory cytokines IL-1β and IL-18 requires cleavage by the serine protease caspase-1 [202]. In conclusion, blocking of caspase-1 should attenuate inflammation, particularly by inhibiting IL-1β, which plays a pivotal role in inflammation [203]. In the present study, IL-1β was measured as indirect proof that caspase-inhibition by zVAD-fmk had functioned. However, this could not be shown, because IL-1β was below the detection limit, also in samples from mice that were not treated with the caspase inhibitor, indicating that the TNF treatment had not triggered IL-1β release.

Only relative cell death in the lung, which was increased per se in $ASM^{-/-}$ mice, possibly due to the onset of lipid storage, was slightly reduced by zVAD-fmk, although this effect was not significant (Fig. 3.18). Of note, relative cell death was measured by quantifying mono- and oligonucleosomes, which does not allow to differentiate between apoptotic and necrotic cell death. Although the fact that cell death was higher in $ASM^{-/-}$ mice indicates that the induction of necroptosis by TNF via ASM played only a minor role in the lungs. Necroptosis is a mechanism by which ASM induces ceramide-dependent cell death in response to TNF. This pathway involves activation of the kinase Rip1 by the p55 receptor. Necroptosis is distinguished from apoptosis not by the initiating stimuli, which can be the same, but by the characteristic morphological changes [204], which could not be analysed in detail here. The high level of relative pulmonary cell death in the TNF-treated groups might result from an impaired apoptotic cell clearance, which was shown to be caused by TNF in the lung [185]. The role of ASM in caspase-independent cell death could not be unravelled in the current model, because neither an increase in cell death was induced by zVAD-fmk in wt mice, nor a reduction of cell death was observed in $ASM^{-/-}$ mice. This can be assigned to the circumstance that TNF had no clear effect in the lung on the one hand as well as to the lipid storage disorder on the other hand. Of note, TNF also activates anti-apoptotic pathways via the transcriptionfactor NFκB [78]. In this pathway also ASM was shown to be involved [107]. Therefore, cell death may not only be enhanced via ceramide generation by ASM, but also reduced via NFκB. In conclusion, in $ASM^{-/-}$ mice not only ceramide-dependent cell death may be reduced, but also the protection of apoptosis by NFκB activation, whereby caspase-dependent apoptosis may be enhanced.

4.3 The acid model

A third model was established with the aim to induce lung injury by a direct insult. The establishment of a reproducible lung injury model was necessary as basis for the investigation of therapeutic strategies. The model of acid-induced lung injury was chosen, because it is characterised by important features of ALI including hypoxemia. The present model stands out from most previous experimental approaches by including the measurement of several clinically relevant physiological parameters, thereby facilitating the transfer of data obtained from animal models to ALI in humans. In this study, mice were ventilated with a high V_T, with the aim to augment the acid-induced lung injury by the increased V_T. Although ventilation was not supposed to be protective, recurrent RM were applied so that the effects of acid-instillation on lung mechanics could be studied without being affected by the ventilation strategy.

4.3.1 The effects of acid-instillation with pH 1.5

The first approach to induce lung injury with instillation of 50 µL acid with pH 1.5 was successful and resulted in strongly impaired lung functions and critical hypoxemia (Fig. 3.25, 3.27). The physiological dysfunction was accompanied by a high lethality after about 330 min so that experiments were shortened to 300 min, allowing blood gas analysis from living mice at the end of the experiment. The control group was instilled with 50 µL of 0.9% NaCl to examine the impact of fluid administration to the lung. It could be shown that lung mechanics were only affected directly after NaCl instillation and were then stabilised, resulting in a relatively normal Horovitz index, which was only about 100 mmHg lower than in un-instilled ventilated mice. Further analysis revealed that physiological dysfunction in the acid-treated mice was associated with a severe inflammatory response, reflected by high levels of IL-6 and KC in the BAL as well as in the plasma. Interestingly, also considerable levels of TNF were present in the lungs (Fig. 3.28). This had not been the case in the ventilation study, where the absence of TNF in the lung was interpreted as a sign of moderate inflammation (chapter 4.1.1). This argument implies that the presence of increased TNF levels may be interpreted as an indicator of severe inflammation and is based on the idea that severe acute inflammation originates from other pathways than a moderate inflammatory response, which can be also beneficial [205]. The inflammatory reaction, which was not detectable in the control group, was further characterised by a strongly increased microvascular permeability, indicated by albumin leakage, and massive neutrophil sequestration, observed by cytospin preparation and histopathological examination. In conclusion, this model fulfilled all experimental criteria of ALI listed in Table 1.1.

The pathogenesis of acid-induced lung injury has been described already two decades ago [50,63], whereas the mechanisms by which acid activates the immune response are not completely understood. It has been suggested that the Toll-like receptor 4, which also mediates endotoxin-induced signalling, is necessary for the development of acid-induced lung injury [206]. Further, a rapid increase in lysophosphatidylcholine (LPC) in response to acid exposure was demonstrated [207]. LPC is produced by hydrolysis of the membrane protein phosphatidylcholine by PLA_2 and is a precursor of dipalmitoylphosphatidylcholine, the surface tension reducing component of surfactant [208]. LPC has an important function as mediator of acute and chronic inflammation [209], suggesting a potential role for LPC in transforming the chemical insult given by acid into an inflammatory response.

Notably, cardiovascular parameters were not affected by this strong inflammatory response or the pulmonary dysfunction (Fig. 3.26). It is very likely that the stable cardiovascular condition was the result of the volume substitution. The literature is inconsistent about the

effect of acid aspiration on haemodynamics. Whereas acid-instillation caused no cardiovascular effects in studies with pigs and rabbits [210], hypotension was observed in studies with ventilated rats [211,212]. The measurement of MAP indicated that dexamethasone had an influence on MAP, although the increase in the group SAD was not significant compared with SA and $NaCl_{5h}$. The induction of hypertension by glucocorticoids is a well-known process, although the mechanisms are only poorly understood. One explanation is the potentiation of endogenous vasoconstrictors by glucocorticoid receptors on vascular smooth muscle cells. Another recently proposed mechanism implicates a decisive role of the glucocorticoid receptors on the vascular endothelium [213].

4.3.2 The effectiveness of dexamethasone in the severe acid model

Glucocorticoids are widely used anti-inflammatory drugs that act on the transcriptional and non-transcriptional level. Although they are very potent also in respiratory diseases e.g. asthma, their usefulness in ALI is still under debate [214]. The application of dexamethasone had no beneficial effect on lung mechanics or oxygenation after exposure to acid pH 1.5, although the inflammatory response was prevented effectively, illustrated by the strongly reduced cytokine levels, low neutrophil numbers and decreased permeability index in the group SAD compared to the group SA. Acid-induced lung injury is described as a biphasic process, in which a first quick response is due to the chemical properties of the acid, followed by a later phase in which the immune response plays a role [63]. The failure of dexamethasone to improve lung functions and oxygenation could indicate that the physiological dysfunction might have not resulted from inflammation, which developed in response to the acid exposure, but was directly caused by the chemical burn due to HCl. This view is strengthened by the fact that neutrophil recruitment, which usually precedes oedema formation and hypoxemia in the pathogenesis of lung injury [47], was circumvented by dexamethasone, whereas oedema formation was not completely abolished. From the present data it cannot be concluded, which consequences the chemical burn actually had in the lung. No evidence for structural changes was found in the small area examined histopathologically. Possibly the burn affected only specific structures, such as the elastic fibres, which would explain the increase in elastance after acid exposure and might have caused microscopically visible changes after a longer period of time. Autopsy cases of patients, who suffered from severe chemical burns and died shortly after, show that the early phase of chemically induced lung injury is characterised by profound oedema and also haemorrhage, whereas no structural changes are visible microscopically [215,216]. In contrast, in a patient, who survived a severe chemical burn, but died of a gun shot 3 months later, structural changes had taken place in the lung. These included strictures in the bronchioles, emphysema, atelectasis and formation of hyaline membranes with infiltration of

fibroblasts or collagenation [216], indicating that a chemical burn results in structural changes which might aggravate over time.

The negative outcome in clinical trials on steroids in ALI is believed to derive from too high dosages at early stages, which strongly repress the immune response, too short therapy or abrupt steroid deprivation [217]. In contrast, prolonged treatment with a moderate dose over a period of several weeks is beneficial regarding oxygenation, reduction of pro-inflammatory mediators and lethality [218,219]. A moderate dose of 1 mg/kg was also administered in the present study, suggesting that the time frame of 5 hours was too short for the development of a beneficial effect of the steroid, regarding the severity of the injury.

Further, it has to be mentioned that glucocorticoid resistance is a major problem in critically ill patients with sepsis or ARDS: Critical illness related corticoid insufficiency (CIRCI) describes a syndrome characterised by insufficient corticoid production as well as unresponsiveness to steroid therapy [220]. Several mechanisms were proposed to be responsible for steroid unresponsiveness. In chronic inflammatory diseases e.g. asthma, resistance to glucocorticoids was related to the high concentrations of cytokines, which were proposed to reduce the binding affinity of steroids to the glucocorticoid receptor by activating protein kinases (p38, JNK and MAPK) and transcription factors (NFκB and Ap-1) [221-223]. Furthermore, high cytokine concentrations were related to a defective nuclear localisation of the glucocorticoid receptor [224]. It is thinkable that the high cytokine levels in the present acid model also influenced the response to dexamethasone, suggesting that the glucocorticoid would be more effective if cytokine levels were lower. In addition, oxidative stress is discussed to cause steroid resistance, e.g. in COPD patients, where smoking is a source of oxidative stress. The proposed mechanism includes that steroids, which inhibit the transcription of pro-inflammatory genes by recruiting histone deacetylases (HDAC), become ineffective when oxidative stress impairs the activity of HDACs [225]. This mechanism can also be relevant when other sources of oxidative stress are involved. In sepsis or ALI, oxidative stress can be caused by support with oxygen (FiO_2: 0.5-0.6), which is often necessary to ensure sufficient arterial oxygenation. Possibly, oxidative stress is also induced by acid-aspiration, even when only a low FiO_2 of 0.3 is applied.

In conclusion, steroid treatment cannot be regarded as salutary in this severe model of injury, since inhibition of the immune response in the early phase of lung injury is not necessarily beneficial and dexamethasone did not restore physiological functionality. The negative side effects of repressing the immune response were shown in several clinical trials, in which the

prophylactic application of steroids in critically ill patients was associated with a higher risk of developing ARDS with lethal outcome [41].

4.3.3 The effects of acid-instillation with pH 1.8

After acid-instillation with pH 1.5 had resulted in pulmonary inflammation and progressive pulmonary dysfunction, which was not susceptible to glucocorticoid therapy, a second approach was designed in which the insult was attenuated. For this purpose, the pH of the acid was raised to 1.8. The correlation of pulmonary compliance with the oxygenation index served to be a suitable indicator to assess the time point at which lung injury was severe enough to result in hypoxemia (Fig. 3.31). As a result, experiments with acid pH 1.8 were prolonged to 330 min. In fact, physiological dysfunction, including lung mechanics and hypoxemia, were less pronounced and also the hallmarks of pulmonary inflammation, i.e. cytokine levels, alveolar neutrophils and albumin leakage, were mitigated compared to the severe acid model, but the experimental criteria for ALI were still fulfilled. The acid-instilled group MA differed significantly from the control group $NaCl_{5.5h}$ in all respects, except from the histopathological lung injury score. Of note, in the acid-model only the right upper lobe of the lung was subjected to histological examination to save tissue for other analysis. Although it can be regarded as advantage to gain as much information from one subject as possible, the examination of such a small part of the lung was also critical, because not all regions of the lungs were always damaged equally by acid-instillation. This might have been one reason, why only a small trend towards an accelerated injury score was observed, when comparing the group MA with the group $NaCl_{5.5h}$. Finally, as expected when considering the observations in the severe acid model, cardiovascular parameters were not affected by acid pH 1.8, but the hypertensive effect of the steroid was slightly more pronounced (Fig. 3.33).

4.3.4 The effectiveness of dexamethasone in the moderate acid model

Interestingly, dexamethasone not only diminished the inflammatory response, but also effectively restored lung mechanics and oxygenation in the moderate acid model (Fig. 3.32, 3.34). These findings indicate that the physiological dysfunction in response to acid pH 1.8, which took more time to develop than in the severe model, derived from the inflammatory reaction and not primarily from the chemical burn. It is well known that a chemical burn occurs within a few seconds and that acid is rapidly neutralised in the lung [61]. This was also observed in the course of the current thesis, as it was not possible to induce lung injury, when acid was administered as an aerosol into the lung, even at pH 1.5 (data not shown). The only aspect in which the beneficial influence of dexamethasone could not be clearly demonstrated was the lung injury score, but this can certainly be ascribed to the fact that the moderate injury hardly increased the score.

The lower increase of pro-inflammatory mediators in the lung in response to acid with pH 1.8 may have contributed to the good response to dexamethasone. As it has already been discussed, the high cytokine levels might have interfered with the action of the steroid in the severe model. Particularly TNF, which has been proposed here to be an indicator for severe injury, was elevated only very moderately and a correlation between high TNF levels and an inhibition of the nuclear transport of the glucocorticoid receptor has been pointed out previously [224]. In addition, also the potential oxidative stress due to the acid treatment could have been reduced at pH 1.8, providing a further explanation for the improved response to dexamethasone.

The severity of the disease was also found to correlate with the beneficial effect of steroids in sepsis. In a meta-analysis including 21 trials on steroids in sepsis a linear relationship between the severity of sepsis and the beneficial effect of steroids on mortality was found. Steroids improved survival in critically ill patients, whereas they were harmful in less severely ill patients, including that in a certain population of patients, which were moderately ill, no effect on mortality was observed at all [214]. Although it appears in the current acid study that steroids are more potent in mild than in severe lung injury, the inconclusive outcome of trials on steroids in ALI and ARDS might be due to a similar linear relationship between the effectiveness of steroids and the severity of lung injury. Therefore, a model in which the severity of injury can be varied is of great advantage when examining the effectiveness of steroids

Apparently, to date only one animal study with inconclusive results has addressed the therapeutic effectiveness of glucocorticoids in acid-induced lung injury [226] and in this case dexamethasone was administered i.t.. Other models of lung injury, including VILI or endotoxin-instillation, returned controversial results, as some showed protective effects on neutrophil sequestration and oedema formation [227,228], while other studies revealed no beneficial influence on oedema formation, although neutrophil numbers were reduced [227,229]. The present study strongly supports that the differential outcome of steroid therapy depends on the grade of lung injury, as it was also shown to be the case in endotoxin-induced lung injury [227].

4.3.5 The effectiveness of quinine in acid-induced lung injury

Quinine was the first effective anti-malaria drug used since the early 17th century [230]. Besides of the antimalarial effect, also anti-pyretic, anti-inflammatory, anti-arrhythmic, analgesic and muscle relaxant properties have been ascribed to this substance. Chloroquine, a derivative of quinine, was shown to be beneficial in moderate and severe asthma

[231,232], revealing anti-inflammatory properties in the lung. Further, quinine was capable of preventing oedema formation in the lung, as demonstrated in PAF- and endotoxin-induced oedema in mice *in vivo* and in PAF-induced oedema in the isolated perfused rat lung [233]. Thus, quinolines exert salutary features, which could also improve the outcome of ALI. Therefore, the effects of quinine were examined in the moderate acid model. However, despite of the very high dose (20 mg/kg) no beneficial outcome could be found in any aspect of injury in the current model. The current data do not indicate why quinine failed to protect from inflammation and oedema formation and the mechanisms by which quinine exerts its beneficial functions are largely unknown.

4.4 Common patterns in the examined injury models

Each study in the current thesis addressed a different aspect of ALI. Finally the question aroused, whether common mechanisms or injury patterns that lead to ALI can be found. Therefore the experimental groups from this thesis were compared by cluster analysis under consideration of four main aspects of ALI: hypoxemia, elastance, albumin leakage and neutrophil infiltration. The cluster analysis revealed that the groups could be assigned to four clusters (Fig. 3.38). Cluster I comprised all groups, which did not fulfil the experimental criteria of ALI. This cluster included all groups from the TNF study, the control groups from the acid models and the high V_T groups from the ventilation study, although they had shown moderate signs of VILI. Of note, the group lowV_TRM5 was very similar to the idealised control group, which further indicates that the ventilation strategy with low V_T and recurrent RM was very protective.

Interestingly, those 6 groups that fulfilled the experimental criteria of ALI were sorted into three distinct clusters (II-IV), revealing that they had different injury patterns. Among these, the group SA was separated from the other groups, as it showed by far the most severe injury. The classification of the steroid-treated group SAD into one cluster with the groups low$V_T$noRM and lowV_TRM60, illustrates that acid pH 1.5 induced not only inflammatory processes. After elimination of inflammation by dexamethasone, the remaining injury pattern was comparable to the mechanical injury in atelectatic lungs. This was unlike the situation in the moderate acid model (cluster III), where lung injury was prevented almost completely by dexamethasone, so that the group MAD was sorted to the 'healthy' groups in cluster I. This indicates that in the moderate acid model only inflammatory, but no mechanical injury, led to physiological dysfunction. An interesting future approach would be to examine the effectiveness of steroids in atelectatic lungs, to verify that physiological dysfunction did not

result from inflammation in this case. Nevertheless, it can be concluded that the injury pattern determined, whether the glucocorticoid therapy was beneficial in the current acid models.

Transferring this rationale to patients with ALI may provide an explanation why some patients benefit from steroid therapy, while others do not. As already pointed out, ALI derives from a broad range of aetiologies and, besides of the four defined clinical criteria, the manifestation of this syndrome can vary from patient to patient. Thus, the systematic analysis of common injury patterns, which allow to predict the susceptibility to steroids, could provide a valuable tool to improve the poor outcome of patients with ALI.

4.5 Conclusion

The current thesis analysed the impact of three different injurious stimuli on the lung in a setup that facilitated the monitoring of clinically relevant physiological parameters and can therefore be regarded as mouse intensive care unit. In the ventilation study, the healthy mouse lung was found to be relatively resistant to MV, even when ventilation strategies were applied that are regarded as not protective. Application of high V_T did not cause relevant lung injury, although comparable settings were used in other studies that investigated VILI. Nonetheless, ventilation without RM at low V_T promoted formation of atelectasis and caused physiological dysfunction. This study demonstrates that protective non-injurious ventilation requires the application of frequent short RM, low V_T and sizeable PEEP to ensure stable lung mechanics.

This thesis further indicates that the healthy lung is not very susceptible to inflammatory stimuli, when the alveolar-capillary barrier is intact. This was illustrated by the fact that the approach to induce extra-pulmonary lung injury by TNF-induced sepsis failed. In general, models that aim to induce lung injury by indirect insults result in a weaker lung injury, but often have stronger systemic effects than models of intra-pulmonary injury. However, the TNF study proved that the mouse intensive care unit established in the course of this thesis is useful to study the effects of sepsis on the lung and the cardiovascular system. Furthermore, a crucial role for ASM in TNF-induced septic shock was revealed.

In addition, it was shown that acid-instillation allows to induce experimental lung injury with variable severity, depending on the pH of the instilled acid. This model was therefore used to examine the therapeutic usefulness of dexamethasone. Instillation of acid with a pH 1.5 produced gross lung injury, characterised by inflammation and profound structural changes in the lung, which could not be prevented by the anti-inflammatory treatment. In contrast, acid with a pH 1.8 caused predominantly inflammatory processes that were susceptible to dexamethasone. A final cluster analysis revealed three injury patterns of ALI, namely inflammation, low-volume injury and chemical damage, and validated that the susceptibility to steroids depended on the severity and type of lung injury. This analysis indicates that a systematic analysis of injury patterns in ALI patients might be a new approach to predict the benefit of steroid treatment.

5 References

1. IRCP. 1994. Human Respiratory Tract Model for Radiological Protection. A Report of a Task Group of the International Commission on Radiological Protection. Ann. ICRP 24: 1-482.

2. Faller A. 1995. Der Körper des Menschen. Thieme; p. 333-375.

3. Weibel ER. 1973. Morphological Basis of Alveolar-Capillary Gas Exchange. Physiol. Rev. 53: 419-495.

4. Sorokin, S. P. 1970. The Cells of the Lungs; Proceedings of a Biology Division, Oak Ridge National Laboratory conference catalogue 73-609398.

5. Schiebler TH. 2005. Anatomie. Springer; p. 475-489.

6. Seliskar M, Rozman D. 2007. Mammalian Cytochromes P450-Importance of Tissue Specificity. Biochim. Biophys. Acta 1770: 458-466.

7. Tierney DF. 1974. Lung Metabolism and Biochemistry. Annu. Rev. Physiol. 36: 209-231.

8. Imai Y, Kuba K, Penninger JM. 2008. The Discovery of Angiotensin-Converting Enzyme 2 and Its Role in Acute Lung Injury in Mice. Exp. Physiol. 93: 543-548.

9. Sobotta J. 1982. Atlas Der Anatomie des Menschen. Urban und Schwarzenberg.

10. Clemets JA, Brown ES, Johnson RP. 1958. Pulmonary Surface Tension and the Mucus Lining of the Lungs: Some Theoretical Considerations. J. Appl. Physiol. 12: 262-268.

11. Cockshutt AM, Possmayer F. 1991. Lysophosphatidylcholine Sensitizes Lipid Extracts of Pulmonary Surfactant to Inhibition by Serum Proteins. Biochim. Biophys. Acta 1086: 63-71.

12. Netter FH. 1982. The Ciba Collection of Medical Illustrations-Respiratory System. Thieme.

13. Bates JH. 1991. Lung Mechanics-the Inverse Problem. Australas. Phys. Eng Sci. Med. 14: 197-203.

14. Bates JH. 2009. Lung Mechanics-an Inverse Modelling Approach. Cambridge University Press.

15. Irvin CG, Bates JH. 2003. Measuring the Lung Function in the Mouse: the Challenge of Size. Respir. Res. 4: 4.

16. Bates JH. 2009. Pulmonary Mechanics: a System Identification Perspective. Conf. Proc. IEEE Eng Med. Biol. Soc. 2009: 170-172.

17. Dubois AB, Brody AW, Lewis DH, Burgess BF, Jr. 1956. Oscillation Mechanics of Lungs and Chest in Man. J. Appl. Physiol. 8: 587-594.

18. LaPrad AS, Lutchen KR. 2008. Respiratory Impedance Measurements for Assessment of Lung Mechanics: Focus on Asthma. Respir. Physiol. Neurobiol. 163: 64-73.

19. Oostveen E, MacLeod D, Lorino H, Farre R, Hantos Z, Desager K, Marchal F. 2003. The Forced Oscillation Technique in Clinical Practice: Methodology, Recommendations and Future Developments. Eur. Respir. J. 22: 1026-1041.

20. Hantos Z, Daroczy B, Suki B, Nagy S, Fredberg JJ. 1992. Input Impedance and Peripheral Inhomogeneity of Dog Lungs. J. Appl. Physiol. 72: 168-178.

21. Tomioka S, Bates JH, Irvin CG. 2002. Airway and Tissue Mechanics in a Murine Model of Asthma: Alveolar Capsule Vs. Forced Oscillations. J. Appl. Physiol. 93: 263-270.

22. Gomes RF, Shen X, Ramchandani R, Tepper RS, Bates JH. 2000. Comparative Respiratory System Mechanics in Rodents. J. Appl. Physiol. 89: 908-916.

23. Hirai T, McKeown KA, Gomes RF, Bates JH. 1999. Effects of Lung Volume on Lung and Chest Wall Mechanics in Rats. J. Appl. Physiol. 86: 16-21.

24. Bates JH, Lutchen KR. 2005. The Interface Between Measurement and Modeling of Peripheral Lung Mechanics. Respir. Physiol. Neurobiol. 148: 153-164.

25. Fredberg JJ, Stamenovic D. 1989. On the Imperfect Elasticity of Lung Tissue. J. Appl. Physiol. 67: 2408-2419.

26. Lutchen KR, Greenstein JL, Suki B. 1996. How Inhomogeneities and Airway Walls Affect Frequency Dependence and Separation of Airway and Tissue Properties. J. Appl. Physiol. 80: 1696-1707.

27. Thorpe CW, Bates JH. 1997. Effect of Stochastic Heterogeneity on Lung Impedance During Acute Bronchoconstriction: a Model Analysis. J. Appl. Physiol. 82: 1616-1625.

28. Sly PD, Collins RA, Thamrin C, Turner DJ, Hantos Z. 2003. Volume Dependence of Airway and Tissue Impedances in Mice. J. Appl. Physiol. 94: 1460-1466.

29. Ashbaugh DG, Bigelow DB, Petty TL, Levine BE. 1967. Acute Respiratory Distress in Adults. Lancet 2: 319-323.

30. Bernard GR, Artigas A, Brigham KL, Carlet J, Falke K, Hudson L, Lamy M, Legall JR, Morris A, Spragg R. 1994. The American-European Consensus Conference on ARDS. Definitions, Mechanisms, Relevant Outcomes, and Clinical Trial Coordination. Am. J. Respir. Crit. Care Med. 149: 818-824.

31. Rubenfeld GD, Caldwell E, Peabody E, Weaver J, Martin DP, Neff M, Stern EJ, Hudson LD. 2005. Incidence and Outcomes of Acute Lung Injury. N. Engl. J. Med. 353: 1685-1693.

32. Deitch EA. 1992. Multiple Organ Failure. Pathophysiology and Potential Future Therapy. Ann. Surg. 216: 117-134.

33. Del SL, Slutsky AS. 2011. Acute Respiratory Distress Syndrome and Multiple Organ Failure. Curr. Opin. Crit. Care 17: 1-6.

34. Matute-Bello G, Downey G, Moore BB, Groshong SD, Matthay MA, Slutsky AS, Kuebler WM. 2011. An Official American Thoracic Society Workshop Report: Features and Measurements of Experimental Acute Lung Injury in Animals. Am. J. Respir. Cell Mol. Biol. 44: 725-738.

35. Pelosi P, Caironi P, Gattinoni L. 2001. Pulmonary and Extrapulmonary Forms of Acute Respiratory Distress Syndrome. Semin. Respir. Crit. Care Med. 22: 259-268.

36. Gattinoni L, Carlesso E, Cadringher P, Valenza F, Vagginelli F, Chiumello D. 2003. Physical and Biological Triggers of Ventilator-Induced Lung Injury and Its Prevention. Eur. Respir. J. Suppl. 47: 15s-25s.

37. Uhlig U, Uhlig S. 2011. Ventilation-Induced Lung Injury. Compr. Physiol. 1: 635-661.

38. Tremblay LN, Slutsky AS. 1998. Ventilator-Induced Injury: From Barotrauma to Biotrauma. Proc. Assoc. Am. Physicians 110: 482-488.

39. ARDSNet. 2000. Ventilation With Lower Tidal Volumes As Compared With Traditional Tidal Volumes for Acute Lung Injury and the Acute Respiratory Distress Syndrome. N. Engl. J Med. 342: 1301-1308.

40. Luh SP, Chiang CH. 2007. Acute Lung Injury/Acute Respiratory Distress Syndrome (ALI/ARDS): the Mechanism, Present Strategies and Future Perspectives of Therapies. J Zhejiang. Univ Sci. B 8: 60-69.

41. Peter JV, John P, Graham PL, Moran JL, George IA, Bersten A. 2008. Corticosteroids in the Prevention and Treatment of Acute Respiratory Distress Syndrome (ARDS) in Adults: Meta-Analysis. BMJ 336: 1006-1009.

42. Sessler CN, Gay PC. 2010. Are Corticosteroids Useful in Late-Stage Acute Respiratory Distress Syndrome? Respir. Care 55: 43-55.

43. Meduri GU, Chinn AJ, Leeper KV, Wunderink RG, Tolley E, Winer-Muram HT, Khare V, Eltorky M. 1994. Corticosteroid Rescue Treatment of Progressive Fibroproliferation in Late ARDS. Patterns of Response and Predictors of Outcome. Chest 105: 1516-1527.

44. Marik PE, Meduri GU, Rocco PR, Annane D. 2011. Glucocorticoid Treatment in Acute Lung Injury and Acute Respiratory Distress Syndrome. Crit. Care Clin. 27: 589-607.

45. St John RC, Dorinsky PM. 1993. Immunologic Therapy for ARDS, Septic Shock, and Multiple-Organ Failure. Chest 103: 932-943.

46. Matute-Bello G, Frevert CW, Martin TR. 2008. Animal Models of Acute Lung Injury. Am. J. Physiol. Lung Cell Mol. Physiol. 295: L379-L399.

47. Reiss LK, Uhlig U, Uhlig S. 2012. Models and Mechanisms of Acute Lung Injury Caused by Direct Insults. Eur. J. Cell Biol. in press.

48. Maniatis NA, Harokopos V, Thanassopoulou A, Oikonomou N, Mersinias V, Witke W, Orfanos SE, Armaganidis A, Roussos C, Kotanidou A, Aidinis V. 2009. A Critical Role for Gelsolin in Ventilator-Induced Lung Injury. Am. J. Respir. Cell Mol. Biol. 41: 426-432.

49. Kantrow SP, Shen Z, Jagneaux T, Zhang P, Nelson S. 2009. Neutrophil-Mediated Lung Permeability and Host Defense Proteins. Am. J. Physiol. Lung Cell Mol. Physiol. 297: L738-L745.

50. Knight PR, Druskovich G, Tait AR, Johnson KJ. 1992. The Role of Neutrophils, Oxidants, and Proteases in the Pathogenesis of Acid Pulmonary Injury. Anesthesiology 77: 772-778.

51. Zarbock A, Allegretti M, Ley K. 2008. Therapeutic Inhibition of CXCR2 by Reparixin Attenuates Acute Lung Injury in Mice. Br. J. Pharmacol. 155: 357-364.

52. Reutershan J, Morris MA, Burcin TL, Smith DF, Chang D, Saprito MS, Ley K. 2006. Critical Role of Endothelial CXCR2 in LPS-Induced Neutrophil Migration into the Lung. J. Clin. Invest. 116: 695-702.

53. Belperio JA, Keane MP, Burdick MD, Londhe V, Xue YY, Li K, Phillips RJ, Strieter RM. 2002. Critical Role for CXCR2 and CXCR2 Ligands During the Pathogenesis of Ventilator-Induced Lung Injury. J. Clin. Invest. 110: 1703-1716.

54. Caironi P, Ichinose F, Liu R, Jones RC, Bloch KD, Zapol WM. 2005. 5-Lipoxygenase Deficiency Prevents Respiratory Failure During Ventilator-Induced Lung Injury. Am. J. Respir. Crit. Care Med. 172: 334-343.

55. Lantz RC, Keller GE, III, Burrell R. 1991. The Role of Platelet-Activating Factor in the Pulmonary Response to Inhaled Bacterial Endotoxin. Am. Rev. Respir. Dis. 144: 167-172.

56. Nagase T, Ishii S, Kume K, Uozumi N, Izumi T, Ouchi Y, Shimizu T. 1999. Platelet-Activating Factor Mediates Acid-Induced Lung Injury in Genetically Engineered Mice. J. Clin. Invest. 104: 1071-1076.

57. Wolthuis EK, Vlaar AP, Choi G, Roelofs JJ, Haitsma JJ, van der PT, Juffermans NP, Zweers MM, Schultz MJ. 2009. Recombinant Human Soluble Tumor Necrosis Factor-Alpha Receptor Fusion Protein Partly Attenuates Ventilator-Induced Lung Injury. Shock 31: 262-266.

58. Ogawa EN, Ishizaka A, Tasaka S, Koh H, Ueno H, Amaya F, Ebina M, Yamada S, Funakoshi Y, Soejima J, Moriyama K, Kotani T, Hashimoto S, Morisaki H, Abraham E, Takeda J. 2006. Contribution of High-Mobility Group Box-1 to the Development of Ventilator-Induced Lung Injury. Am. J. Respir. Crit. Care Med. 174: 400-407.

59. Jerng JS, Hsu YC, Wu HD, Pan HZ, Wang HC, Shun CT, Yu CJ, Yang PC. 2007. Role of the Renin-Angiotensin System in Ventilator-Induced Lung Injury: an in Vivo Study in a Rat Model. Thorax 62: 527-535.

60. MENDELSON CL. 1946. The Aspiration of Stomach Contents into the Lungs During Obstetric Anesthesia. Am. J. Obstet. Gynecol. 52: 191-205.

61. Engelhardt T, Webster NR. 1999. Pulmonary Aspiration of Gastric Contents in Anaesthesia. Br. J. Anaesth. 83: 453-460.

62. Schwartz DJ, Wynne JW, Gibbs CP, Hood CI, Kuck EJ. 1980. The Pulmonary Consequences of Aspiration of Gastric Contents at PH Values Greater Than 2.5. Am. Rev. Respir. Dis. 121: 119-126.

63. Kennedy TP, Johnson KJ, Kunkel RG, Ward PA, Knight PR, Finch JS. 1989. Acute Acid Aspiration Lung Injury in the Rat: Biphasic Pathogenesis. Anesth. Analg. 69: 87-92.

64. Wynne JW, Ramphal R, Hood CI. 1981. Tracheal Mucosal Damage After Aspiration. A Scanning Electron Microscope Study. Am. Rev. Respir. Dis. 124: 728-732.

65. Perl M, Lomas-Neira J, Venet F, Chung CS, Ayala A. 2011. Pathogenesis of Indirect (Secondary) Acute Lung Injury. Expert. Rev. Respir. Med. 5: 115-126.

66. Brigham KL, Meyrick B. 1986. Endotoxin and Lung Injury. Am. Rev. Respir. Dis. 133: 913-927.

67. Schuster DP. 1994. ARDS: Clinical Lessons From the Oleic Acid Model of Acute Lung Injury. Am. J. Respir. Crit. Care Med. 149: 245-260.

68. Sakuma T, Takahashi K, Ohya N, Kajikawa O, Martin TR, Albertine KH, Matthay MA. 1999. Ischemia-Reperfusion Lung Injury in Rabbits: Mechanisms of Injury and Protection. Am. J. Physiol. 276: L137-L145.

69. Matute-Bello G, Frevert CW, Kajikawa O, Skerrett SJ, Goodman RB, Park DR, Martin TR. 2001. Septic Shock and Acute Lung Injury in Rabbits With Peritonitis: Failure of the Neutrophil Response to Localized Infection. Am. J. Respir. Crit. Care Med. 163: 234-243.

70. Carswell EA, Old LJ, Kassel RL, Green S, Fiore N, Williamson B. 1975. An Endotoxin-Induced Serum Factor That Causes Necrosis of Tumors. Proc. Natl. Acad. Sci. U. S. A 72: 3666-3670.

71. Fiers W. 1991. Tumor Necrosis Factor. Characterization at the Molecular, Cellular and in Vivo Level. FEBS Lett. 285: 199-212.

72. Sethu S, Melendez AJ. 2011. New Developments on the TNFalpha-Mediated Signalling Pathways. Biosci. Rep. 31: 63-76.

73. Yang G, Hamacher J, Gorshkov B, White R, Sridhar S, Verin A, Chakraborty T, Lucas R. 2010. The Dual Role of TNF in Pulmonary Edema. J. Cardiovasc. Dis. Res. 1: 29-36.

74. Michie HR, Manogue KR, Spriggs DR, Revhaug A, O'Dwyer S, Dinarello CA, Cerami A, Wolff SM, Wilmore DW. 1988. Detection of Circulating Tumor Necrosis Factor After Endotoxin Administration. N. Engl. J. Med. 318: 1481-1486.

75. Hesse DG, Tracey KJ, Fong Y, Manogue KR, Palladino MA, Jr., Cerami A, Shires GT, Lowry SF. 1988. Cytokine Appearance in Human Endotoxemia and Primate Bacteremia. Surg. Gynecol. Obstet. 166: 147-153.

76. Michie HR, Spriggs DR, Manogue KR, Sherman ML, Revhaug A, O'Dwyer ST, Arthur K, Dinarello CA, Cerami A, Wolff SM, . 1988. Tumor Necrosis Factor and Endotoxin Induce Similar Metabolic Responses in Human Beings. Surgery 104: 280-286.

77. Natanson C, Eichenholz PW, Danner RL, Eichacker PQ, Hoffman WD, Kuo GC, Banks SM, MacVittie TJ, Parrillo JE. 1989. Endotoxin and Tumor Necrosis Factor Challenges in Dogs Simulate the Cardiovascular Profile of Human Septic Shock. J. Exp. Med. 169: 823-832.

78. Cauwels A, Janssen B, Waeytens A, Cuvelier C, Brouckaert P. 2003. Caspase Inhibition Causes Hyperacute Tumor Necrosis Factor-Induced Shock Via Oxidative Stress and Phospholipase A2. Nat. Immunol. 4: 387-393.

79. Waage A, Halstensen A, Espevik T. 1987. Association Between Tumour Necrosis Factor in Serum and Fatal Outcome in Patients With Meningococcal Disease. Lancet 1: 355-357.

80. Freeman BD, Natanson C. 2000. Anti-Inflammatory Therapies in Sepsis and Septic Shock. Expert. Opin. Investig. Drugs 9: 1651-1663.

81. Tracey KJ, Fong Y, Hesse DG, Manogue KR, Lee AT, Kuo GC, Lowry SF, Cerami A. 1987. Anti-Cachectin/TNF Monoclonal Antibodies Prevent Septic Shock During Lethal Bacteraemia. Nature 330: 662-664.

82. Beutler B, Cerami A. 1988. The Common Mediator of Shock, Cachexia, and Tumor Necrosis. Adv. Immunol. 42: 213-231.

83. Abraham E. 1998. Cytokine Modifiers: Pipe Dream or Reality? Chest 113: 224S-227S.

84. Rice TW, Wheeler AP, Morris PE, Paz HL, Russell JA, Edens TR, Bernard GR. 2006. Safety and Efficacy of Affinity-Purified, Anti-Tumor Necrosis Factor-Alpha, Ovine Fab for Injection (CytoFab) in Severe Sepsis. Crit. Care Med. 34: 2271-2281.

85. Reinhart K, Wiegand-Lohnert C, Grimminger F, Kaul M, Withington S, Treacher D, Eckart J, Willatts S, Bouza C, Krausch D, Stockenhuber F, Eiselstein J, Daum L, Kempeni J. 1996. Assessment of the Safety and Efficacy of the Monoclonal Anti-Tumor Necrosis Factor Antibody-Fragment, MAK 195F, in Patients With Sepsis and Septic Shock: a Multicenter, Randomized, Placebo-Controlled, Dose-Ranging Study. Crit. Care Med. 24: 733-742.

86. Fisher CJ, Jr., Opal SM, Dhainaut JF, Stephens S, Zimmerman JL, Nightingale P, Harris SJ, Schein RM, Panacek EA, Vincent JL, . 1993. Influence of an Anti-Tumor Necrosis Factor Monoclonal Antibody on Cytokine Levels in Patients With Sepsis. The CB0006 Sepsis Syndrome Study Group. Crit. Care Med. 21: 318-327.

87. Millar AB, Foley NM, Singer M, Johnson NM, Meager A, Rook GA. 1989. Tumour Necrosis Factor in Bronchopulmonary Secretions of Patients With Adult Respiratory Distress Syndrome. Lancet 2: 712-714.

88. Meduri GU, Kohler G, Headley S, Tolley E, Stentz F, Postlethwaite A. 1995. Inflammatory Cytokines in the BAL of Patients With ARDS. Persistent Elevation Over Time Predicts Poor Outcome. Chest 108: 1303-1314.

89. Goncalves de Moraes V, Vargaftig BB, Lefort J, Meager A, Chignard M. 1996. Effect of Cyclo-Oxygenase Inhibitors and Modulators of Cyclic AMP Formation on Lipopolysaccharide-Induced Neutrophil Infiltration in Mouse Lung. Br. J. Pharmacol. 117: 1792-1796.

90. Horgan MJ, Palace GP, Everitt JE, Malik AB. 1993. TNF-Alpha Release in Endotoxemia Contributes to Neutrophil-Dependent Pulmonary Edema. Am. J. Physiol. 264: H1161-H1165.

91. Guery BP, Welsh DA, Viget NB, Robriquet L, Fialdes P, Mason CM, Beaucaire G, Bagby GJ, Neviere R. 2003. Ventilation-Induced Lung Injury Is Associated With an Increase in Gut Permeability. Shock 19: 559-563.

92. Wilson MR, Choudhury S, Takata M. 2005. Pulmonary Inflammation Induced by High-Stretch Ventilation Is Mediated by Tumor Necrosis Factor Signaling in Mice. Am. J. Physiol. Lung Cell Mol. Physiol. 288: L599-L607.

93. Johnson J, Meyrick B, Jesmok G, Brigham KL. 1989. Human Recombinant Tumor Necrosis Factor Alpha Infusion Mimics Endotoxemia in Awake Sheep. J. Appl. Physiol. 66: 1448-1454.

94. Gaskill HV, III. 1988. Continuous Infusion of Tumor Necrosis Factor: Mechanisms of Toxicity in the Rat. J. Surg. Res. 44: 664-671.

95. Grell M, Wajant H, Zimmermann G, Scheurich P. 1998. The Type 1 Receptor (CD120a) Is the High-Affinity Receptor for Soluble Tumor Necrosis Factor. Proc. Natl. Acad. Sci. U. S. A 95: 570-575.

96. Lucas R, Verin AD, Black SM, Catravas JD. 2009. Regulators of Endothelial and Epithelial Barrier Integrity and Function in Acute Lung Injury. Biochem. Pharmacol. 77: 1763-1772.

97. Lo SK, Everitt J, Gu J, Malik AB. 1992. Tumor Necrosis Factor Mediates Experimental Pulmonary Edema by ICAM-1 and CD18-Dependent Mechanisms. J. Clin. Invest. 89: 981-988.

98. Hocking DC, Phillips PG, Ferro TJ, Johnson A. 1990. Mechanisms of Pulmonary Edema Induced by Tumor Necrosis Factor-Alpha. Circ. Res. 67: 68-77.

99. Yang Y, Yin J, Baumgartner W, Samapati R, Solymosi EA, Reppien E, Kuebler WM, Uhlig S. 2010. Platelet-Activating Factor Reduces Endothelial Nitric Oxide Production: Role of Acid Sphingomyelinase. Eur. Respir. J. 36: 417-427.

100. Mukhopadhyay S, Hoidal JR, Mukherjee TK. 2006. Role of TNFalpha in Pulmonary Pathophysiology. Respir. Res. 7: 125.

101. Corda S, Laplace C, Vicaut E, Duranteau J. 2001. Rapid Reactive Oxygen Species Production by Mitochondria in Endothelial Cells Exposed to Tumor Necrosis Factor-Alpha Is Mediated by Ceramide. Am. J. Respir. Cell Mol. Biol. 24: 762-768.

102. Goldblum SE, Hennig B, Jay M, Yoneda K, McClain CJ. 1989. Tumor Necrosis Factor Alpha-Induced Pulmonary Vascular Endothelial Injury. Infect. Immun. 57: 1218-1226.

103. Wilson MR, Goddard ME, O'Dea KP, Choudhury S, Takata M. 2007. Differential Roles of P55 and P75 Tumor Necrosis Factor Receptors on Stretch-Induced Pulmonary Edema in Mice. Am. J. Physiol. Lung Cell Mol. Physiol. 293: L60-L68.

104. Yang Y, Uhlig S. 2011. The Role of Sphingolipids in Respiratory Disease. Ther. Adv. Respir. Dis. 5: 325-344.

105. Bao HF, Zhang ZR, Liang YY, Ma JJ, Eaton DC, Ma HP. 2007. Ceramide Mediates Inhibition of the Renal Epithelial Sodium Channel by Tumor Necrosis Factor-Alpha Through Protein Kinase C. Am. J. Physiol. Renal Physiol. 293: F1178-F1186.

106. Wiegmann K, Schutze S, Machleidt T, Witte D, Kronke M. 1994. Functional Dichotomy of Neutral and Acidic Sphingomyelinases in Tumor Necrosis Factor Signaling. Cell 78: 1005-1015.

107. Schütze S, Potthoff K, Machleidt T, Berkovic D, Wiegmann K, Kronke M. 1992. TNF Activates NF-Kappa B by Phosphatidylcholine-Specific Phospholipase C-Induced "Acidic" Sphingomyelin Breakdown. Cell 71: 765-776.

108. Huwiler A, Fabbro D, Pfeilschifter J. 1998. Selective Ceramide Binding to Protein Kinase C-Alpha and -Delta Isoenzymes in Renal Mesangial Cells. Biochemistry 37: 14556-14562.

109. Frindt G, Palmer LG, Windhager EE. 1996. Feedback Regulation of Na Channels in Rat CCT. IV. Mediation by Activation of Protein Kinase C. Am. J. Physiol. 270: F371-F376.

110. De Palma C, Meacci E, Perrotta C, Bruni P, Clementi E. 2006. Endothelial Nitric Oxide Synthase Activation by Tumor Necrosis Factor Alpha Through Neutral Sphingomyelinase 2, Sphingosine Kinase 1, and Sphingosine 1 Phosphate Receptors: a Novel Pathway Relevant to the Pathophysiology of Endothelium. Arterioscler. Thromb. Vasc. Biol. 26: 99-105.

111. Barsacchi R, Perrotta C, Bulotta S, Moncada S, Borgese N, Clementi E. 2003. Activation of Endothelial Nitric-Oxide Synthase by Tumor Necrosis Factor-Alpha: a Novel Pathway Involving Sequential Activation of Neutral Sphingomyelinase, Phosphatidylinositol-3' Kinase, and Akt. Mol. Pharmacol. 63: 886-895.

112. Johns DG, Jin JS, Webb RC. 1998. The Role of the Endothelium in Ceramide-Induced Vasodilation. Eur. J. Pharmacol. 349: R9-10.

113. Uhlig S, Gulbins E. 2008. Sphingolipids in the Lungs. Am. J. Respir. Crit. Care Med. 178: 1100-1114.

114. Claus RA, Bunck AC, Bockmeyer CL, Brunkhorst FM, Losche W, Kinscherf R, Deigner HP. 2005. Role of Increased Sphingomyelinase Activity in Apoptosis and Organ Failure of Patients With Severe Sepsis. FASEB J. 19: 1719-1721.

115. Dhami R, He X, Gordon RE, Schuchman EH. 2001. Analysis of the Lung Pathology and Alveolar Macrophage Function in the Acid Sphingomyelinase--Deficient Mouse Model of Niemann-Pick Disease. Lab. Invest. 81: 987-999.

116. Schuchman EH. 2010. Acid Sphingomyelinase, Cell Membranes and Human Disease: Lessons From Niemann-Pick Disease. FEBS Lett. 584: 1895-1900.

117. Haimovitz-Friedman A, Cordon-Cardo C, Bayoumy S, Garzotto M, McLoughlin M, Gallily R, Edwards CK, III, Schuchman EH, Fuks Z, Kolesnick R. 1997. Lipopolysaccharide Induces Disseminated Endothelial Apoptosis Requiring Ceramide Generation. J. Exp. Med. 186: 1831-1841.

118. Göggel R, Winoto-Morbach S, Vielhaber G, Imai Y, Lindner K, Brade L, Brade H, Ehlers S, Slutsky AS, Schutze S, Gulbins E, Uhlig S. 2004. PAF-Mediated Pulmonary Edema: a New Role for Acid Sphingomyelinase and Ceramide. Nat. Med. 10: 155-160.

119. von Bismarck P, Wistadt CF, Klemm K, Winoto-Morbach S, Uhlig U, Schutze S, Adam D, Lachmann B, Uhlig S, Krause MF. 2008. Improved Pulmonary Function by Acid Sphingomyelinase Inhibition in a Newborn Piglet Lavage Model. Am. J. Respir. Crit. Care Med. 177: 1233-1241.

120. Morita Y, Perez GI, Paris F, Miranda SR, Ehleiter D, Haimovitz-Friedman A, Fuks Z, Xie Z, Reed JC, Schuchman EH, Kolesnick RN, Tilly JL. 2000. Oocyte Apoptosis Is Suppressed by Disruption of the Acid Sphingomyelinase Gene or by Sphingosine-1-Phosphate Therapy. Nat. Med. 6: 1109-1114.

121. Elmore S. 2007. Apoptosis: a Review of Programmed Cell Death. Toxicol. Pathol. 35: 495-516.

122. Jarvis WD, Grant S, Kolesnick RN. 1996. Ceramide and the Induction of Apoptosis. Clin. Cancer Res. 2: 1-6.

123. Rotolo JA, Zhang J, Donepudi M, Lee H, Fuks Z, Kolesnick R. 2005. Caspase-Dependent and -Independent Activation of Acid Sphingomyelinase Signaling. J. Biol. Chem. 280: 26425-26434.

124. Santana P, Pena LA, Haimovitz-Friedman A, Martin S, Green D, McLoughlin M, Cordon-Cardo C, Schuchman EH, Fuks Z, Kolesnick R. 1996. Acid Sphingomyelinase-Deficient Human Lymphoblasts and Mice Are Defective in Radiation-Induced Apoptosis. Cell 86: 189-199.

125. Strelow A, Bernardo K, dam-Klages S, Linke T, Sandhoff K, Kronke M, Adam D. 2000. Overexpression of Acid Ceramidase Protects From Tumor Necrosis Factor-Induced Cell Death. J. Exp. Med. 192: 601-612.

126. Hauber HP, Karp D, Goldmann T, Vollmer E, Zabel P. 2010. Effect of Low Tidal Volume Ventilation on Lung Function and Inflammation in Mice. BMC. Pulm. Med. 10: 21.

127. Cannizzaro V, Berry LJ, Nicholls PK, Zosky GR, Turner DJ, Hantos Z, Sly PD. 2009. Lung Volume Recruitment Maneuvers and Respiratory System Mechanics in Mechanically Ventilated Mice. Respir. Physiol Neurobiol. 169: 243-251.

128. Thammanomai A, Majumdar A, Bartolak-Suki E, Suki B. 2007. Effects of Reduced Tidal Volume Ventilation on Pulmonary Function in Mice Before and After Acute Lung Injury. J. Appl. Physiol. 103: 1551-1559.

129. Allen GB, Suratt BT, Rinaldi L, Petty JM, Bates JH. 2006. Choosing the Frequency of Deep Inflation in Mice: Balancing Recruitment Against Ventilator-Induced Lung Injury. Am. J. Physiol. Lung Cell Mol. Physiol. 291: L710-L717.

130. Müller HC, Hellwig K, Rosseau S, Tschernig T, Schmiedl A, Gutbier B, Schmeck B, Hippenstiel S, Peters H, Morawietz L, Suttorp N, Witzenrath M. 2010. Simvastatin Attenuates Ventilator-Induced Lung Injury in Mice. Crit. Care 14: R143.

131. Hoetzel A, Dolinay T, Vallbracht S, Zhang Y, Kim HP, Ifedigbo E, Alber S, Kaynar AM, Schmidt R, Ryter SW, Choi AM. 2008. Carbon Monoxide Protects Against Ventilator-Induced Lung Injury Via PPAR-Gamma and Inhibition of Egr-1. Am. J. Respir. Crit. Care Med. 177: 1223-1232.

132. Vaneker M, Halbertsma FJ, van Egmond J, Netea MG, Dijkman HB, Snijdelaar DG, Joosten LA, van der Hoeven JG, Scheffer GJ. 2007. Mechanical Ventilation in Healthy Mice Induces Reversible Pulmonary and Systemic Cytokine Elevation With Preserved Alveolar Integrity: an in Vivo Model Using Clinical Relevant Ventilation Settings. Anesthesiology 107: 419-426.

133. Wolthuis EK, Vlaar AP, Choi G, Roelofs JJ, Juffermans NP, Schultz MJ. 2009. Mechanical Ventilation Using Non-Injurious Ventilation Settings Causes Lung Injury in the Absence of Pre-Existing Lung Injury in Healthy Mice. Crit. Care 13: R1.

134. Chavolla-Calderon M, Bayer MK, Fontan JJ. 2003. Bone Marrow Transplantation Reveals an Essential Synergy Between Neuronal and Hemopoietic Cell Neurokinin Production in Pulmonary Inflammation. J. Clin. Invest. 111: 973-980.

135. Finigan JH, Boueiz A, Wilkinson E, Damico R, Skirball J, Pae HH, Damarla M, Hasan E, Pearse DB, Reddy SP, Grigoryev DN, Cheadle C, Esmon CT, Garcia JG, Hassoun PM. 2009. Activated Protein C Protects Against Ventilator-Induced Pulmonary Capillary Leak. Am. J. Physiol. Lung Cell Mol. Physiol. 296: L1002-L1011.

136. Bai KJ, Spicer AP, Mascarenhas MM, Yu L, Ochoa CD, Garg HG, Quinn DA. 2005. The Role of Hyaluronan Synthase 3 in Ventilator-Induced Lung Injury. Am. J. Respir. Crit. Care Med. 172: 92-98.

137. Hong SB, Huang Y, Moreno-Vinasco L, Sammani S, Moitra J, Barnard JW, Ma SF, Mirzapoiazova T, Evenoski C, Reeves RR, Chiang ET, Lang GD, Husain AN, Dudek SM, Jacobson JR, Ye SQ, Lussier YA, Garcia JG. 2008. Essential Role of Pre-B-Cell Colony Enhancing Factor in Ventilator-Induced Lung Injury. Am. J. Respir. Crit. Care Med. 178: 605-617.

138. Dolinay T, Wu W, Kaminski N, Ifedigbo E, Kaynar AM, Szilasi M, Watkins SC, Ryter SW, Hoetzel A, Choi AM. 2008. Mitogen-Activated Protein Kinases Regulate Susceptibility to Ventilator-Induced Lung Injury. PLoS One 3: e1601.

139. Kacmarek RM, Kallet RH. 2007. Respiratory Controversies in the Critical Care Setting. Should Recruitment Maneuvers Be Used in the Management of ALI and ARDS?. Respir. Care 52: 622-631.

140. J.Mead CC. 1959. Relation of Volume History of Lungs to Respiratory Mechanics in Anesthetized Dogs. J. Appl. Physiol. 14: 669-678.

141. Uhlig S, Wollin L. 1994. An Improved Setup for the Isolated Perfused Rat Lung. J Pharmacol. Toxicol. Methods 31: 85-94.

142. von Bethmann AN, Brasch F, Nusing R, Vogt K, Volk HD, Muller KM, Wendel A, Uhlig S. 1998. Hyperventilation Induces Release of Cytokines From Perfused Mouse Lung. Am J Respir. Crit. Care Med. 157: 263-272.

143. Hodgson C, Keating JL, Holland AE, Davies AR, Smirneos L, Bradley SJ, Tuxen D. 2009. Recruitment Manoeuvres for Adults With Acute Lung Injury Receiving Mechanical Ventilation. Cochrane. Database. Syst. Rev. CD006667.

144. Verbrugge SJ, Bohm SH, Gommers D, Zimmerman LJ, Lachmann B. 1998. Surfactant Impairment After Mechanical Ventilation With Large Alveolar Surface Area Changes and Effects of Positive End-Expiratory Pressure. Br. J. Anaesth. 80: 360-364.

145. Halter JM, Steinberg JM, Gatto LA, DiRocco JD, Pavone LA, Schiller HJ, Albert S, Lee HM, Carney D, Nieman GF. 2007. Effect of Positive End-Expiratory Pressure and Tidal Volume on Lung Injury Induced by Alveolar Instability. Crit. Care 11: R20.

146. Seah AS, Grant KA, Aliyeva M, Allen GB, Bates JH. 2011. Quantifying the Roles of Tidal Volume and PEEP in the Pathogenesis of Ventilator-Induced Lung Injury. Ann. Biomed. Eng 39: 1505-1516.

147. Haitsma JJ, Lachmann B. 2006. Lung Protective Ventilation in ARDS: the Open Lung Maneuver. Minerva Anestesiol. 72: 117-132.

148. Hedrich HJ, Bullock G. 2004. The Laboratory Mouse. Elsevier.

149. Bateman RM, Ellis CG, Sharpe MD, Mehta S, Freeman DJ. 2001. Effect of Hemolyzed Plasma on the Batch Measurement of Nitrate by Nitric Oxide Chemiluminescence. Clin. Chem. 47: 1847-1851.

150. Cuellar JM, Antognini JF, Carstens E. 2004. An in Vivo Method for Recording Single Unit Activity in Lumbar Spinal Cord in Mice Anesthetized With a Volatile Anesthetic. Brain Res. Brain Res. Protoc. 13: 126-134.

151. Yamamoto N, Tsuchiya H, Hoffman RM. 2011. Tumor Imaging With Multicolor Fluorescent Protein Expression. Int. J. Clin. Oncol. 16: 84-91.

152. Berul CI, Aronovitz MJ, Wang PJ, Mendelsohn ME. 1996. In Vivo Cardiac Electrophysiology Studies in the Mouse. Circulation 94: 2641-2648.

153. Beck-Schimmer B, Schimmer RC. 2010. Perioperative Tidal Volume and Intra-Operative Open Lung Strategy in Healthy Lungs: Where Are We Going? 1. Best. Pract. Res. Clin. Anaesthesiol. 24: 199-210.

154. Weingarten TN, Cata JP, O'Hara JF, Prybilla DJ, Pike TL, Thompson GB, Grant CS, Warner DO, Bravo E, Sprung J. 2010. Comparison of Two Preoperative Medical Management Strategies for Laparoscopic Resection of Pheochromocytoma. Urology 76: 508-511.

155. Futier E, Constantin JM, Pelosi P, Chanques G, Kwiatkoskwi F, Jaber S, Bazin JE. 2010. Intraoperative Recruitment Maneuver Reverses Detrimental Pneumoperitoneum-Induced Respiratory Effects in Healthy Weight and Obese Patients Undergoing Laparoscopy. Anesthesiology 113: 1310-1319.

156. Pinheiro de Oliveira R, Hetzel MP, dos Anjos SM, Dallegrave D, Friedman G. 2010. Mechanical Ventilation With High Tidal Volume Induces Inflammation in Patients Without Lung Disease. Crit. Care 14: R39.

157. Lim SC, Adams AB, Simonson DA, Dries DJ, Broccard AF, Hotchkiss JR, Marini JJ. 2004. Intercomparison of Recruitment Maneuver Efficacy in Three Models of Acute Lung Injury. Crit. Care Med. 32: 2371-2377.

158. Vaporidi K, Voloudakis G, Priniannakis G, Kondili E, Koutsopoulos A, Tsatsanis C, Georgopoulos D. 2008. Effects of Respiratory Rate on Ventilator-Induced Lung Injury at a Constant PaCO2 in a Mouse Model of Normal Lung. Crit. Care Med. 36: 1277-1283.

159. Laffey JG, Engelberts D, Duggan M, Veldhuizen R, Lewis JF, Kavanagh BP. 2003. Carbon Dioxide Attenuates Pulmonary Impairment Resulting From Hyperventilation. Crit. Care Med. 31: 2634-2640.

160. Halbertsma FJ, Vaneker M, Pickkers P, Snijdelaar DG, van Egmond J, Scheffer GJ, van der Hoeven HG. 2008. Hypercapnic Acidosis Attenuates the Pulmonary Innate Immune Response in Ventilated Healthy Mice. Crit. Care Med. 36: 2403-2406.

161. Zosky GR, Janosi TZ, Adamicza A, Bozanich EM, Cannizzaro V, Larcombe AN, Turner DJ, Sly PD, Hantos Z. 2008. The Bimodal Quasi-Static and Dynamic Elastance of the Murine Lung. J. Appl. Physiol. 105: 685-692.

162. Soutiere SE, Mitzner W. 2004. On Defining Total Lung Capacity in the Mouse. J Appl. Physiol. 96: 1658-1664.

163. Bates JH, Allen GB. 2006. The Estimation of Lung Mechanics Parameters in the Presence of Pathology: a Theoretical Analysis. Ann. Biomed. Eng. 34: 384-392.

164. Muscedere JG, Mullen JB, Gan K, Slutsky AS. 1994. Tidal Ventilation at Low Airway Pressures Can Augment Lung Injury. Am J Respir. Crit. Care Med. 149: 1327-1334.

165. Hubmayr RD. 2002. Perspective on Lung Injury and Recruitment: a Skeptical Look at the Opening and Collapse Story. Am. J. Respir. Crit. Care Med. 165: 1647-1653.

166. Verbrugge SJ, Lachmann B, Kesecioglu J. 2007. Lung Protective Ventilatory Strategies in Acute Lung Injury and Acute Respiratory Distress Syndrome: From Experimental Findings to Clinical Application. Clin. Physiol Funct. Imaging 27: 67-90.

167. Gharib SA, Liles WC, Klaff LS, Altemeier WA. 2009. Noninjurious Mechanical Ventilation Activates a Proinflammatory Transcriptional Program in the Lung. Physiol Genomics 37: 239-248.

168. Tsangaris I, Lekka ME, Kitsiouli E, Constantopoulos S, Nakos G. 2003. Bronchoalveolar Lavage Alterations During Prolonged Ventilation of Patients Without Acute Lung Injury. Eur. Respir. J. 21: 495-501.

169. Meier T, Lange A, Papenberg H, Ziemann M, Fentrop C, Uhlig U, Schmucker P, Uhlig S, Stamme C. 2008. Pulmonary Cytokine Responses During Mechanical Ventilation of Noninjured Lungs With and Without End-Expiratory Pressure. Anesth. Analg. 107: 1265-1275.

170. Uhlig S. 2002. Ventilation-Induced Lung Injury and Mechanotransduction: Stretching It Too Far?. Am. J. Physiol. Lung Cell Mol. Physiol. 282: L892-L896.

171. Ranieri VM, Suter PM, Tortorella C, De Tullio R, Dayer JM, Brienza A, Bruno F, Slutsky AS. 1999. Effect of Mechanical Ventilation on Inflammatory Mediators in Patients With Acute Respiratory Distress Syndrome: a Randomized Controlled Trial 1. JAMA 282: 54-61.

172. Cannas A, Calvo L, Chiacchio T, Cuzzi G, Vanini V, Lauria FN, Pucci L, Girardi E, Goletti D. 2010. IP-10 Detection in Urine Is Associated With Lung Diseases. BMC. Infect. Dis. 10: 333.

173. Jiang Y, Xu J, Zhou C, Wu Z, Zhong S, Liu J, Luo W, Chen T, Qin Q, Deng P. 2005. Characterization of Cytokine/Chemokine Profiles of Severe Acute Respiratory Syndrome. Am. J. Respir. Crit. Care Med. 171: 850-857.

174. Haitsma JJ, Uhlig S, Goggel R, Verbrugge SJ, Lachmann U, Lachmann B. 2000. Ventilator-Induced Lung Injury Leads to Loss of Alveolar and Systemic Compartmentalization of Tumor Necrosis Factor-Alpha. Intensive Care Med. 26: 1515-1522.

175. Villar J, Kacmarek RM, Perez-Mendez L, guirre-Jaime A. 2006. A High Positive End-Expiratory Pressure, Low Tidal Volume Ventilatory Strategy Improves Outcome in Persistent Acute Respiratory Distress Syndrome: a Randomized, Controlled Trial. Crit. Care Med. 34: 1311-1318.

176. Meade MO, Cook DJ, Guyatt GH, Slutsky AS, Arabi YM, Cooper DJ, Davies AR, Hand LE, Zhou Q, Thabane L, Austin P, Lapinsky S, Baxter A, Russell J, Skrobik Y, Ronco JJ, Stewart TE. 2008. Ventilation Strategy Using Low Tidal Volumes, Recruitment Maneuvers, and High Positive End-Expiratory Pressure for Acute Lung Injury and Acute Respiratory Distress Syndrome: a Randomized Controlled Trial. JAMA 299: 637-645.

177. Uhlig S, Ranieri M, Slutsky AS. 2004. Biotrauma Hypothesis of Ventilator-Induced Lung Injury. Am. J Respir. Crit. Care Med. 169: 314-315.

178. dos Santos CC, Slutsky AS. 2006. The Contribution of Biophysical Lung Injury to the Development of Biotrauma. Annu. Rev. Physiol. 68: 585-618.

179. Khimenko PL, Bagby GJ, Fuseler J, Taylor AE. 1998. Tumor Necrosis Factor-Alpha in Ischemia and Reperfusion Injury in Rat Lungs. J. Appl. Physiol. 85: 2005-2011.

180. Koh Y, Hybertson BM, Jepson EK, Repine JE. 1996. Tumor Necrosis Factor Induced Acute Lung Leak in Rats: Less Than With Interleukin-1. Inflammation 20: 461-469.

181. Shimizu M, Hasegawa N, Nishimura T, Endo Y, Shiraishi Y, Yamasawa W, Koh H, Tasaka S, Shimada H, Nakano Y, Fujishima S, Yamaguchi K, Ishizaka A. 2009. Effects of TNF-Alpha-Converting Enzyme Inhibition on Acute Lung Injury Induced by Endotoxin in the Rat. Shock 32: 535-540.

182. Mong PY, Petrulio C, Kaufman HL, Wang Q. 2008. Activation of Rho Kinase by TNF-Alpha Is Required for JNK Activation in Human Pulmonary Microvascular Endothelial Cells. J. Immunol. 180: 550-558.

183. Koss M, Pfeiffer GR, Wang Y, Thomas ST, Yerukhimovich M, Gaarde WA, Doerschuk CM, Wang Q. 2006. Ezrin/Radixin/Moesin Proteins Are Phosphorylated by TNF-Alpha and Modulate Permeability Increases in Human Pulmonary Microvascular Endothelial Cells. J. Immunol. 176: 1218-1227.

184. Thomson EM, Williams A, Yauk CL, Vincent R. 2012. Overexpression of Tumor Necrosis Factor-Alpha in the Lungs Alters Immune Response, Matrix Remodeling, and Repair and Maintenance Pathways. Am. J. Pathol.

185. Borges VM, Vandivier RW, McPhillips KA, Kench JA, Morimoto K, Groshong SD, Richens TR, Graham BB, Muldrow AM, Van HL, Henson PM, Janssen WJ. 2009. TNFalpha Inhibits Apoptotic Cell Clearance in the Lung, Exacerbating Acute Inflammation. Am. J. Physiol. Lung Cell Mol. Physiol. 297: L586-L595.

186. Bertok S, Wilson MR, Morley PJ, de WR, Bayliffe A, Takata M. 2012. Selective Inhibition of Intra-Alveolar P55 TNF Receptor Attenuates Ventilator-Induced Lung Injury. Thorax 67: 244-251.

187. Kolesnick RN, Kronke M. 1998. Regulation of Ceramide Production and Apoptosis. Annu. Rev. Physiol. 60: 643-665.

188. Gowda S, Yeang C, Wadgaonkar S, Anjum F, Grinkina N, Cutaia M, Jiang XC, Wadgaonkar R. 2011. Sphingomyelin Synthase 2 (SMS2) Deficiency Attenuates LPS-Induced Lung Injury. Am. J. Physiol. Lung Cell Mol. Physiol. 300: L430-L440.

189. Kuemmel TA, Thiele J, Schroeder R, Stoffel W. 1997. Pathology of Visceral Organs and Bone Marrow in an Acid Sphingomyelinase Deficient Knock-Out Mouse Line, Mimicking Human Niemann-Pick Disease Type A. A Light and Electron Microscopic Study. Pathol. Res. Pract. 193: 663-671.

190. Cauwels A, Van MW, Janssen B, Everaerdt B, Huang P, Fiers W, Brouckaert P. 2000. Protection Against TNF-Induced Lethal Shock by Soluble Guanylate Cyclase Inhibition Requires Functional Inducible Nitric Oxide Synthase. Immunity. 13: 223-231.

191. Dahaba AA, Metzler H. 2009. Procalcitonin's Role in the Sepsis Cascade. Is Procalcitonin a Sepsis Marker or Mediator? Minerva Anestesiol. 75: 447-452.

192. Alexander RB, Rosenberg SA. 1991. Biologic Therapy of Cancer. J.B. Lippincott Company; p. 378-392.

193. Fink MP, Heard SO. 1990. Laboratory Models of Sepsis and Septic Shock. J. Surg. Res. 49: 186-196.

194. Wolfe TA, Dasta JF. 1995. Use of Nitric Oxide Synthase Inhibitors As a Novel Treatment for Septic Shock. Ann. Pharmacother. 29: 36-46.

195. Kuhl SJ, Rosen H. 1998. Nitric Oxide and Septic Shock. From Bench to Bedside. West J. Med. 168: 176-181.

196. Kilbourn RG, Gross SS, Jubran A, Adams J, Griffith OW, Levi R, Lodato RF. 1990. NG-Methyl-L-Arginine Inhibits Tumor Necrosis Factor-Induced Hypotension: Implications for the Involvement of Nitric Oxide. Proc. Natl. Acad. Sci. U. S. A 87: 3629-3632.

197. Lopez A, Lorente JA, Steingrub J, Bakker J, McLuckie A, Willatts S, Brockway M, Anzueto A, Holzapfel L, Breen D, Silverman MS, Takala J, Donaldson J, Arneson C, Grove G, Grossman S, Grover R. 2004. Multiple-Center, Randomized, Placebo-Controlled, Double-Blind Study of the Nitric Oxide Synthase Inhibitor 546C88: Effect on Survival in Patients With Septic Shock. Crit. Care Med. 32: 21-30.

198. Künstle G, Leist M, Uhlig S, Revesz L, Feifel R, MacKenzie A, Wendel A. 1997. ICE-Protease Inhibitors Block Murine Liver Injury and Apoptosis Caused by CD95 or by TNF-Alpha. Immunol. Lett. 55: 5-10.

199. Piguet PF, Vesin C, Donati Y, Barazzone C. 1999. TNF-Induced Enterocyte Apoptosis and Detachment in Mice: Induction of Caspases and Prevention by a Caspase Inhibitor, ZVAD-Fmk. Lab. Invest. 79: 495-500.

200. Vercammen D, Beyaert R, Denecker G, Goossens V, Van LG, Declercq W, Grooten J, Fiers W, Vandenabeele P. 1998. Inhibition of Caspases Increases the Sensitivity of L929 Cells to Necrosis Mediated by Tumor Necrosis Factor. J. Exp. Med. 187: 1477-1485.

201. Garcia-Ruiz C, Colell A, Mari M, Morales A, Calvo M, Enrich C, Fernandez-Checa JC. 2003. Defective TNF-Alpha-Mediated Hepatocellular Apoptosis and Liver Damage in Acidic Sphingomyelinase Knockout Mice. J. Clin. Invest. 111: 197-208.

202. Bryant C, Fitzgerald KA. 2009. Molecular Mechanisms Involved in Inflammasome Activation. Trends Cell Biol. 19: 455-464.

203. Dinarello CA. 2011. A Clinical Perspective of IL-1beta As the Gatekeeper of Inflammation. Eur. J. Immunol. 41: 1203-1217.

204. Degterev A, Yuan J. 2008. Expansion and Evolution of Cell Death Programmes. Nat. Rev. Mol. Cell Biol. 9: 378-390.

205. Medzhitov R. 2008. Origin and Physiological Roles of Inflammation. Nature 454: 428-435.

206. Imai Y, Kuba K, Neely GG, Yaghubian-Malhami R, Perkmann T, van Loo G, Ermolaeva M, Veldhuizen R, Leung YH, Wang H, Liu H, Sun Y, Pasparakis M, Kopf M, Mech C, Bavari S, Peiris JS, Slutsky AS, Akira S, Hultqvist M, Holmdahl R, Nicholls J, Jiang C, Binder CJ, Penninger JM. 2008. Identification of Oxidative Stress and Toll-Like Receptor 4 Signaling As a Key Pathway of Acute Lung Injury. Cell 133: 235-249.

207. Baum KF, Beckman DL. 1976. Aspiration Pneumonitis and Pulmonary Phospholipids. J. Trauma 16: 782-787.

208. Chen X, Hyatt BA, Mucenski ML, Mason RJ, Shannon JM. 2006. Identification and Characterization of a Lysophosphatidylcholine Acyltransferase in Alveolar Type II Cells. Proc. Natl. Acad. Sci. U. S. A 103: 11724-11729.

209. Schmitz G, Ruebsaamen K. 2010. Metabolism and Atherogenic Disease Association of Lysophosphatidylcholine. Atherosclerosis 208: 10-18.

210. Folkesson HG, Matthay MA, Hebert CA, Broaddus VC. 1995. Acid Aspiration-Induced Lung Injury in Rabbits Is Mediated by Interleukin-8-Dependent Mechanisms. J. Clin. Invest. 96: 107-116.

211. Pawlik MT, Schreyer AG, Ittner KP, Selig C, Gruber M, Feuerbach S, Taeger K. 2005. Early Treatment With Pentoxifylline Reduces Lung Injury Induced by Acid Aspiration in Rats. Chest 127: 613-621.

212. Schreiber T, Hueter L, Gaser E, Schmidt B, Schwarzkopf K, Karzai W. 2007. Effects of a Catecholamine-Induced Increase in Cardiac Output on Lung Injury After Experimental Unilateral Pulmonary Acid Instillation. Crit. Care Med. 35: 1741-1748.

213. Goodwin JE, Zhang J, Gonzalez D, Albinsson S, Geller DS. 2011. Knockout of the Vascular Endothelial Glucocorticoid Receptor Abrogates Dexamethasone-Induced Hypertension. J. Hypertens. 29: 1347-1356.

214. Minneci PC, Deans KJ, Natanson C. 2009. Corticosteroid Therapy for Severe Sepsis and Septic Shock. JAMA 302: 1643-1645.

215. Kozawa S, Kakizaki E, Muraoka E, Koketsu H, Setoyama M, Yukawa N. 2009. An Autopsy Case of Chemical Burns by Hydrochloric Acid. Leg. Med. (Tokyo) 11 Suppl 1: S535-S537.

216. Chu CS, Ouyang BY, Zhang Q. 1982. Early and Late Pathological Changes in Severe Chemical Burn to the Respiratory Tract Complicated With Acute Respiratory Failure. Burns Incl. Therm. Inj. 8: 387-390.

217. Bernard GR, Luce JM, Sprung CL, Rinaldo JE, Tate RM, Sibbald WJ, Kariman K, Higgins S, Bradley R, Metz CA, . 1987. High-Dose Corticosteroids in Patients With the Adult Respiratory Distress Syndrome. N. Engl. J. Med. 317: 1565-1570.

218. Meduri GU, Headley AS, Golden E, Carson SJ, Umberger RA, Kelso T, Tolley EA. 1998. Effect of Prolonged Methylprednisolone Therapy in Unresolving Acute Respiratory Distress Syndrome: a Randomized Controlled Trial. JAMA 280: 159-165.

219. Meduri GU, Marik PE, Chrousos GP, Pastores SM, Arlt W, Beishuizen A, Bokhari F, Zaloga G, Annane D. 2008. Steroid Treatment in ARDS: a Critical Appraisal of the ARDS Network Trial and the Recent Literature. Intensive Care Med. 34: 61-69.

220. Marik PE, Pastores SM, Annane D, Meduri GU, Sprung CL, Arlt W, Keh D, Briegel J, Beishuizen A, Dimopoulou I, Tsagarakis S, Singer M, Chrousos GP, Zaloga G, Bokhari F, Vogeser M. 2008. Recommendations for the Diagnosis and Management of Corticosteroid Insufficiency in Critically Ill Adult Patients: Consensus Statements From an International Task Force by the American College of Critical Care Medicine. Crit. Care Med. 36: 1937-1949.

221. Szefler SJ, Leung DY. 1997. Glucocorticoid-Resistant Asthma: Pathogenesis and Clinical Implications for Management. Eur. Respir. J. 10: 1640-1647.

222. Irusen E, Matthews JG, Takahashi A, Barnes PJ, Chung KF, Adcock IM. 2002. P38 Mitogen-Activated Protein Kinase-Induced Glucocorticoid Receptor Phosphorylation Reduces Its Activity: Role in Steroid-Insensitive Asthma. J. Allergy Clin. Immunol. 109: 649-657.

223. Bantel H, Schmitz ML, Raible A, Gregor M, Schulze-Osthoff K. 2002. Critical Role of NF-KappaB and Stress-Activated Protein Kinases in Steroid Unresponsiveness. FASEB J. 16: 1832-1834.

224. Webster JC, Oakley RH, Jewell CM, Cidlowski JA. 2001. Proinflammatory Cytokines Regulate Human Glucocorticoid Receptor Gene Expression and Lead to the Accumulation of the Dominant Negative Beta Isoform: a Mechanism for the Generation of Glucocorticoid Resistance. Proc. Natl. Acad. Sci. U. S. A 98: 6865-6870.

225. Barnes PJ. 2004. Corticosteroid Resistance in Airway Disease. Proc. Am. Thorac. Soc. 1: 264-268.

226. Funda A, Guniz M, Sibel E, Huseyin O. 2005. The Effects of Intratracheal Dexamethasone on Acute Lung Injury in Rabbits--Experimental Study. Middle East. J. Anesthesiol. 18: 161-171.

227. Jansson AH, Eriksson C, Wang X. 2005. Effects of Budesonide and N-Acetylcysteine on Acute Lung Hyperinflation, Inflammation and Injury in Rats. Vascul. Pharmacol. 43: 101-111.

228. Tang HF, Lu JJ, Tang JF, Zheng X, Liang YQ, Wang XF, Wang YJ, Mao LG, Chen JQ. 2010. Action of a Novel PDE4 Inhibitor ZL-n-91 on Lipopolysaccharide-Induced Acute Lung Injury. Int. Immunopharmacol. 10: 406-411.

229. O'Leary EC, Marder P, Zuckerman SH. 1996. Glucocorticoid Effects in an Endotoxin-Induced Rat Pulmonary Inflammation Model: Differential Effects on Neutrophil Influx, Integrin Expression, and Inflammatory Mediators. Am. J. Respir. Cell Mol. Biol. 15: 97-106.

230. Toovey S. 2004. The Miraculous Fever-Tree. The Cure That Changed the World Fiametta Rocco; Harper Collins, San Francisco, 2004, 348 Pages, Paperback, ISBN 0-00-6532357. Travel. Med. Infect. Dis. 2: 109-110.

231. Charous BL, Halpern EF, Steven GC. 1998. Hydroxychloroquine Improves Airflow and Lowers Circulating IgE Levels in Subjects With Moderate Symptomatic Asthma. J. Allergy Clin. Immunol. 102: 198-203.

232. Charous BL. 1990. Open Study of Hydroxychloroquine in the Treatment of Severe Symptomatic or Corticosteroid-Dependent Asthma. Ann. Allergy 65: 53-58.

233. Falk S, Goggel R, Heydasch U, Brasch F, Muller KM, Wendel A, Uhlig S. 1999. Quinolines Attenuate PAF-Induced Pulmonary Pressor Responses and Edema Formation. Am. J. Respir. Crit. Care Med. 160: 1734-1742.

6 Supplements

6.1 Statistical group comparisons

The tables below show exemplary, which groups were compared for calculation of the p-values in the single models. The same groups were also compared in all other analyses within those models.

6.1.1 Lung mechanics with PEEP = 2 cmH_2O

Table 6.1: P-values ranges for lung mechanics with PEEP = 2 cmH_2O

	C	R	G	H	R_{aw}
LowV_TRM5 – Low$V_T$noRM	0.001	0.001	0.05	0.001	0.001
LowV_TRM5 – HighV_TRM5	n.s.	0.05	n.s.	n.s.	0.05
LowV_TRM5 – LowV_TRM60a	0.001	0.001	0.01	0.001	0.001
LowV_TRM5 – LowV_TRM60b	0.01	0.01	0.05	0.01	0.001
HighV_TRM5 – High$V_T$noRM	0.001	0.001	0.05	0.001	0.001
Low$V_T$noRM – LowV_TRM60b	0.01	0.01	0.05	0.001	0.001
Low$V_T$noRM – High$V_T$noRM	0.01	0.001	n.s.	0.01	0.001
LowV_TRM60a – LowV_TRM60b	0.01	0.05	0.05	0.05	0.01

C: compliance, R: resistance, G: tissue damping, H: tissue elastance, R_{aw}: airway resistance. $p \leq 0.05$ was considered as statistically significant, n.s. not significant.

6.1.2 Lung mechanics with PEEP = 6 cmH_2O

Table 6.2: P-value ranges for lung mechanics with PEEP = 6 cmH_2O

	C	R	G	H
PEEP6_RM5 – PEEP6_RM60a	0.001	0.01	0.001	0.001
PEEP6_RM5 – PEEP6_RM60b	0.001	0.05	0.001	0.001
PEEP6_RM5 – PEEP6_noRM	0.001	0.001	0.001	0.001
PEEP6_noRM – PEEP6_RM60a	n.s.	n.s.	n.s.	0.05
PEEP6_noRM – PEEP6_RM60b	0.01	0.001	0.001	0.001
PEEP6_RM60a – PEEP6_RM60b	0.05	0.05	0.05	0.01

C: compliance, R: resistance, G: tissue damping, H: tissue elastance. $p \leq 0.05$ was considered as statistically significant, n.s. not significant.

6.1.3 Group comparisons for one-way ANOVA analyses in the TNF model

wt-zVAD – wt+zVAD

$ASM^{-/-}$-zVAD – $ASM^{-/-}$+zVAD

wt-zVAD – $ASM^{-/-}$-zVAD

wt+zVAD – $ASM^{-/-}$+zVAD

$ASM^{-/-}$sham – $ASM^{-/-}$-zVAD

$ASM^{-/-}$sham – $ASM^{-/-}$+zVAD

$ASM^{-/-}$sham – wt-zVAD

$ASM^{-/-}$sham – wt+zVAD

6.1.4 Lung mechanics in the severe acid model

Table 6.3: P-value ranges for lung mechanics in the severe acid model

	C	R	G	H	R_{aw}
$NaCl_{5h}$ – SA	0.001	0,05	0.001	0.001	n.s.
$NaCl_{5h}$ – SAD	0.001	0.001	0.001	0.001	n.s.
SA – SAD	n.s.	n.s.	n.s.	n.s.	n.s.

NACl: control with NaCl it, SA: severe acid (pH 1.5) it, SAD: severe acid it + dexamethasone iv; C: compliance, R: resistance, G: tissue damping, H: tissue elastance, R_{aw}: airway resistance. $p \leq 0.05$ was considered as statistically significant, n.s. not significant.

6.1.5 Lung mechanics in the moderate acid model

Table 6.4: P-value ranges for lung mechanics in the moderate acid model

	C	R	G	H	R_{aw}
NaCl – MA	0.01	0.01	0.01	0.01	n.s.
NaCl – MAD	n.s.	n.s.	n.s.	n.s.	n.s.
NaCl – MAQ	0.01	0.01	0.01	0.001	n.s.
MA – MAD	0.01	0.01	0.01	0.001	n.s.
MA – MAQ	n.s.	n.s.	n.s.	n.s.	n.s.
MAD – MAQ	0.01	0.01	0.05	0.001	n.s.

C: compliance, R: resistance, G: tissue damping, H: tissue elastance, R_{aw}: airway resistance. $p \leq 0.05$ was considered as statistically significant, n.s. not significant.

6.2 List of figures

6.3 List of tables

6.4 Publications

Original articles

Reiss LK, Kowallik A, Uhlig S. 2011. Recurrent recruitment manoeuvres improve lung mechanics and minimize lung injury during mechanical ventilation of healthy mice. PLoS One, 6 (9): e24527.

Kobbe P, Lichte P, Schreiber H, Reiss LK, Uhlig S, Pape HC, Pfeifer R. 2012. Inhalative IL-10 attenuates pulmonary inflammation following hemorrhagic shock without major alterations of the systemic inflammatory response. Mediators Inflamm., 2012: 512974.

Review article

Reiss LK, Uhlig U, Uhlig S. 2012. Models and mechanisms of acute lung injury caused by direct insults. Eur. J. Cell Biol., in press.

Oral presentations

Reiss LK, Yang Y, Adam D, Uhlig S. 2011. TNF-α induced septic shock does not trigger acute lung injury in mechanically ventilated mice. ESSR annual congress Aachen, abstract OP6-6.

Reiss LK, Uhlig S. 2011. Conditions for stable lung functions and hemodynamics in mechanically ventilated mice. ESSR annual congress Aachen, abstract OP6-5.

Reiss LK, Yang Y, Adam D, Uhlig S. 2011. TNF-alpha induced septic shock is attenuated in acid sphingomyelinase-deficient mice. ERS annual congress Amsterdam, abstract 2938.

Reiss LK, Adam D, Uhlig S. 2012. Acid sphingomyelinase-deficient mice are protected from the lethal cardiovascular effects in TNF-induced septic shock. DGPT Dresden 2012, abstract ID-239.

Poster

Reiss LK, Martin C, Gao J, Lex D, Uhlig U, Uhlig S. 2010. Absence of lung injury in mice during high-tidal volume ventilation when other physiological parameters are maintained in a physiological range. Am. J. Respir. Crit. Care Med. 181; 2010: A3025.

Gao J, Reiss LK, Martin C, Uhlig U, Uhlig S. 2010. Strain and vehicle dependence of zymosan-induced lung injury. Am. J. Respir. Crit. Care Med. 181; 2010: A2774.

Reiss LK, Uhlig S. 2011. Impact of tidal volume and recruitment manoeuvres on lung functions in mechanically ventilated mice. Naunyn-Schmiedeberg´s Arch. Pharmacol. 383 (Suppl 1): P043.

Reiss LK, Uhlig S. 2011. Recurrent recruitment manoeuvres are required to maintain lung functions during low tidal volume ventilation of healthy mice. ERS Amsterdam 2011 annual congress, abstract 800.

Verjans E, Reiss LK, Wagner N, Uhlig S, Tenbrock K, Martin C. 2011. Function of cAMP response element modulator in a murine asthma model. ERS Amsterdam 2011 annual congress, abstract 956.

6.5 Curriculum vitae

Persönliche Daten

Name:	Reiss
Vorname:	Lucy Kathleen
Geburtstag**:**	28. Juli 1975
Geburtsort:	London
Staatsangehörigkeit:	britisch

Qualifikationen

1995	Abitur am Privaten Franziskus Gymnasium Vossenack, Kreis Düren
1995 - 2002	Vordiplom in Biologie an der RWTH Aachen University
2002 - 2007	Diplom in Biologie an der RWTH Aachen University
Seit 2008	Promotion am Institut für Pharmakologie und Toxikologie des Universitätsklinikums der RWTH Aachen University

6.6 Acknowledgement

Zuallererst möchte ich Herrn Univ.-Prof. Dr. Stefan Uhlig herzlich dafür danken, dass er mir die Promotion am Institut für Pharmakologie und Toxikologie unter seiner Betreuung ermöglicht hat. Er hat stets großes Vertrauen in meine Arbeit gesetzt und meine wissenschaftliche Laufbahn weit über die Promotion hinaus gefördert.

Herrn Univ.-Prof. Dr. Werner Baumgartner vom Institut für Biologie II der RWTH Aachen University möchte ich für die freundliche Übernahme des Koreferates danken.

Weiterhin möchte ich Herrn PD Dr. Christian Martin ganz herzlich dafür danken, dass er meine Arbeit durch seinen beratenden und motivierenden Beistand unterstützt hat.

Bei Herrn Univ.-Prof. Dr. Dieter Adam, unserem Kooperationspartner vom Institut für Immunologie an der Christian-Albrechts-Universität zu Kiel, möchte ich mich für die fruchtbare Zusammenarbeit sowie die Bereitstellung von Mäusen bedanken.

An dieser Stelle möchte mich allen Mitarbeitern des Institutes für Pharmakologie und Toxikologie für die freundliche und hilfsbereite Arbeitsatmosphäre danken. Insbesondere Frau Nadine Ruske und Frau Birgit Feulner haben mich stets tatkräftig unterstützt. Betonen möchte ich auch, dass Frau Ulrike Uhlig, Frau Marion Peters und Frau Vera Lothmann immer ein offenes Ohr für mich hatten und so manches Problem für mich gelöst haben.

Mein besonderer Dank gilt Herrn Dr. Marco Schlepütz, der mich freundschaftlich auf meinem bisherigen wissenschaftlichen Weg begleitet hat, und Frau Anke Kowallik, die meine Arbeit durch ihre großartige Hilfe unterstützt hat.

Meiner lieben Familie danke ich dafür, dass sie mir immer zur Seite steht, wenn auch teilweise aus der Ferne. Nur gut, dass es das Telefon gibt…

Abschließend möchte ich meinen größten Dank an Erik und Spencer richten: Danke, dass Ihr immer für mich da seid!